

ÉCOLE DE TECHNOLOGIE SUPÉRIEURE
UNIVERSITÉ DU QUÉBEC

MASTER'S THESIS SUBMITTED TO
ÉCOLE DE TECHNOLOGIE SUPÉRIEURE

IN PARTIAL FULFILLMENT OF THE
REQUIREMENTS FOR THE
MASTER'S DEGREE IN MECHANICAL ENGINEERING
M.Eng.

BY
JUN ZENG

FINITE ELEMENT MODELING AND SIMULATION OF ROLL BENDING
PROCESS FOR FORMING A THICK CONICAL HOLLOW SHAPE

MONTREAL, July 4 2007

© copyright reserved by Jun Zeng

THIS THESIS HAS BEEN EVALUATED
BY THE FOLLOWING BOARD OF EXAMINERS

M. Vladimir Brailovski, President of the Board of Examiners
Département de génie mécanique à l'École de technologie supérieure

M. Zhaoheng Liu, Thesis supervisor
Département de génie mécanique à l'École de technologie supérieure

M. Henri Champlaud, Thesis co-supervisor
Département de génie mécanique à l'École de technologie supérieure

M. Hakim Bouzid, Membre of the Board of Examiners
Département de génie mécanique à l'École de technologie supérieure

THIS THESIS HAS BEEN PRESENTED AND DEFENDED
BEFORE A BOARD OF EXAMINERS AND PUBLIC

July 4 2007

AT ÉCOLE DE TECHNOLOGIE SUPÉRIEURE

MODÈLE D'ÉLÉMENT FINIS ET SIMULATION DE ROULAGE DE TÔLE ÉPAISSE POUR FORMER UN CÔNE CREUX

Jun Zeng

SOMMAIRE

L'objectif du projet exposé dans ce mémoire est de modéliser et de simuler le procédé dynamique du roulage des tôles fortes pour former des troncs de cônes. Le projet est réalisé en utilisant la méthode des éléments finis (MÉF) intégrée dans le logiciel ANSYS/LS-DYNA. Dans cette étude, la configuration pyramidale de roulage continu par flexion avec trois rouleaux est utilisée pour former une pièce conique à partir de tôles planes épaisses. La finalité est de fournir un outil de simulation permettant l'optimisation des paramètres du procédé, et de montrer sa faisabilité pour réaliser des géométries coniques adaptées à la fabrication de couronnes de turbine Francis.

Les relations cinématiques et géométriques du processus sont d'abord développées: elles permettent de minimiser le glissement entre la pièce et les rouleaux en utilisant des rouleaux coniques. Les étapes détaillées de la modélisation par éléments finis incluant le choix des types d'éléments, le maillage, les surfaces de contact avec frottement, les conditions frontières et les liaisons cinématiques sont ensuite présentés. Cette simulation 3D est basée sur la méthode explicite des éléments finis pouvant traiter le comportement de déformation non-linéaire élasto-plastique. Par la suite, la faisabilité de la modélisation du procédé à l'aide de cet outil numérique est exposée à travers un exemple typique. Les résultats du processus dynamique du roulage allant de la tôle plane initiale jusqu'à sa forme conique finale sont visualisés, c'est-à-dire changement progressif de la géométrie ainsi qu'évolution de la distribution des contraintes dans la pièce. Un test de convergence, faisant varier la résolution du maillage, est aussi réalisé pour s'assurer de la pertinence de la taille des éléments choisis. De plus, les forces de réaction et les contraintes résiduelles obtenues par la simulation numérique sont comparées aux résultats d'un calcul analytique simplifié. Pour mesurer la précision géométrique de la forme générée par rapport à celle spécifiée, un algorithme de vérification dimensionnelle a été développé. Cet algorithme, basé sur la méthode d'optimisation non-linéaire de Levenberg-Marquardt, permet de faire un lissage, selon une surface conique, des coordonnées des nœuds de la forme finale obtenue. Par la suite, les déviations sont calculées afin d'analyser les effets des variables du procédé et des paramètres de la simulation sur le résultat final du formage. Ces paramètres incluent le coefficient de frottement, l'épaisseur de la tôle, les propriétés des matériaux, l'agencement spatial des rouleaux et la température de la plaque formée. Cette étude de sensibilité évalue l'influence des paramètres sur les forces de réaction, les contraintes résiduelles et la conformité géométrique de la pièce formée.

FINITE ELEMENT MODELING AND SIMULATION OF ROLL BENDING PROCESS FOR FORMING A THICK CONICAL HOLLOW SHAPE

Jun Zeng

ABSTRACT

The objective of the project presented in this thesis is to model and simulate the dynamic roll-bending process for forming a thick plate to a conical hollow shape. The project is realized using the Finite Element Method (FEM), which is integrated into the ANSYS/LS-DYNA software. In this study, the continuous three-roll pyramidal configuration is applied to form a thick plate to a conical hollow shape. The final goal is to provide a simulation tool that allows the optimization of the parameters of the process, and to demonstrate the feasibility of fulfilling the conical geometry adapted to the manufacture of Francis turbine crowns.

The kinematic and geometric relationships of the process are developed first: they allow sliding to be kept to a minimum between the workpiece and the rolls using conical rolls. Detailed steps for modeling the Finite Elements (FM), including the element type, the meshing, the contact surfaces, the boundary conditions and the constraints, are then presented. This 3D simulation is based on the explicit finite element method, which is able to deal with nonlinear elasto-plastic deformation behavior. Next, a typical example is presented to demonstrate the feasibility of modeling the process using this numerical tool. The results of the dynamic roll-bending process, going from the initial plate plane to its final conical form are examined, that is, the progressive change in the geometry along with the evolution of the residual stress distribution in the workpiece. A convergence test, which varies the meshing size, is also carried out in order to ensure that the proper element sizes are chosen. Furthermore, the reaction forces and the residual stress obtained through the numerical simulation are compared with the results of a simplified analytic calculation. To compare the geometric precision of the shape generated with that of that specified, a dimensional verification algorithm was developed. The algorithm, which is based on the Levenberg-Marquardt nonlinear optimization method, allows the smoothing of the coordinates of the nodes of the final shape obtained, based on a conical surface. Next, the deviations are calculated in order to analyze the effects of the variables of the process and of the simulation parameters on the final forming results. These parameters include the friction coefficient, the plate thickness, the materials properties, the spatial arrangement of the outer rolls and the plate temperature. This sensitivity study evaluates the influence of the parameter on the reaction forces, the residual stresses and the geometric compliance of the final formed piece.

RÉSUMÉ EN FRANÇAIS

Le marché de la réparation des turbines hydrauliques dans les centrales hydroélectriques est grandissant, car beaucoup d'entre elles arrivent vers la fin de leur vie utile. Afin de minimiser les pertes dues à l'arrêt d'une turbine, les exploitants des centrales fixent des délais auxquels les manufacturiers doivent se soumettre. Dans le cas des turbines de type Francis, le temps de fabrication de la couronne par moulage empêche les fabricants d'être en mesure de répondre aux exigences des exploitants. Ainsi, d'autres procédés de fabrication doivent être étudiés pour atteindre les objectifs en termes de délai de livraison. Le procédé dont il sera question dans ce projet est le roulage pyramidal des tôles épaisses.

Le roulage est un des moyens efficaces pour former un tube cylindrique ou conique à partir d'une plaque plane métallique. Il existe plusieurs techniques de roulage. Le procédé le plus courant est le roulage pyramidal, qui utilise trois rouleaux dont un est en contact avec la surface supérieure de la plaque tandis que les deux autres sont en contact avec la surface inférieure. La plaque est menée par les forces de friction à l'interface de la plaque et des deux rouleaux inférieurs. Le rouleau supérieur est utilisé pour contrôler le rayon de courbure. D'autres procédés tels que le roulage à quatre rouleaux et le roulage à trois rouleaux croque ont été aussi développés dans l'industrie pour améliorer le formage. Cependant, le procédé pyramidal est le plus général et le plus utilisé dans la pratique. Par conséquent, dans ce projet l'étude s'est concentrée sur la modélisation et la simulation dynamique du procédé de roulage pyramidal par la méthode des éléments finis.

Le but de cette recherche sur le roulage est d'optimiser la précision du formage par roulage, d'estimer les dimensions nécessaires des rouleaux pour effectuer ce travail, de déterminer la force d'attraction et les forces de réactions entre les différentes composantes du procédé. D'après une revue de la littérature, il existe peu de travaux de

recherche antérieurs portant sur l'étude de faisabilité de la fabrication d'une couronne par roulage de troncs de cônes.

Le roulage est un processus complexe dont il reste beaucoup à apprendre et à comprendre. Dans cette optique, la méthode des éléments finis (MEF), avec la capacité de modélisation dynamique constitue, un outil intéressant pour permettre d'étudier en profondeur ce procédé. ANSYS® est un logiciel d'analyse des contraintes d'origine thermique ou mécanique par la méthode des éléments finis. Avec l'intégration de LS-DYNA®, ANSYS® a la capacité de simuler le processus dynamique, avec de grandes déformations et de grands déplacements, ainsi que les phénomènes complexes d'impacts. Dans le procédé du roulage, où de grands déplacements sont observés, ANSYS® avec LS-DYNA® intégré permet de simuler et d'étudier ce procédé particulier. Dans ce document, une modélisation paramétrique de la simulation du roulage pyramidal est présentée, en utilisant ANSYS® avec LS-DYNA® pour étudier la faisabilité du formage d'un cône par cette technique. La simulation numérique permet d'évaluer l'influence des paramètres du procédé sur les forces appliquées, la qualité du formage et la distribution des contraintes résiduelles.

La première étape importante dans la simulation de formage consiste à construire le modèle géométrique. Puisque la procédure du roulage doit satisfaire la relation cinématique, il faut créer un modèle géométrique pour lequel cette relation cinématique est respectée et dont le rayon de courbure est facile à contrôler. Dans le cadre de ce projet, pour faire suite à cette considération, des rouleaux coniques seront utilisés pour former un cône par roulage. Dans la construction du modèle géométrique, les paramètres de configuration tels que la position, la taille des rouleaux et la position de la plaque sont optimisés. De plus, la flexibilité du modèle géométrique créé permet de réaliser des études paramétriques. Les détails du modèle géométrique sont présentés dans le chapitre 1.

Il est à noter que dans la conception du modèle, le critère suivi est sa facilité et sa flexibilité d'utilisation et de réutilisation tout au long de l'étude. Ceci veut dire que ce

modèle doit être capable de simuler la procédure du roulage en choisissant différentes tailles de cônes, différents matériaux, différentes températures et différentes configurations de rouleaux. *L'architecture modulaire* est donc un point essentiel dans la création de ce modèle comportant plusieurs modules bien définis qui exécutent différentes tâches de modélisation de façon structurée. Ce type de modèle est plus fiable et les composants sont récupérables. Un autre avantage de ce modèle est son extensibilité. Les nouveaux modules sont faciles à modifier pour intégrer d'autres fonctionnalités. Le chapitre 2 présente en détail les différentes étapes des analyses dynamiques effectuées dans cette étude. Les commandes principales du logiciel utilisé ainsi que l'architecture modulaire du code de simulation sont présentées. Dans la dernière section du chapitre, quelques résultats de simulation, utilisant le modèle établi, sont présentés.

Les résultats de la simulation dans ANSYS® donnent la position atteinte par les nœuds, les forces sur les surfaces de contact et les contraintes résiduelles. ANSYS® permet également de visualiser le processus dynamique de formage jusqu'à la forme désirée à l'aide de l'animation graphique. À la suite d'une simulation, il faut évaluer la différence géométrique entre la pièce formée et le cône désiré. Cependant, la déviation ne peut pas être évaluée directement parce que la pièce formée n'est pas un cône exact. Pour cette raison, un nouvel algorithme de lissage de données non linéaire a été mis en place afin de mesurer quantitativement la déviation géométrique. Dans ce mémoire, cette procédure est appelée la vérification géométrique. Avec cette méthode, la distorsion provenant de la procédure et l'écart entre la pièce réelle et la pièce idéale peuvent être calculés. C'est l'algorithme non linéaire Levenberg-Marquardt qui est utilisé pour lisser un cône dont la somme des carrés des distances est minimum. Ce cône, appelé le cône des moindres carrés, est obtenu par l'algorithme d'optimisation non linéaire mentionné. Le résultat de la position des nœuds générés par ANSYS® est importé dans MATLAB® pour le calcul numérique. Par la suite, l'écart entre la géométrie de la pièce formée et celle du cône désiré est calculé. Après avoir obtenu le cône des moindres carrés, la vérification géométrique s'effectue et permet de quantifier la conformité et la qualité de

la pièce formée par le procédé. Le chapitre 3 présente en détail la procédure de vérification géométrique, la fonction objective et l'algorithme non linéaire. Un cas de calcul est donné à titre d'exemple.

À la suite de l'obtention des résultats de la simulation et de la vérification géométrique, la sensibilité des paramètres est étudiée. Il est assez évident que, pour le processus du roulage, les variations de la dimension du cône désiré, des propriétés de matériaux et de la configuration des rouleaux peuvent influencer les résultats de formage. Dans l'analyse, chaque rouleau est considéré comme un corps rigide et sa dimension est déterminée par les dimensions spécifiques du cône à former. La configuration des rouleaux est alors représentée par la distance entre les deux rouleaux inférieurs. Dans l'évaluation de l'influence des paramètres du procédé, les principaux résultats sont donc la qualité du formage, la force exercée sur les rouleaux et les contraintes résiduelles.

Dans l'étude de la qualité du formage, les différents matériaux (acier inoxydable ASTM A743 grade CA-6NM, acier ASTM A36, alliage d'Aluminium et de Cuivre AA 6063, Cuivre recuit) sont considérés. Les résultats montrent que la configuration des rouleaux joue un rôle important sur la qualité du formage. Pour un type de matériau donné, il existe une configuration optimale avec laquelle une meilleure qualité de formage peut être atteinte. Une série de simulations, pour différents types de matériaux et dimensions de couronnes, a été réalisée afin de déterminer la meilleure configuration des rouleaux pour une combinaison donnée.

Dans l'étude de la force exercée sur les rouleaux, le facteur épaisseur de la plaque est particulièrement intéressant, car c'est ce paramètre qui donne l'effet le plus significatif. Pour cette partie de l'étude, les dimensions du cône désiré sont : 2 mètres de rayon au sommet, 3 mètres de rayon à la base et 4 mètres de hauteur. Le matériel est de l'acier inoxydable ASTM A743 grade CA-6NM. L'analyse de la sensibilité de l'épaisseur de la plaque fait varier ce paramètre de 1 cm à 10 cm. Les résultats montrent que la force exercée sur les rouleaux augmente en fonction de l'épaisseur sous forme d'une relation quasiment linéaire. De plus, l'effet de la température de formage de la plaque (20 °C,

200 °C, 400 °C, 600 °C, 800 °C, 1000 °C) est aussi étudié. Les résultats montrent logiquement que la force exercée sur les rouleaux diminue lorsque la température augmente.

Les résultats des contraintes résiduelles générées dans le cône par le procédé de roulage sont en relation avec les forces exercées sur les rouleaux. La variation des contraintes résiduelles est également étudiée pour différentes épaisseurs de plaque et différentes températures. Avec l'augmentation de la température, la plaque devient plus malléable et il est ainsi plus facile de la former. L'intensité des contraintes résiduelles s'en trouve diminuée.

La friction entre les surfaces en contact est aussi étudiée pour vérifier sa sensibilité sur la qualité du formage. En général, un coefficient de friction de l'ordre de 0.3-0.4 est suffisant pour permettre l'entraînement de la plaque par les rouleaux. L'étude de sensibilité montre que la friction entre deux composants (rouleau et plaque) n'affecte pas la qualité de la géométrie formée tant que le coefficient de friction demeure supérieur à 0.3.

Toutes les études paramétriques sont réalisées avec des rouleaux coniques. Cependant, des comparaisons ont été effectuées avec des simulations du roulage utilisant des rouleaux cylindriques. Les résultats montrent que l'utilisation de rouleaux coniques permet de contrôler plus facilement le rayon de courbure et de satisfaire la relation cinématique entre la plaque formée et les rouleaux. Les détails de la discussion des résultats sont exposés dans le chapitre 4.

En résumé, les principales étapes de l'étude du roulage présentées dans ce mémoire peuvent être décrites comme suit : En premier lieu, le modèle géométrique est construit en utilisant des rouleaux coniques. Ensuite, un modèle d'éléments finis est établi et la simulation dynamique de la procédure du roulage est exécutée dans ANSYS® avec LS-DYNA®. Avec le résultat de la position des nœuds, le cône des moindres carrés est obtenu dans MATLAB® afin de réaliser la vérification géométrique. La sensibilité

paramétrique est étudiée en se basant sur les résultats de la simulation et de la vérification géométrique. Selon les différentes analyses de l'étude, les conclusions suivantes sont tirées :

- Pour un cône donné avec un type de matériau spécifique, la qualité du formage dépend de la configuration de rouleaux. Il y a une configuration pour laquelle la qualité optimale du formage peut être obtenue.

- Pour une configuration donnée et un type de matériau spécifique, la force exercée sur les rouleaux augmente en fonction de l'épaisseur de la plaque d'une façon quasiment linéaire. Cependant, pour un cône donné avec un type de matériau spécifique, les forces exercées sur les rouleaux diminuent lorsque la distance entre les deux rouleaux inférieurs est augmentée.

- Même si la configuration influence directement la qualité du formage, il n'existe toujours pas de formulation analytique permettant de calculer la meilleure configuration possible des rouleaux. Il est clair que la simulation numérique telle qu'établie dans cette étude s'est avérée utile et pertinente pour déterminer la valeur optimale de ce paramètre.

Bien que le procédé de roulage des couronnes coniques soit étudié avec succès à l'aide d'un modèle des éléments finis, plusieurs aspects peuvent être améliorés et peuvent constituer la suite de ce travail de recherche :

- Premièrement, tous les rouleaux dans ce modèle sont coniques. Ce type de rouleau est plus coûteux à fabriquer que des rouleaux cylindriques. Si les rouleaux cylindriques sont utilisés, il est plus difficile de contrôler le rayon de courbure du cône formé et la relation cinématique ne peut pas être satisfaite. Cependant, utiliser les rouleaux cylindriques est plus économique et polyvalent.

Il serait donc intéressant et utile d'établir un modèle de roulage avec des rouleaux cylindriques et d'étudier la faisabilité et la précision atteinte dans ce cas.

- Deuxièmement, tous les rouleaux du modèle actuel sont rigides dans le but de simplifier la construction du modèle. Pour rendre la simulation plus précise, il faudrait étudier le procédé avec des rouleaux déformables.
- Une troisième amélioration du présent travail consisterait à accélérer le calcul numérique. La simulation actuelle prend trop de temps de calcul, spécialement quand la taille des éléments est petite. Une des solutions envisageables pour palier à ce problème est de faire appel au calcul parallèle, ce qui diminuerait le temps de calcul.
- Enfin, un modèle de simulation en boucle fermée pour automatiser le processus de choix des paramètres optimaux serait un atout important. Le modèle actuel permet de déterminer la relation entre la qualité du formage et la configuration des rouleaux. Néanmoins, ce modèle est en boucle ouverte. La mesure de la qualité du formage est indépendante de la configuration des rouleaux. Un modèle en boucle fermée pourrait être plus efficace dans la détermination de la meilleure configuration des rouleaux. Si la qualité du formage est mesurée et transférée à l'entrée du modèle afin d'ajuster à mesure la configuration des rouleaux, la convergence vers une meilleure qualité du formage pourrait être accélérée.

ACKNOWLEDGEMENT

First of all, I would like to extend my appreciation to my director, Professor Zhaoheng Liu and my co-director, Professor Henri Champliaud, who provided me with tons of instructions on how to advance with my work, on how to analyze results, and on how to carry out a geometric verification of this project. These invaluable instructions guided me in the right direction, and extended my thought process in my Master's project.

Next, I would like to acknowledge the contribution of my wife and daughter. During the course of this project, they offered me all the support I needed in order to dedicate myself fully to my studies. Thanks to them for their understanding and encouragement, particularly during those moments when I encountered difficulties in my project.

Last, but not least, I would also like to thank all my colleagues for their help in this project. I have learnt a lot from them, I will forever cherish the experience I gained from working with them.

TABLE OF CONTENTS

	Page
SOMMAIRE	iii
ABSTRACT	iv
RÉSUMÉ EN FRANÇAIS	v
ACKNOWLEDGEMENT	xii
LIST OF FIGURES	xvi
LIST OF TABLES	xix
ABBREVIATIONS	xxi
NOMENCLATURE	xxii
INTRODUCTION	1
CHAPTER	GEOMETRIC SETUP OF THE CONICAL ROLL BENDING PROCESS
	10
1.1	Determination of roll the type
	11
1.1.1	Curvature control
	11
1.1.2	Kinematic relationship
	12
1.1.3	Application of conical rolls
	13
1.2	Determination of roll diameter
	14
1.3	Determination of the geometric parameters
	17
1.3.1	Hypothesis and illustration of the final geometric parameters
	19
1.3.2	The dimension of the target cone
	21
1.3.3	The dimension of the rolls
	21
1.3.3.1	The dimension of the outer roll
	22
1.3.3.2	The dimension of the inner roll
	22
1.3.4	The outer and inner apex of the target cone
	23
1.3.5	The roll position
	24
1.3.5.1	The outer roll position
	25
1.3.5.2	The inner roll position
	26
1.3.6	The dimension and position of the plate
	27
1.3.7	The initial position of the inner roll
	29
1.4	Significance of the geometric setup
	30

CHAPTER 2	FINITE ELEMENT MODELING AND SIMULATION IN ANSYS AND LS-DYNA	32
2.1	Introduction to ANSYS and LS-DYNA simulation program structure	32
2.1.1	Analysis procedure using ANSYS	32
2.1.2	Structure of the simulation program	33
2.2	Finite Element Model	36
2.2.1	Element type	36
2.2.2	Solid modeling	38
2.2.3	Meshing strategy	40
2.2.4	Contact surfaces and friction model	41
2.2.5	Constraints and boundary conditions of guiding cylinders and rolls	43
2.2.6	Material specification	45
2.2.7	Loads specification	46
2.2.7.1	Tilt angle of the inner roll	47
2.2.7.2	Rotation angular speed of the outer roll	48
2.3	A typical simulation example and its numerical results	49
2.3.1	The contour display of the final shape	50
2.3.2	The reaction force on the roll	51
2.4	Discussion of convergence and number of passes in the process ..	52
2.4.1	Convergence studies and comparison of performance	53
2.4.2	Number of passes	55
2.5	Comparison between FEM results and the theoretical calculation for the roll-bending of a cylindrical shape	56
2.5.1	Validation of reaction force	57
2.5.2	Validation of residual stress	59
2.6	Summary	61
CHAPTER 3	VERIFICATION OF THE GEOMETRIC ACCORDANCE OF THE FINAL PIECE	63
3.1	Purpose of geometric verification	63
3.1.1	Assessment of the circularity and the distortion	64
3.1.1.1	Comparison of circularity	64
3.1.1.2	Comparison of distortion	65
3.1.2	Assesment of the deviation between the fitted cone and the target cone	66
3.1.3	Analysis of sensitivity of the bending quality	66
3.2	Realization of geometric verification	67
3.2.1	Procedure of geometric verification	68
3.3	Geometric verification criteria	68
3.3.1	Similarity to an exact cone	68
3.3.2	Deviation from the target cone	69

3.4	Levenberg-Marquardt Algorithm [25].....	70
3.4.1	The problem.....	70
3.4.2	The solution.....	71
3.4.3	Choice of damping parameter.....	72
3.4.4	Algorithm.....	72
3.5	Determination of fitted cone.....	73
3.5.1	Distance from a point to a plane (g_i) and to a line (f_i).....	74
3.5.1.1	Distance from a point to a plane.....	75
3.5.1.2	Distance from a point to a line.....	75
3.5.2	The derivation for f_i and g_i	76
3.5.3	Distance between the point and the plane.....	77
3.5.4	Objective function.....	78
3.5.5	Normalization.....	78
3.6	Typical example of geometric verification.....	79
CHAPTER 4	SENSITIVITY ANALYSIS OF THE THREE-ROLL BENDING PROCESS.....	82
4.1	Study parameters and approach.....	82
4.1.1	Input parameters and output results.....	82
4.1.2	The study approach.....	83
4.2	Sensitivity of geometric parameters.....	84
4.2.1	Influence of plate thickness on bending quality.....	85
4.2.2	Influence of plate thickness on reaction forces on the rolls.....	86
4.2.3	Influence of plate thickness on residual stresses.....	87
4.2.4	Influence of the semi-angle of the target cone on bending quality.....	88
4.3	Sensitivity of material properties.....	89
4.3.1	Influence of temperature on the bending quality.....	91
4.3.2	Influence of temperature on the reaction forces on the rolls.....	92
4.3.3	Influence of temperature on residual stress.....	92
4.4	Configuration parameters.....	93
4.4.1	Influence of span of the outer rolls on bending quality.....	94
4.4.2	Influence of span of outer rolls on the reaction forces on the rolls.....	98
4.4.3	Influence of span of the outer rolls on residual stress.....	99
4.4.4	Sensitivity of friction to the bending process.....	100
4.5	Summary.....	101
CONCLUSION	103
RECOMMENDATIONS	106

LIST OF FIGURES

		Page
Figure 1	3-D illustration and image of the Francis Turbine [2, 3]	1
Figure 2	The three components of the Francis Turbine.....	2
Figure 3	The three-roll continuous pyramidal bending model.....	5
Figure 4	Illustration of three-roll continuous bending machine [16]	7
Figure 5	Comparison of two configurations of the roll bending machine used to bend conical shapes [16]	7
Figure 6	The input and output parameters for geometric setup procedure.....	11
Figure 7	Illustration of perfect conical shape (a) and distorted conical shape (b)	12
Figure 8	Kinematic relationship of tangent speed for driving a pre-bent sector plate in roll-bending process	13
Figure 9	Illustration of application of conical rolls in roll bending process: 3D image and 2D section demonstration	14
Figure 10	Deflection of roll when changing the roll diameter	16
Figure 11	Parameters needed for determining the geometric parameters of the roll-bending process	18
Figure 12	Illustration of geometric parameters of the target cone and rolls.....	20
Figure 13	Illustration of angle between axes of rolls and the XY, YZ, XZ planes	25
Figure 14	Illustration for calculating the dimension and position of the sector plate and the position of the inner roll	28
Figure 15	Structure of simulation program	35
Figure 16	Illustration of the Finite Element Model.....	36
Figure 17	Illustration of SHELL163	37
Figure 18	Integration points of SHELL163 element.....	38

Figure 19	Entities of solid model in ANSYS	39
Figure 20	Illustration of meshing plate by specifying width division and arc division.....	41
Figure 21	Friction model of rolls and plates in the roll-bending process.....	42
Figure 22	Constraints of the bottom and top central node of the outer rolls.....	44
Figure 23	Real behaviour and simplifying behaviour of bilinear material.....	46
Figure 24	Illustration of the tilt angle for pressing down the upper roll in the three-pass process.....	47
Figure 25	Tilt angle of the upper roll used for pressing the plate during the process.....	48
Figure 26	The angular speed of the outer roll for driving the plate forward and backward in the 3-pass roll-bending process	49
Figure 27	The contour display of the final shape formed in a typical simulation. .	51
Figure 28	Reaction forces on the upper roll	52
Figure 29	Convergence study conducted by comparing the reaction force of the inner roll in the Y direction when applying different mesh sizes	54
Figure 30	Rapid increase in run-time along with the increase of element	55
Figure 31	Two views of the contour display of the final shape obtained by applying the single-pass roll bending process.....	56
Figure 32	Parameters for the theoretical estimation of the reaction forces on the inner roll.....	58
Figure 33	Determination of residual stress using graphic interpretation [5].....	61
Figure 34	Comparison of circularity on different configurations.....	65
Figure 35	Comparison of distortion on different configurations.....	65
Figure 36	Relationship between configuration and bending quality.....	67
Figure 37	Geometric verification procedure	68
Figure 38	Procedure for Levenberg-Marquardt algorithm.....	73
Figure 39	Demonstration of fitting cone	74
Figure 40	Distance from point to line and distance from point to plane.....	75

Figure 41	Distance from i^{th} point to fitted cone	77
Figure 42	Simulation and geometric verification sequence	80
Figure 43	Graphical comparison of the target cone and fitted cone.....	81
Figure 44	Relation between input parameters and output results.....	83
Figure 45	Variation of bending quality with different plate thicknesses	86
Figure 46	Tendency of reaction forces as plate thickness is increased	87
Figure 47	Variation of residual stress with changes in plate thickness	88
Figure 48	Influence of the semi-angle of the target shape on the bending quality.....	89
Figure 49	Bending quality obtained at different temperatures	91
Figure 50	Reaction force of three rolls at different temperatures in the Y direction	92
Figure 51	Trend of residual stress with increase in temperature.....	93
Figure 52	Deviation of the final shape from the target cone on different spans of the outer rolls when applying the ASTM A743 grade CA-6NM material.....	95
Figure 53	Deviation of the final shape from the target cone on different spans of the outer rolls when applying the ASTM A36 Steel material.....	96
Figure 54	Deviation of the final shape from the target cone on different spans of the outer rolls when applying the AA 6063 Aluminum Alloy material.....	97
Figure 55	Variation of reaction force when applying different spans of the outer rolls	98
Figure 56	Residual stress on the application of different span of the outer rolls ..	99
Figure 57	Comparison of the final shape at frictions of 0.1, 0.3 and 0.7	100

LIST OF TABLES

		Page
Table I	The four-roll continuous bending procedure.....	5
Table II	The three-roll pinching-bending procedure	6
Table III	Equations for calculating the geometric parameters of the target cone	21
Table IV	Equations for calculating the geometric parameters of the outer roll	22
Table V	Equations for calculating the geometric parameters of the inner roll	23
Table VI	Equations for calculating the coordinate of the bottom center of the outer roll.....	25
Table VII	Equations for calculating the angles between the axis of the outer roll and the planes XY, YZ and XZ.....	26
Table VIII	Equations for calculating the coordinates of the bottom center of the inner roll.....	26
Table IX	Equations for calculating the angles between the axis of the inner roll and the XY, YZ and XZ planes.....	27
Table X	Equations for calculating the dimension and position of the plate	28
Table XI	Equations for calculating the initial position of the bottom center of the inner roll.....	29
Table XII	Equations for calculating the initial angles between the axis of the inner roll and the XY, YZ and XZ planes	30
Table XIII	Friction between certain components and the plate	43
Table XIV	Validation of reaction force on the inner roll with the theoretical result.....	59
Table XV	Comparison of residual stress in simulation with the theoretical result	60
Table XVI	Numerical comparison of the target cone and the fitted cone.....	81
Table XVII	Constant parameters for studying plate thickness sensitivity	85
Table XVIII	Constant parameters for studying the sensitivity of the temperature.....	90

Table XIX	Material ASTM A743 grade CA-6NM at different temperatures.....	90
Table XX	Constant parameters for studying the sensitivity of the span of outer rolls.....	94
Table XXI	Material properties of ASTM A36 Steel.....	96
Table XXII	Material properties of AA 6063 Aluminum Alloy.....	97

ABBREVIATIONS

FEM/FEA	Finite Element Method / Finite Element Analysis
LSTC	Livermore Software Technology Corporation
ANSYS	Product of ANSYS corporation; FE analysis and static simulation software
LS-DYNA	Product of LSTC corporation; FE analysis and dynamic simulation software
APDL	ANSYS Parametric Design Language

NOMENCLATURE

R_p	Outer radius of the sector plate
r_p	Inner radius of the sector plate
V_o	Outer tangent speed of the sector plate
V_i	Inner tangent speed of the sector plate
R_{ro}	Bottom radius of outer roll
r_{ro}	Top radius of outer roll
R	Bottom radius of the target cone
r	Top radius of the target cone
h	Height of the target cone
φ	Angle of the target cone
t	Plate thickness
R_r	Bottom radius of roll
d	Distance between outer rolls
P	Apex of outer profile of the target cone
S	Apex of inner profile of the target cone
α	Angle between the axis of outer roll and the axis of the target cone
α'	Angle between the axis of the inner roll and the axis of the target cone
β	Angle of outer conical roll
β'	Angle of inner conical roll
l_{ro}	Length of outer roll
l_{ri}	Length of inner roll
θ_{xy}	Angle between the roll's axis projected on XY plane and Y-axis
θ_{yz}	Angle between the roll's axis projected on YZ plane and Z-axis
θ_{xz}	Angle between the roll's axis projected on XZ plane and Z-axis

f_i	Distance between i^{th} point and the axis of the cone
g_i	Distance between i^{th} point and the bottom plane of the cone
P	Vector (p_x, p_y, p_z) ; a point on the axis of the cone (not the apex)
\vec{a}	Vector (a_x, a_y, a_z) ; the direction point from p to apex of the cone
φ	Apex semi-angle of the cone
s	Orthogonal distance from point p to the cone
σ_x	Stress in X direction
σ_y	Stress in Y direction
σ_z	Stress in Z direction
τ_{xy}	Shear stress on XY plane
τ_{yz}	Shear stress on YZ plane
τ_{xz}	Shear stress on XZ plane
σ_{eqv}	Equivalent stress
ε_{ex}	Elastic strain in X direction
ε_{ey}	Elastic strain in Y direction
ε_{ez}	Elastic strain in Z direction
ε_{exy}	Elastic strain on XY plane
ε_{eyz}	Elastic strain on YZ plane
ε_{exz}	Elastic strain on XZ plane
$\varepsilon_{\text{eeqv}}$	Equivalent elastic strain
ε_{px}	Plastic strain in X direction
ε_{py}	Plastic strain in Y direction
ε_{pz}	Plastic strain in Z direction
ε_{pxy}	Plastic strain on XY plane

ε_{pyz}	Plastic strain on YZ plane
ε_{pxz}	Plastic strain on XZ plane
ε_{peqv}	Equivalent plastic strain
f_x	Reaction force in X direction
f_y	Reaction force in Y direction
f_z	Reaction force in Z direction
d_R	Deviation of radius between fitted cone and target cone
d_h	Deviation of height between fitted cone and target cone
R_f	Radius of fitted cone
R_t	Radius of target cone
H_f	Height of fitted cone
H_t	Height of target cone
E_s	Sliding energy
E_t	Total energy
σ_Y	Yield stress
σ_r	Residual stress

INTRODUCTION

Background

The hydropower generation equipment market is growing rapidly. Much of the equipment that is already in service needs to be replaced, and many new hydropower projects require even more such equipment. The problem faced by all hydropower generation system providers is that current manufacturing methods take too long to satisfy customers' requirements.

The Francis Turbine shown in Figure 1 is a major piece of equipment in the hydro generation system. It has a diameter of up to 10 m (Three Gorges project in China), and a plate thickness of up to 10 cm. The Francis Turbine is comprised of three components: the Crown, Blades and the Band. The Crown has a conical hollow shape, as illustrated in Figure 2 [1]. This project is aimed at developing an efficient technique for producing the Francis Turbine Crown.

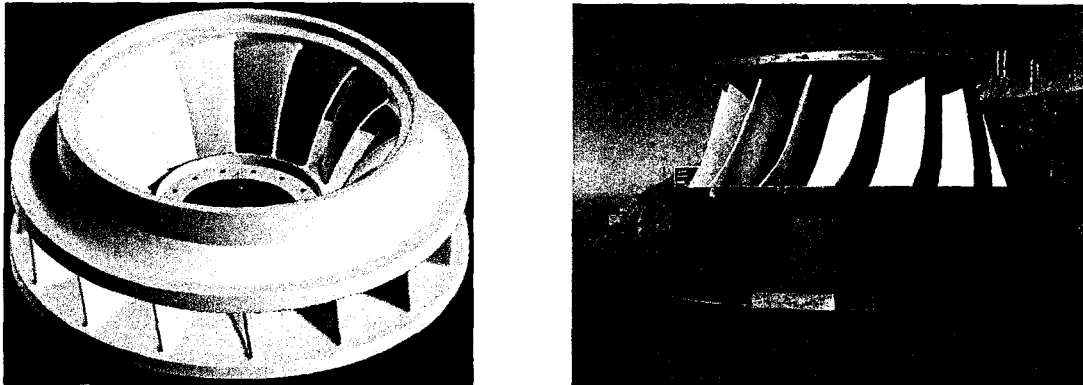


Figure 1 3-D illustration and image of the Francis Turbine [2, 3]

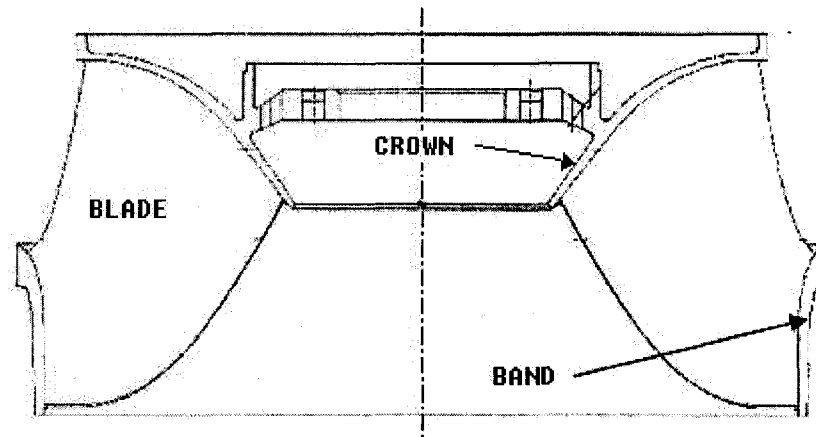


Figure 2 The three components of the Francis Turbine

The manufacturing technique currently used to form the Crown consists of the Foundry and Welding processes. First, a few pieces of the Crown are produced by Foundry, and are then joined together by Welding. The base material used for the Crown is stainless steel (ASTM A743 grade CA-6NM), which has a strong mechanical resistance against corrosion and cavitations. However, this property can be problematic in the Foundry process, particularly because the chrome presented in the material can oxidize, and cause internal faults. Moreover, to ensure that the grains of the steel used are pure, a very slow annealing process is necessary. During the Welding process, preheating is required to reduce residual stresses. This has a major impact on the manufacturing period and for a single crown can be 12-18 months, thus justifying the development of a new manufacturing process.

Several manufacturing methods can be applied in forming the Crown of the Francis Turbine. Generally, the manufacturing process involves a combination of certain metal forming techniques, such as Foundry and Welding (which is also current process [1]), or a combination of the Punching or Forging and Welding processes, or a combination of the Roll Bending and Welding processes.

The continuous roll bending process is an efficient metal forming technique commonly used to produce medium and large cylindrical tubular sections. Several bending machines capable of forming the conical tube are currently available in the market. However, no published studies have examined the roll bending process to produce thick conical tubular section of large diameter. This project use FEM, and implements a simulation to study the feasibility of the roll bending process to produce a conical hollow shape.

Introduction to the roll bending process

Bending is the plastic deformation of metals about a linear axis with little or no change in the surface area. Multiple bends can be conducted simultaneously, but to be classified as true bending, and calculated by simple bending theory, each axis must be linear and independent of all others. Roll bending is a continuous form of three-point bending, in which plates, sheets, beams, pipes, and even rolled shapes and extrusions are bent to a desired curvature using forming rolls [4]. In the metal bending industry, the large or medium size of tubular section is usually formed by first bending the metal sheet using stamp bending, and then welding it to form a larger seamed tube. Compared with these techniques, roll bending can be used to form the plate or sheet to a wide range of bend radii. The smallest radius in such cases is just larger than the top roll, while the largest may take up as much room as a workshop. Roll bending is an efficient technique which dramatically reduces the number of seams on the piece as a result of the continuity of the process involved. To obtain a different curvature, the only work required is to choose the right rolls and their right configurations.

A description of the basic principle and the operation of the roll bending process can be found in [4, 5]. C. Bouhelier [5] gives the formulas for calculating the spring-back, the reaction forces and the essential power required. Unfortunately, the author does not clearly discuss the process mechanism, and as a result, the final shape is difficult to

estimate using the formulas. Yang, Ming [6] constructed a simulation model for estimating the deformation seen at different periods of the roll bending process. M. Hua [7-12] conducted extensive work studying the four-roll bending process. From his experiments, he discussed the roll bending process mechanism. In 2001, Weilong Hu [13] applied the FEM to study the roll bending process mechanism and came up with a new model, which separated the top or bottom rolls into two parts. In 2004, Zafer Tekiner [14] studied the spring-back of metal sheets with different materials and different thickness in bending dies.

There are three major types of roll bending models available for use, depending on the position of the rolls and their respective functions in the process: the three-roll pyramidal model, the three-roll pinching model, and the four-roll symmetric model. The most common model is the three-roll pyramidal model, as shown in Figure 3, which consists of one top roll and two symmetric bottom rolls. Generally, the diameter of the outer roll is 60-90% that of the inner roll [5]. This model is applied in this project because it is usually employed to bend thick plates [7]. During the bending process, the inner roll presses down to a specified position to control the curvature, and the outer rolls rotate to drive the plate forward. Figure 3 illustrates the whole bending process. This model is easier to set up, but the straight edge part is always present. To resolve this problem, the four-roll model can be applied. Table I shows the whole process, using the four-roll model. By setting roll 1 and roll 3 in step 3 and step 5 respectively, the straight edge part can be decreased effectively. The disadvantage of this model is that it requires one more roll, which increases cost and leads to a more complex configuration. The other three-roll model, the pinching model, applies the same idea as in the four-roll model to resolve straight edge part problem. Table II presents the process using the three-roll pinching model. When this model is applied, the two outer rolls need to be pinched separately during the edge bending process, in order to eliminate the edge part.

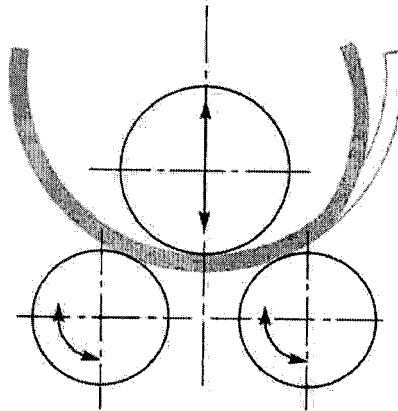


Figure 3 The three-roll continuous pyramidal bending model

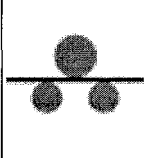
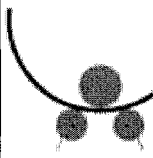
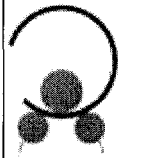
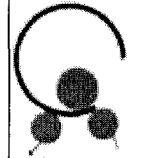
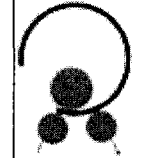
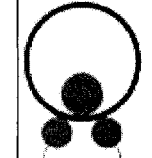
Table I

The four-roll continuous bending procedure

1	2	3	4	5	6	7
Feed the work to center	No. 2 roll move up	No. 1 roll move up	Rolls	No. 1 roll down, No. 3 roll up	Rolls	No. 2 and No. 3 rolls down Take out the work

Table II

The three-roll pinching-bending procedure

Feed the work	Rough forming 1	Rough forming 2	Edge bending 1	Edge bending 2	R forming
1	2	3	4	5	6
					

Depending on the number of the passes, the roll bending process can be arranged into single-pass and multi-pass categories. The single-pass is more efficient, but requires more bending forces. In some situations, such as with the thick plate, the plate usually needs to undergo pre-bending when applying the single-pass, resulting in increased cost. The multi-pass process for its part does not require pre-bending. As illustrated in Table II, the first pass involves rough bending, and the second pass, refined bending. The multi-pass process is therefore the method of choice in the bending of a thick plate or sheet.

In the current roll bending machine market, the three-roll model is the most common configuration encountered. However, the four-roll, and even the two-roll models are also employed in the industry. The roll may be manually-, hydraulically, or electrically-driven, or through a combination of all the preceding configurations. The thickness of the bend plate or of the bend sheet can go up to 25 cm [15]. The conical tubular section can be bent using conical rolls or cylindrical rolls with certain standard equipment.

Figure 4 illustrates a roll-bending machine with a three-roll configuration. Figure 5 illustrates the roll-bending machine used to form a conical tube.

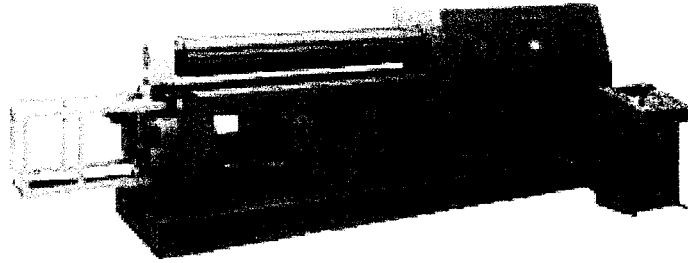
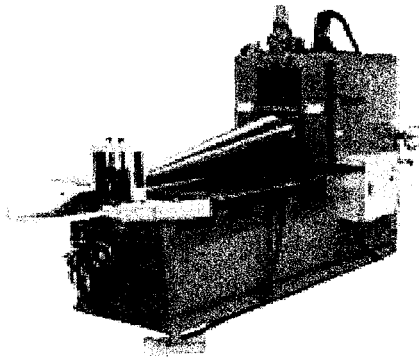
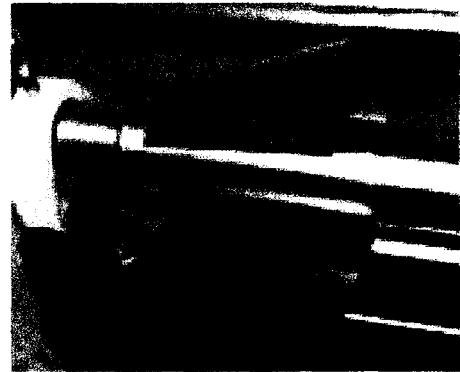


Figure 4 Illustration of three-roll continuous bending machine [16]



a: conical rolls configuration



b: cylindrical rolls configuration

Figure 5 Comparison of two configurations of the roll bending machine used to bend conical shapes [16]

Conical rolls are applied according to Figure 5-a, and their use presents the following advantages:

- Better bending quality
- Easy to configure

However, compared to cylindrical rolls, type *a* is more costly.

The roll bending process mechanism is a complex dynamic problem. The Finite Element Analysis (FEA) is the approach most commonly used to solve this type of problem. ANSYS is a commercially available software application used to solve the FE problem. With the integration of LS-DYNA, the complex dynamic problem can even be simulated in ANSYS.

The ANSYS program has many finite element analysis capabilities, and offers solutions ranging from a simple, linear, static analysis to a complex, nonlinear, transient dynamic analysis. The analysis guide manuals in the ANSYS documentation set describe specific procedures for performing analyses for different engineering disciplines. The next few sections of this chapter cover general steps that are common to most analyses.

A typical ANSYS analysis involves three distinct steps: [17]

1. Build the model.
2. Apply loads and obtain the solution.
3. Review the results.

Geometry can be transferred between ANSYS and ANSYS LS-DYNA in order to perform sequential implicit-explicit/explicit-implicit analyses, such as those required for drop test, spring-back, and other applications. [18]

The procedure for an explicit dynamic analysis is similar to that for any other analysis that is available in the ANSYS program, which is mentioned above.

Limited-duration events (such as severe collisions and blade containment) and large, permanent deformations (within the stamping and forming industries) present engineers with unique simulation challenges. ANSYS LS-DYNA meets these challenges by combining LSTC's LS-DYNA explicit dynamic solver technology with the pre-/post-processing power of the ANSYS software. [19]

ANSYS LS-DYNA supports both 2-D and 3-D explicit elements, and features an extensive set of single-surface, surface-to-surface, and node-to-surface contacts as well as a contact analysis option that automatically creates contact surfaces. ANSYS LS-DYNA also provides optional methods for fast solution processing. The symmetric multiprocessing (SMP) and massively parallel processing (MMP) methods optimize the power of multiple CPUs to deliver explicit simulation results in a fraction of the time. [19]

ANSYS and LS-DYNA support many kinds of materials (refer to [19]). The bilinear isotropic material is selected because the material used in the Francis Turbine manifests bilinear behavior, and bilinear isotropic materials support the parametric definition at different temperatures.

This project aims to setup a FEM model and to simulate the roll bending process using ANSYS with LS-DYNA for forming a thick plate to a conical hollow shape.

CHAPTER 1

GEOMETRIC SETUP OF THE CONICAL ROLL BENDING PROCESS

The geometric setup is the procedure used to determine the dimension and the position of all components involved in the roll bending process. For some components, the initial position and final position must be determined.

According to the introduction to the roll bending process presented in the last section, conical rolls or cylindrical rolls can be applied to form the conical hollow shape. Before the geometric setup procedure is defined, a decision must be made with respect the type of rolls to be selected. During the roll bending process, the inner roll is pressed down, and so both its initial and final positions must be determined.

The geometric setup is especially important for the simulations. The type of rolls, and the position and the dimension of all components greatly influence the final shape. Before the geometric setup is chosen, certain parameters must be determined: The dimensions of the desired cone, including the bottom radii, the top radii and the height, and the thickness of the plate must be determined by the client, while the bottom radius of the roll and the span of the outer rolls must be determined by the designer. The geometric setup must calculate all necessary geometric parameters according to these pre-determined parameters. Figure 6 illustrates the input and output parameters of the geometric setup. Section 1.2 in this chapter discusses the procedure for determining its value. The other parameter, the span of the outer rolls, as shown in Figure 11, directly influences the final shape. Different values can therefore be chosen for the simulation in order to observe its control to the final shape.

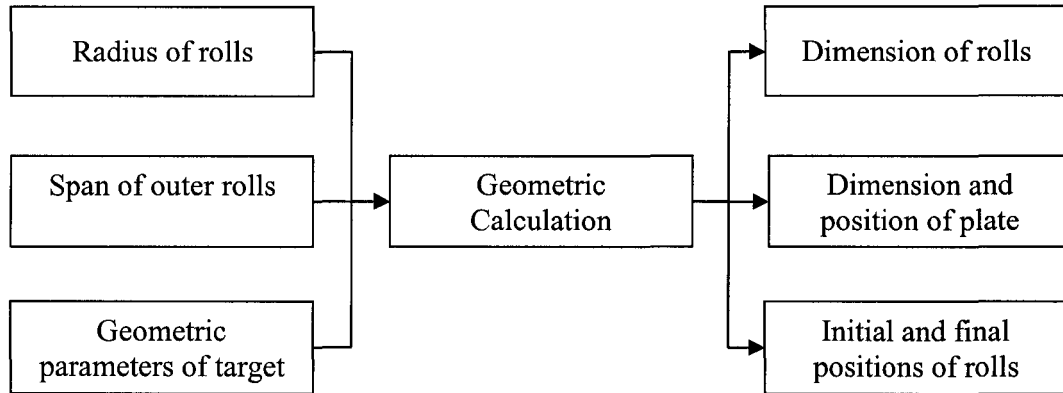


Figure 6 The input and output parameters for geometric setup procedure

1.1 Determination of roll the type

This first step is to determine the roll type. As discussed in the Introduction, two types of rolls - conical and cylindrical - are currently available in the market. However, applying a conical roll can be beneficial in term of:

- Ease of controlling curvature
- Satisfying the kinematic relationship

1.1.1 Curvature control

For any given cone, the intersection of any plane orthogonal to its axis is a circle. All circles, including those on the top and bottom planes, have the same circularity, but different diameters. When the roll bending process is applied, all circles cannot have the same circularity, unless the contact lines intersect at the apex of the cone. The relationship is shown in Figure 7. In this illustration, L_1 and L_2 are the lines representing the contact lines between the cone and the outer rolls, respectively. Only in the situation where L_1 and L_2 intersect at the apex of the cone can the circularity of the cone be satisfied (as shown in Figure 7 a). However, if L_1 and L_2 do not intersect at the apex of

the cone (as shown in Figure 7 b), the curvature does not satisfy the requirement, and the workpiece will be distorted. The discussion above is based on the ideal situation, where there is no sliding between the roll and the plate. Any sliding will distort the final workpiece.

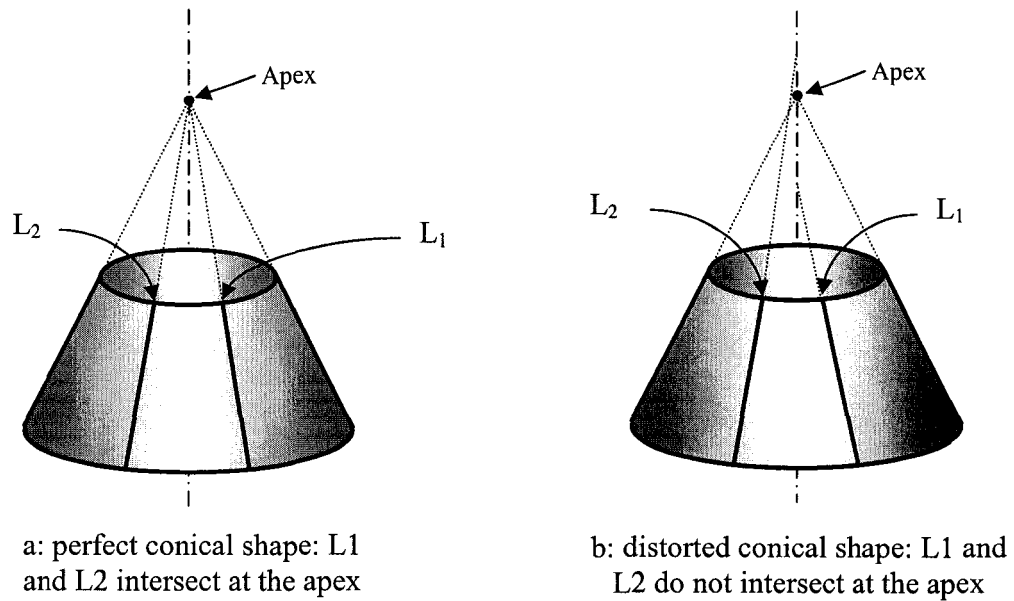


Figure 7 Illustration of perfect conical shape (a) and distorted conical shape (b)

1.1.2 Kinematic relationship

The plate that is pre-bent to form a cone is a sector, which is shown in Figure 8. Point O is the center of this sector plate; V_o and V_i are the outer tangent speed and inner tangent speed, respectively, and r_p and R_p represent the inner and outer radii of the sector plate, respectively. During the period of bending process, this sector plate must rotate around the center O. Therefore, V_o and V_i must satisfy the following relationship:

$$\frac{V_o}{V_i} = \frac{R_p}{r_p} \quad (1.1)$$

where:

R_p, r_p : Outer and inner radius of the sector plate
 V_o, V_i : Outer and inner tangent speed

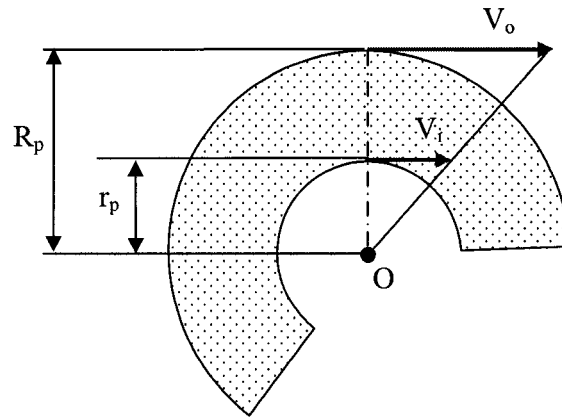


Figure 8 Kinematic relationship of tangent speed for driving a pre-bent sector plate in roll-bending process

1.1.3 Application of conical rolls

As discussed above, conical rolls can easily satisfy the two requirements for bending a conical hollow shape. As illustrated in Figure 9, this project employs conical rolls for the simulations. According to this figure, the axes of all rolls intersect at the apex of the desired cone. Point P is the outer apex of the cone and point S is the inner apex. Based on this relationship, the following equation is obtained.

$$\frac{R_o}{r_o} = \frac{V_o}{V_i} = \frac{R_p}{r_p} = \frac{R}{r} \quad (1.2)$$

where:

R_o, r_o : Bottom and top radius of outer roll
 R, r : Outer bottom and top radius of target cone

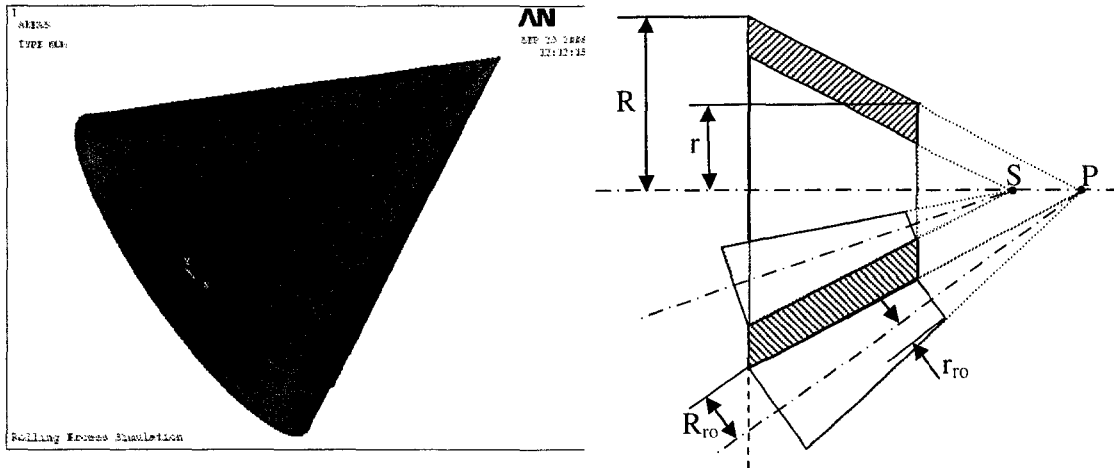


Figure 9 Illustration of application of conical rolls in roll bending process: 3D image and 2D section demonstration

For the same reason, the dimension of the inner roll is determined as follows:

$$\frac{R_i}{r_i} = \frac{R'}{r'} \quad (1.3)$$

where:

- R_i, r_i : Bottom and top radii of the inner roll
 R', r' : Inner bottom and top radii of the target cone

1.2 Determination of roll diameter

Before we can set up a geometric model, the dimension and the position of all rolls must be determined. As already pointed out, the proportion of the top-bottom radius of the roll must be the same as that of the target cone. If one roll radius is known, then the dimension of all the rolls can be determined.

In this simulation, all rolls are considered as rigid bodies. However, in real applications, the rolls exhibit deflections. Therefore the radius of the roll must be carefully determined to limit deflection to a reasonable range. The following section discusses the procedure for determining the radius of a roll.

Hypothesis:

To simplify the calculation, the conditions below are present:

- Cylindrical roll
- Material is steel with elastic modulus (E) of 200GPa
- Uniform pressure
- Simply supported ends

Therefore, the maximum deflection is calculated as follows: [20, 21]

$$v_{\max} = \frac{5wL^4}{384EI} = \frac{5wL^4}{12E\pi d^4} \quad (1.4)$$

where:

- w : Distributed load on the beam
 L : Length of the beam
 E : Elastic modulus
 I : Moment of inertia

From the result of section 2.5.1, the reaction force on the lower roll is almost 1978 kN. Suppose the roll is cylindrical and the load is distributed uniformly, and that the length and elastic modulus are known. The deflection of the roll is therefore a function of the radius of the roll. This relation is illustrated in Figure 10:



Figure 10 Deflection of roll when changing the roll diameter

As illustrated in Figure 10, the maximum deflection is 0.6 mm when diameter of the roll is 0.5 m. This value is nearly 0.1% of the radius of the target cone and therefore is acceptable. Actually, equation 1.4 is based on the hypothesis of cylindrical roll. In this simulation, 0.25 m is the radius of the smaller side. Therefore, the deflection must be less than 0.3 mm when applying conical rolls.

Note: The discussion above is based on the outer roll. For the pyramid model (refer to Figure 3), the radius of the inner roll is 1.2-1.5 times of the radius of the outer roll [5].

1.3 Determination of the geometric parameters

The determination of the geometric parameters involves those of the initial status and of the final status. *Initial status* denotes the status prior to bending while *final status* denotes the status when roll-bending process is completed. In fact, the set-up of rolls can be determined according to the dimensions of the plate, the dimensions of the target cone and the span of the outer rolls. All these pre-determined parameters are known, except for the span of the outer rolls which is varied and will be determined by the designer.

The following list presents the known parameters for determining the final geometric parameters (see Figure 11).

Parameters specified by client

- R: Bottom radius
- r: Top radius
- h: Height
- t: Plate thickness

Parameters determined by engineer

- R_r : Bottom radius of roll; determined by material strength
- d: Span of outer rolls; no equation to determine it: try many values; the optimal value is determined by the simulation

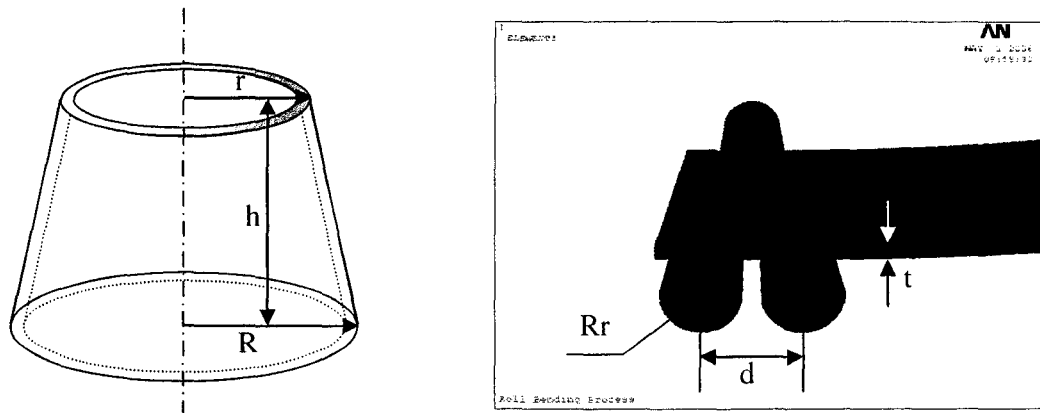


Figure 11 Parameters needed for determining the geometric parameters of the roll-bending process

Parameters to be determined (see Figure 12 and Figure 13):

- P: Apex of outer profile of the bended cone
- S: Apex of inner profile of the bended cone
- α : Angle between the axis of the outer roll and the axis of the desired cone
- α' : Angle between the axis of the inner roll and the axis of the desired cone
- β : Angle of outer conical rolls
- β' : Angle of inner conical roll
- L: Length of outer line of the target cone
- L': Length of inner line of the target cone
- L_{ro} : Distance from bottom to the apex
- l_{ro} : Length of outer rolls
- L_{ri} : Distance from bottom to the apex
- l_{ri} : Length of inner rolls
- φ : Angle of the desired cone
- θ_{xy} : Angle between roll axis projected on XY plane and Y-axis
- θ_{yz} : Angle between roll axis projected on YZ plane and Z-axis
- θ_{xz} : Angle between roll axis projected on XZ plane and Z-axis

1.3.1 Hypothesis and illustration of the final geometric parameters

Figure 12 illustrates the final position of the rolls and the target cone. The positions of the rolls are determined based on the following hypothesis:

- The length of the roll is equal to the width of the plate.
- All rolls have a conical shape the radius of which conforms to the relationships of equation 2.2 and equation 2.3.

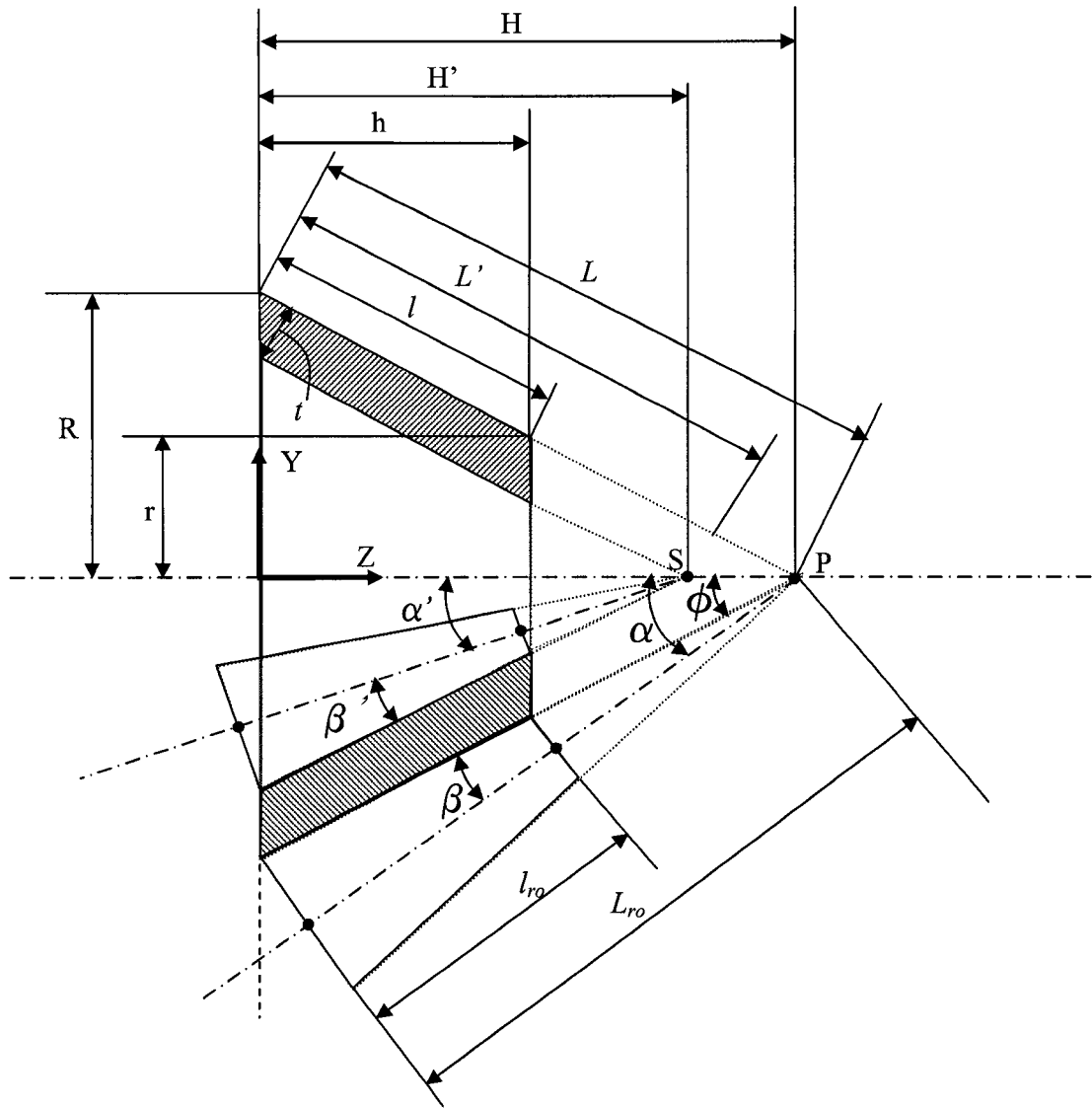


Figure 12 Illustration of geometric parameters of the target cone and rolls

The parameters illustrated in Figure 12 are determined in sections 1.3.2 to 1.3.5.

1.3.2 The dimension of the target cone

Table III lists the equations used to calculate the geometric parameters of the target cone. The given geometric parameters of the target cone are the bottom and top radii, the height of the target cone, and the plate thickness. With these parameters, the semi-angle of the target cone φ , the distance from inner apex S to bottom L' and distance from outer apex P to bottom L can be calculated (see Figure 12).

Table III

Equations for calculating the geometric parameters of the target cone

Angle of the target cone	$\varphi = \tan^{-1}\left(\frac{R-r}{h}\right)$
Distance from outer apex P to bottom	$L = \frac{R}{\sin(\varphi)}$
Distance from inner apex S to bottom	$L' = \frac{R - \frac{t}{\cos(\varphi)}}{\sin(\varphi)}$

1.3.3 The dimension of the rolls

As described above, the roll is assumed to be a rigid body with a conical shape. Therefore, the radius of all rolls is determined by the bottom radius of outer roll R_o . Section 1.2 discusses the method used to determine R_o . The radius of the inner roll is $(1.2-1.5)R_o$. The dimension of all rolls can be obtained based on R_o and the dimension of the target cone.

1.3.3.1 The dimension of the outer roll

Table IV lists the equations used to calculate the geometric parameters of the outer roll, including the bottom radius R_{ro} , the semi-angle of the roll β , the angle between the roll axis and the target cone axis α , and the length of the roll l_{ro} (see Figure 12). With these parameters, a roll can be created directly in ANSYS.

Table IV

Equations for calculating the geometric parameters of the outer roll

Bottom radius	$R_{ro} = R_r$
Angle of the roll	$\beta = \sin^{-1}\left(\frac{R_r}{L}\right)$
Angle between the axis of the cone and the axis of the roll	$\alpha = \varphi + \beta$
Full length of the roll	$L_{ro} = L \cdot \cos(\beta)$
Length of the roll	$l_{ro} = l \cdot \cos(\beta)$

1.3.3.2 The dimension of the inner roll

Table V lists the equations used to calculate the geometric parameters of the inner roll, including the bottom radius R_{ri} , the semi-angle of the roll β' , the angle between the axis of the roll and the axis of the target cone α' , the full length of the roll L_{ri} and the length of the roll l_{ri} .

Table V

Equations for calculating the geometric parameters of the inner roll

Bottom radius	$R_{ri} = (1.2 \square 1.5)R_r$
Angle of the roll	$\beta' = \sin^{-1}\left(\frac{R_{ri}}{L'}\right)$
Angle between the axis of cone and the axis of the roll	$\alpha' = \varphi - \beta'$
Full length of the roll	$L_{ri} = L' \cos(\beta')$
Length of the roll	$l_{ri} = l' \cdot \cos(\beta')$

1.3.4 The outer and inner apex of the target cone

The equations below present the method for calculating the apex of the target cone. P is the outer apex and S is the inner apex (see Figure 12). H is the height from the bottom of the target cone to its apex.

$$P = \left[0, 0, \frac{R}{\tan(\varphi)}\right] \quad (1.5)$$

$$S = \left[0, 0, Z_p - \frac{e}{\sin(\varphi)}\right] \quad (1.6)$$

where:

R : Bottom radius of the target cone

φ : Semi-angle of the target cone

Z_p : Z-coordinate of point P

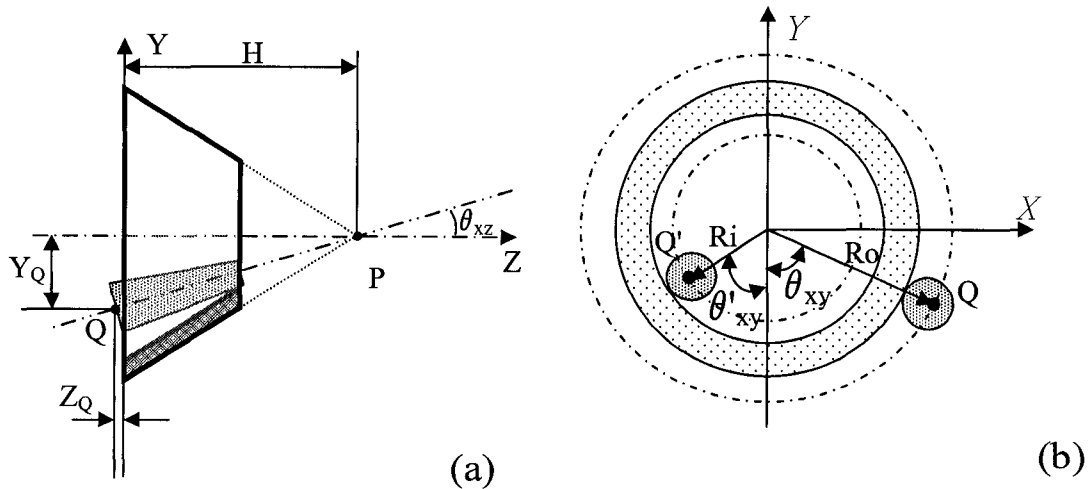
e : Thickness of the plate

φ : Semi angle of the target cone

1.3.5 The roll position

The last sections have provided the equations for calculating the dimensions of the rolls. This section for its part discusses the method for obtaining the positions of all rolls. Because the axes of the two outer rolls intersect at the apex of the target cone, the factors used to determine their positions are the angle between the axis and the XY, XZ and YZ planes, as shown in Figure 13. Likewise, the position of the inner roll is determined by the angle between its axis and the three planes. Figure 13 (a), (b) and (c) represent the front view, the left view and the top view, respectively. In Figure 13, point Q is the bottom center of the outer roll, and Q' is the bottom center of the inner roll.

The outer broken-line circle is the enveloped circle of the bottom center of the outer roll, and the inner broken-line circle is the enveloped circle of the bottom center of the inner roll. R_o is the radius of the outer enveloped circle and R_i is the radius of the inner enveloped circle.



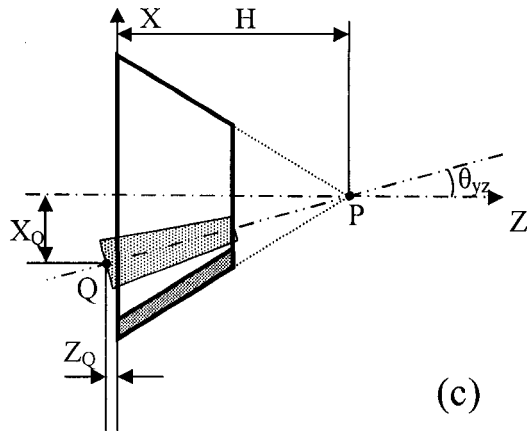


Figure 13 Illustration of angle between axes of rolls and the XY, YZ, XZ planes
 (a) View of YZ plane; (b) View of XY plane; (c) View of XZ plane

1.3.5.1 The outer roll position

Table VI lists the equations used to calculate the coordinates of the bottom center of the outer roll. Table VII lists the equations used to calculate the angles between the axis of the outer roll and the XY, YZ, XZ planes.

Table VI

Equations for calculating the coordinate of the bottom center of the outer roll

R_Q	$R_Q = L_{ro} \sin(\alpha)$
X_Q	$X_Q = \frac{d}{2}$
Y_Q	$Y_Q = \sqrt{R_Q^2 - X_Q^2}$
Z_Q	$Z_Q = R_{ro} \sin(\alpha)$

Table VII

Equations for calculating the angles between the axis of the outer roll and the planes XY, YZ and XZ

Angle between the axis and the XY plane	$\theta_{xy} = \sin^{-1}\left(\frac{X_Q}{R_o}\right)$
Angle between the axis and the YZ plane	$\theta_{yz} = \tan^{-1}\left(\frac{X_Q}{H - Z_Q}\right)$
Angle between the axis and the XZ plane	$\theta_{xz} = \sin^{-1}\left(\frac{Y_Q}{H - Z_Q}\right)$

1.3.5.2 The inner roll position

Table VIII lists the equations for calculating the coordinates of the bottom center of the inner roll. Table IX lists the equations for calculating the angle between the axis of the inner roll and the XY, YZ, XZ planes.

Note: The position of the inner roll determined in this section is the final position of the inner roll. Furthermore, the initial position of the inner roll must be determined as well. This will be discussed in 1.3.7.

Table VIII

Equations for calculating the coordinates of the bottom center of the inner roll

R_i	$R_i = L_{ri} \sin(\alpha')$
$X_{Q'}$	$X_{Q'} = 0$
$Y_{Q'}$	$Y_{Q'} = R_i$
$Z_{Q'}$	$Z_{Q'} = R_{ri} \sin(\alpha')$

Table IX

Equations for calculating the angles between the axis of the inner roll and the XY, YZ and XZ planes

Angle between the axis and the XY plane	$\theta_{xy} = \sin^{-1}\left(\frac{X_{Q'}}{R_i}\right)$
Angle between the axis and the YZ plane	$\theta_{yz} = \tan^{-1}\left(\frac{X_{Q'}}{H' - Z_{Q'}}\right)$
Angle between the axis and the XZ plane	$\theta_{xz} = \sin^{-1}\left(\frac{Y_{Q'}}{H' - Z_{Q'}}\right)$

1.3.6 The dimension and position of the plate

The pre-bended plate has a sector shape (see Figure 8). Its dimension, including its outer radius R_p , its inner radius r_p and its length, can be determined from the geometry of the target cone. The position of pre-bended plate depends on the angle between the plate and plane XZ θ'_p . Figure 14 illustrates the geometric parameters in question.

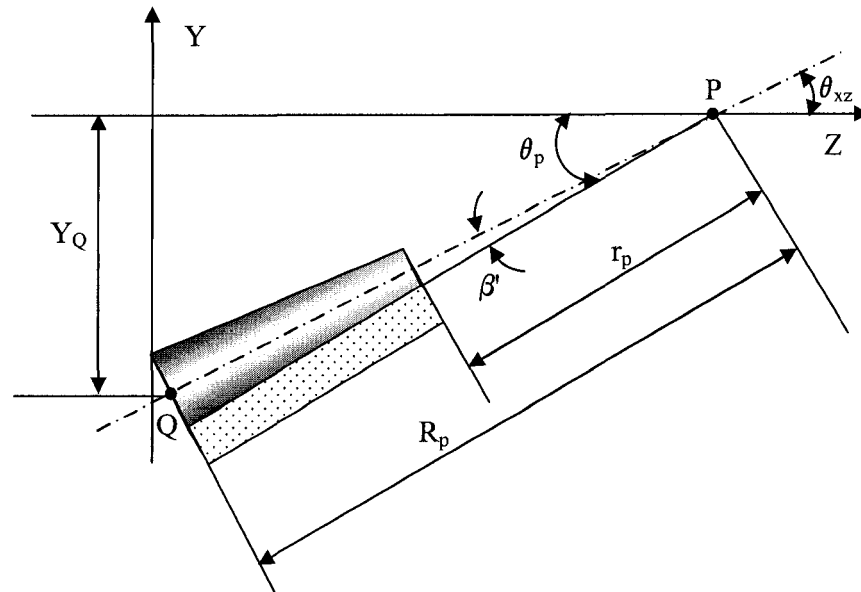


Figure 14 Illustration for calculating the dimension and position of the sector plate and the position of the inner roll

Table X lists the equations for calculating the geometric parameters of the plate.

Table X

Equations for calculating the dimension and position of the plate

Outer radius	$R_p = L$
Inner radius	$r_p = \frac{r}{R} \cdot L$
Angle to XZ plane	$\theta_p = \theta_{xzo} - \beta$
Start angle	$\phi_s = \sin^{-1} \left(\frac{d}{2 \cdot L_{ro}} \right)$
Length	$\phi_l = \frac{R_{ro}}{R_p} \cdot 360^\circ$

1.3.7 The initial position of the inner roll

Section 1.3.5.2 discussed the final position of the inner roll. To ensure bending quality, the inner roll must be guaranteed to contact the plate completely during the process, in which case the pressure on the plate will be uniform. The initial position of the inner roll must therefore be determined carefully in order to ensure proper contact, as illustrated in Figure 14.

Table XI and Table XII list the equations used to calculate the initial position of the inner roll, including the coordinates of the bottom of roll ($X_{Q'i}$, $Y_{Q'i}$, $Z_{Q'i}$) and the angle between the axis of the roll and the XY, YZ, XZ planes.

Table XI

Equations for calculating the initial position of the bottom center of the inner roll

X-coordinate of the bottom center of the inner roll	$X_{Q'i} = 0$
Y-coordinate of the bottom center of the inner roll	$Y_{Q'i} = R_{ii}$
Z-coordinate of the bottom center of the inner roll	$Z_{Q'i} = R_{ri} \sin(\theta_{xzi})$

Table XII

Equations for calculating the initial angles between the axis of the inner roll and the XY, YZ and XZ planes

Angle between the axis and XY plane	$\theta_{xyi} = \sin^{-1}\left(\frac{X_{Q'i}}{R_i}\right)$
Angle between the axis and YZ plane	$\theta_{yzi} = \tan^{-1}\left(\frac{X_{Q'i}}{H' - Z_{Q'i}}\right)$
Angle between the axis and XZ plane	$\theta_{xzi} = \theta_{xzi}$

The outer roll has no initial position because it does not move during entire roll bending process. The displacement of the inner roll is the difference between the initial position and the final position.

1.4 Significance of the geometric setup

The geometric setup is a necessary step prior to the simulation in ANSYS. The calculation procedure discussed in this chapter is implemented in ANSYS using ANSYS Parametric Design Language (APDL) programming.

The geometric setup is especially important for obtaining a correct final shape. During the development of this project, a very small error in the calculation of the geometric parameters will cause the distortion or inaccurate curvature to the final shape. To avoid calculation complications, conical rolls are employed. In addition, some hypotheses are given for simplifying the calculation.

In the next chapter, a procedure for establishing the simulation in ANSYS will be described. It involves the finite element type, the contact surface and friction model, the constraint and boundary conditions, the material specification, the solid model, etc. A

typical simulation will then be given to illustrate the process. Moreover, the convergence and the number of passes (single pass or 3-pass bending) will also be discussed based on certain simulation results.

CHAPTER 2

FINITE ELEMENT MODELING AND SIMULATION IN ANSYS AND LS-DYNA

This chapter discusses the simulation of the roll bending process in ANSYS with LS-DYNA. Firstly, a brief introduction of ANSYS will be given in order to describe the basic analysis procedure using ANSYS with LS-DYNA to resolve a dynamic problem. Then, a design process chart will be presented to demonstrate the modular design for this project. Next, the finite element modeling will be described comprehensively, and will cover among other things, *the finite element model, the element type, solid modeling, the mesh strategy, the contact surface, friction specification and load application* etc. Finally, the result of a simulation will be presented as an example. Moreover, the FEA convergence will be discussed, and the model will be validated by comparing the reaction forces obtained by FEA with the theoretical ones.

2.1 Introduction to ANSYS and LS-DYNA simulation program structure

The ANSYS computer application is a large-scale multipurpose finite element program which may be used for solving several classes of engineering analysis. The analysis capabilities of ANSYS include the ability to solve static and dynamic structural analyses, steady-state and transient heat transfer problems, mode-frequency and buckling eigenvalue problems, static or time-varying magnetic analyses, and various types of field and coupled-field applications.

2.1.1 Analysis procedure using ANSYS

A typical ANSYS analysis involves three distinct steps:

1. Build the model. (PREP7)
2. Apply loads and obtain the solution. (SOLU)
3. Review the results. (POST1 and POST26)

The finite element model is established in step 1 (PREP7). In this step, the element type, the material properties and the real constants are specified; as well, the solid model is constructed and the meshing finished. In step 2 (SOLU), the contact surfaces and friction, the load, the constraints, and boundary conditions are specified. We can then start solving the process using the SOLVE command. In step 3, postprocessor (POST1 and POST26), the result is reviewed. Two kinds of postprocessors are provided in ANSYS. POST1 is a general result reviewer with which the results of all models are reviewed at specified time intervals. The results, including stress, pressure and deformation, etc., can be presented by animation, by contour display, through a data list, etc. Another postprocessor is POST26, which is a time-history postprocessor. POST26 is used to review Time-History results, such as reaction forces on the contact surfaces, stress and energy, etc., which occurred on specific elements during the entire process.

2.1.2 Structure of the simulation program

Figure 15 illustrates the procedure and structure of the simulation program.

In addition to the description in the last section, Figure 15 presents one more step - Geometric calculation, which is used to calculate the geometric parameters of all components, as discussed in the last chapter. Certain modules are created in the program in order to increase maintainability and extendibility. These modules are represented by the small rectangles in Figure 15. Applying modules to the program brings the following advantages:

- Reusability

Reusability improves design efficiency. Certain components with similar characteristics can be designed with a simple interface, after which such a component is created just by calling the module, rather than creating them one-by-one. For example, this simulation involves three rolls with different

dimensions and positions. A roll component is produced just by calling the created roll module with certain parameters such as the position, the dimension, the material and the meshing information. A well meshed roll is then placed at right place.

- Reliability

By applying many modules in the program, a complex problem can be broken down into many small and simple modules. Small modules are easier to debug and maintain, making them more reliable than a big complex system. Secondly, the modules isolate the problem, making it easier to locate any problem, which in turn makes it carry out any necessary debugging. Thirdly, adding new functions does not significantly interfere with the operation of the original program.

- Extensibility

Applying modules to the program makes it more extendable. If a function needs to be added or removed, all that will be needed is simply to add or remove a single module. For example, say we have two modules in this simulation: p1 to run postprocessor POST1 and p26 to run postprocessor POST26. If the simulation does not need the POST26 result review, then we can simply remove the p26 module from the program. A modular design program should be open and extendable. For instance, while the current roll is conical in shape, a cylindrical roll might be applied in a future work. This extensibility is provided by the modular design.

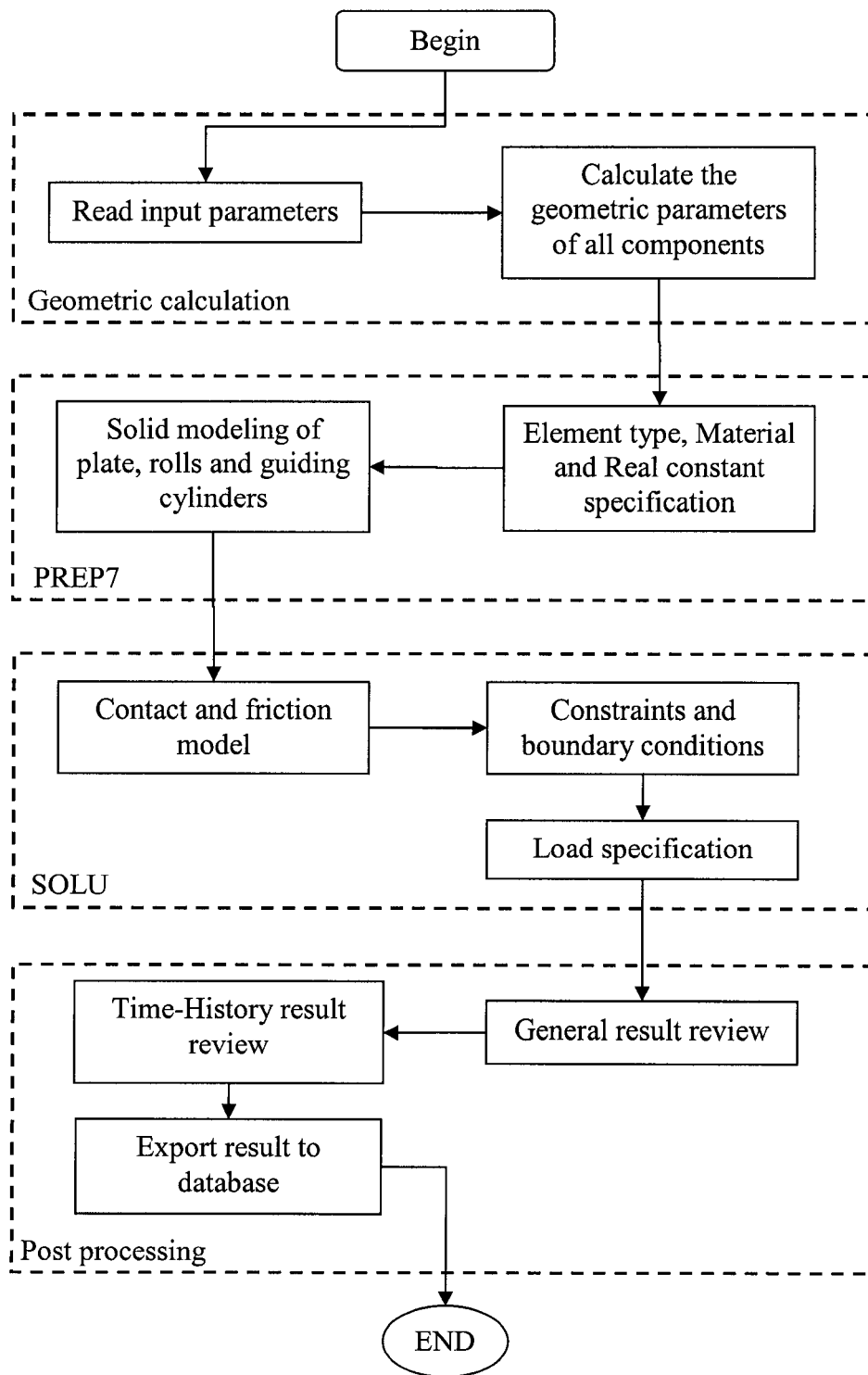


Figure 15 Structure of simulation program

2.2 Finite Element Model

The finite element model comprises three types of components: the sector plate, the rolls and the guiding cylinders, which are illustrated in Figure 16. The role of the plate and the rolls is discussed in section 1. The four cylinders are used to restrict the movement of the plate and avoid sliding between the rolls and the plate, as sliding will cause a distortion in the final shape.

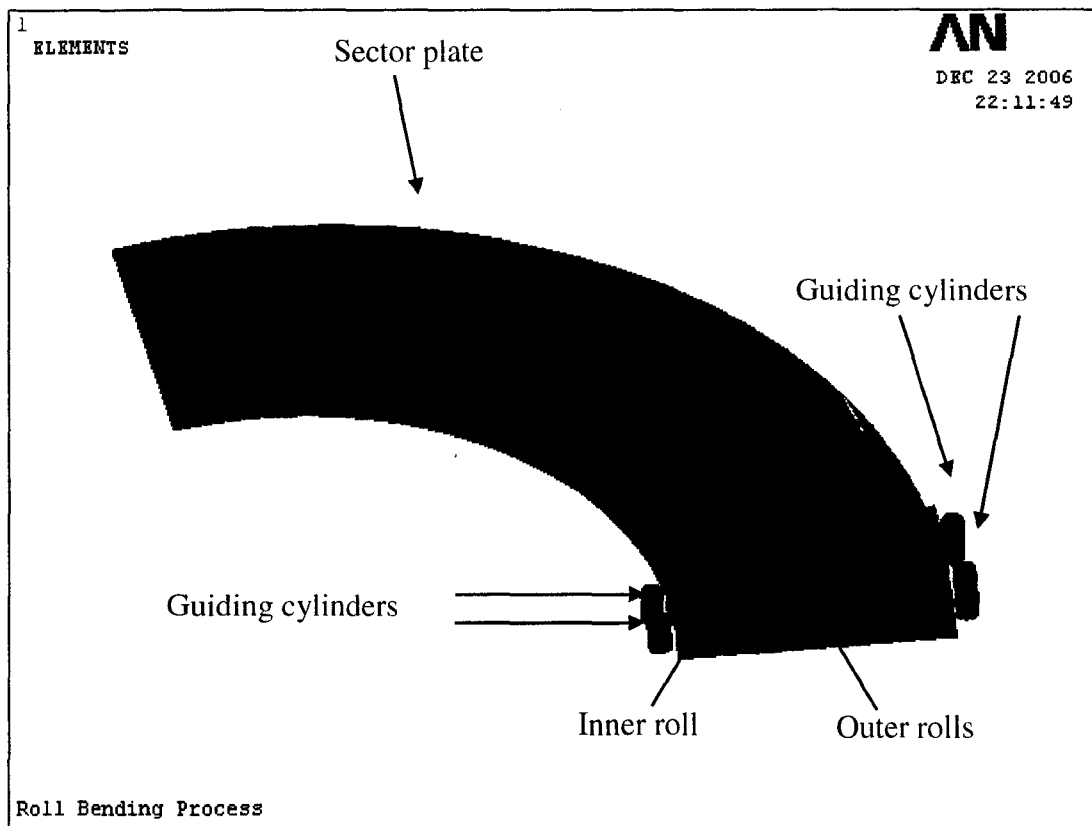


Figure 16

Illustration of the Finite Element Model

2.2.1 Element type

Considering the fact that the sector plate is very thin with a very small thickness-width ratio, this type of structure is generally modeled with SHELL elements. Since the problem would become more difficult to solve if mixed SHELL and SOLID elements

were used, all rolls are then meshed with rigid SHELL163 elements as well to facilitate the modeling and simulation in this work.

SHELL163 is a 4-node element (Figure 17-a) with both bending and membrane capabilities. Both in-plane and normal loads are permitted. The element has 12 degrees of freedom at each node: translations, accelerations, and velocities in the nodal x, y, and z directions and rotations about the nodal x-, y-, and z-axes. Another option for SHELL163 is 3-node triangular element shown in Figure 17-b, but this is not recommended. SHELL163 is used only in explicit dynamic analysis. For additional details on SHELL163, refer to lecture [18].

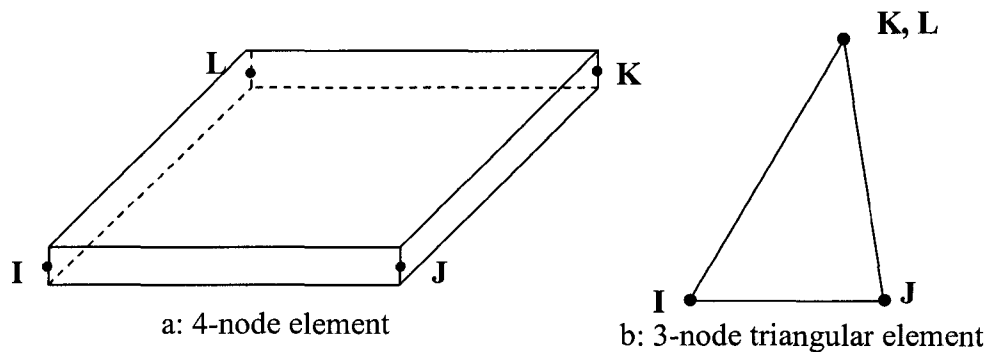


Figure 17 Illustration of SHELL163

All shell element formulations can have an arbitrary number of integration points through the thickness. Typically, 2 integration points (default) are required through the thickness for an elastic behaviour to be present, while 3 or more integration points are required for a plastic behaviour. The number of integration points through the thickness is controlled using the second real constant:

$R, NSET, R2$, where $R2$ = number of integration points (NIP).

The integration points are stacked vertically at the centroid of the element, as shown in Figure 18.

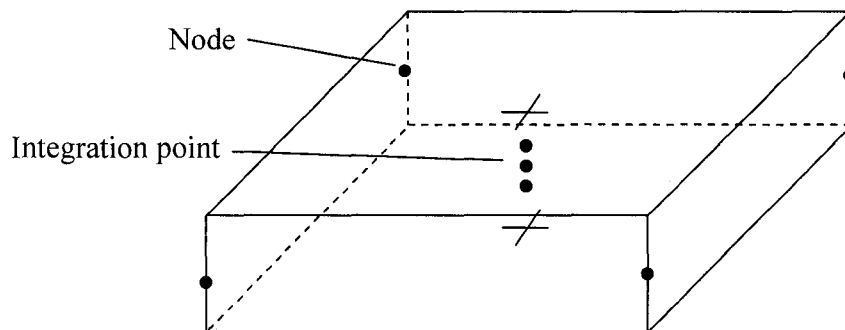


Figure 18 Integration points of SHELL163 element

Two integration points are sufficient for linear elastic materials, while more points are required for nonlinear ones. Stress output is given at the outermost integration points, not at the surfaces. For elastic materials, stresses can be extrapolated to the surfaces. For nonlinear materials, the usual procedure is to choose four or five integration points through the thickness and to ignore any inaccuracy. Five integration points are chosen in this simulation. Suppose the mid plane is 0 and the outer surface is 1, the outermost integration point will be 0.9062 when five integration points are chosen.

2.2.2 Solid modeling

Any solid model, irrespective of whether it is assembled from the bottom-up or from the top-down, is defined in terms of keypoints, lines, areas, and volumes. Figure 19 illustrates the entities of a solid model.

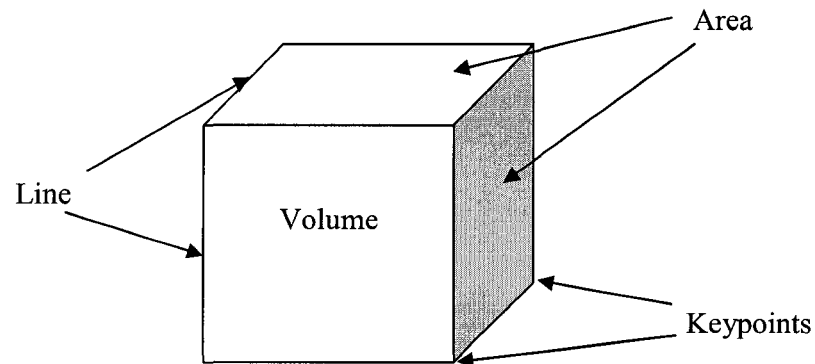


Figure 19 Entities of solid model in ANSYS

ANSYS provides two methods for constructing the solid model: from bottom-up and from the top-down. Modeling from the bottom-up implies creating a solid model through the following steps: Keypoint→ Line→ Area→ Volume. However, modeling from the top-down implies creating a volume, and then automatically producing all areas, lines and keypoints. Bottom-up modeling is generally used to create an irregular shape. In this simulation, all volumes are regular bodies, which means modeling from the top-down is easier for constructing a volume.

The following commands are used in solid modeling:

PCIRC: To create the sector plate

CONE: To create the conical rolls

CYLINDER: To create the guiding cylinders

However, there should be no volume because only the SHELL element is applied in this simulation. The commands above create the volumes. Therefore, the following commands are used to remove all volumes:

VSEL,ALL

VDEL,ALL

2.2.3 Meshing strategy

To simplify the analysis, all rolls are assumed to be rigid bodies. The unique deformable body is the plate. In accordance with the description of SHELL163, the triangular-shaped element is not recommended. Therefore, a mapped mesh is used for the plate and the quadrilateral-shaped element is specified in order to avoid the production of some triangular elements. In ANSYS, the operation is implemented using the following two commands:

```
MSHKEY, 1          ! Mapped Mesh  
MSHAPE, 0, 2D     ! Specify quadrilateral-shaped element
```

The geometric shape of the plate is very simple, and the load on it is distributed uniformly. Consequently, the size of all the elements on the plate is identical. The element size is defined by the length division and the arc division of the plate respectively, as shown in Figure 20.

For the rolls, it is difficult to avoid the triangular element because the two sides are circular in shape. However, the triangular element has no bearing on the analysis result because the rolls are rigid bodies, and their deformation is not considered in the current simulation.

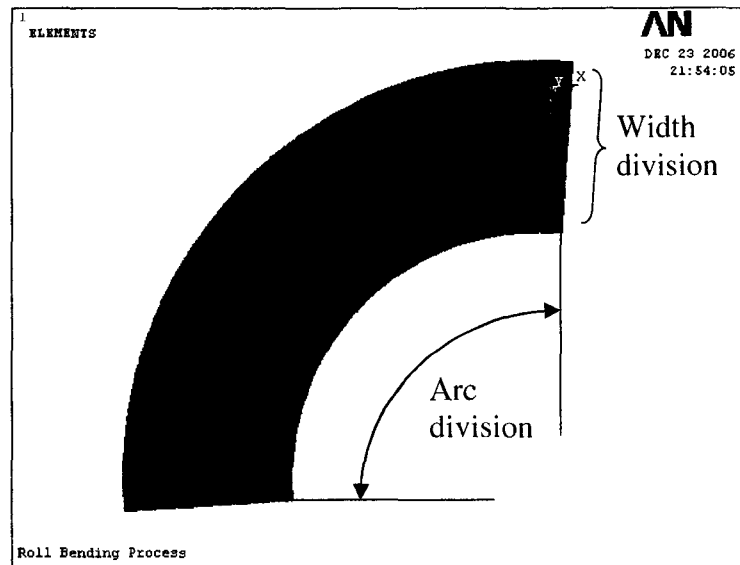


Figure 20 Illustration of meshing plate by specifying width division and arc division

2.2.4 Contact surfaces and friction model

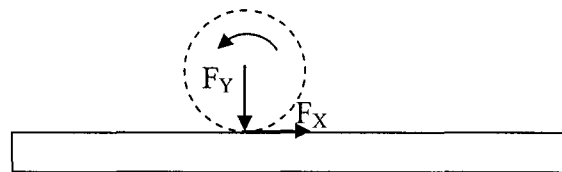
As can be seen in Figure 16, there are three main contact surfaces between the rolls and the workpiece for the pyramidal roll-bending configuration. In the simulation presented here, since we propose the installation of four guiding cylinders in order to restrict the longitudinal motion of the workpiece, there are four additional contact surfaces between the plate and the guiding cylinders. Contact surfaces play an important role in the modeling of the roll-bending process. In fact, it is through these contact surfaces that the workpiece is driven and deformed to its final shape.

Contact surfaces define the type of interaction between components in a model. It should be noted that contact is represented differently in an explicit dynamic analysis (LS-DYNA) from that in other types of ANSYS analyses (for example, static analysis). In a typical static analysis, the contact is represented by a “contact element”. However, for an explicit dynamic analysis, there are no contact elements to be defined. Instead, the contact surfaces, the type of contact, and other parameters related to the contact, need to be indicated through a command.

There are different contact types available in the software as options. For most typical analyses, three options are recommended: Single Surface, Node-to-Surface, and Surface-to-Surface. As the contact is located between a cylindrical part and a plane for a roll-bending process, the Automatic Node-to-Surface (ANTS) is therefore the most appropriate contact type for this project. This contact type is most efficient when a smaller surface comes into contact with a larger surface. For all contact surfaces in this simulation, the plate is always defined as the target component since the cylinder's nodes can penetrate into the plate during the process. The command used to define the contact surfaces is given by:

EDCGEN, Option, Cont, Targ, FS, FD, DC, VC, VDC, V1, V2, V3, V4, BTIME, DTIME, BOXID1, BOXID2

The friction coefficient is also specified when defining the contact surface. The friction model on the contact surfaces is illustrated in Figure 21.



$$F_x = \mu_c \cdot F_y$$

F_x and F_y are the friction and the normal force executed by the cylinder to the plate, respectively

Figure 21 Friction model of rolls and plates in the roll-bending process

In Figure 21, the tangent force F_x is determined by the applied force F_y and the friction coefficient μ_c . In this equation, the friction coefficient is calculated from the parameters

specified in command EDCGEN and the relative velocities of the two contacting parts as follows:

$$\mu_c = FD + (FS - FD)e^{-DC(v_{rel})} \quad (2.1)$$

where FD is the dynamic friction coefficient, FS is the static friction coefficient, DC is the exponential decay coefficient, and v_{rel} is the relative velocity between the two contacting parts at the contact point.

The FD , FS and DC in Equation (2.1) must also be specified in the command EDCGEN. In this work, the outer rolls are used for the motorization of the process. Therefore, the friction between the outer rolls and the plate should be high enough to cause motion without excessive sliding. On the other hand, there should be as little friction as possible between the other elements and the plate. Table XIII lists the typical friction levels of some of the components in this simulation. The value 0.3 is the friction coefficient between steel and steel without a lubricant present. The friction coefficient between the plate and the inner roll and the guiding cylinders is set to zero since they are passive contacts, and no driving forces are transmitted in these pairs.

Table XIII

Friction between certain components and the plate

	Static Friction	Dynamic Friction
Outer rolls	0.3	0.3
Inner roll	0	0
Guiding cylinders	0	0

2.2.5 Constraints and boundary conditions of guiding cylinders and rolls

In this simulation, the two outer rolls have only a rotation but no translation. Therefore, the top and bottom central nodes of these two rolls are constrained as shown in Figure 22. The inner roll has no self-rotation but is tilted to press the deformed plate. As a

result, the inner roll is constrained in rotation. The four guiding cylinders have both constraints in translation and rotation. The plate is not constrained by the program, but by all rolls and the four guiding cylinders in the simulation.

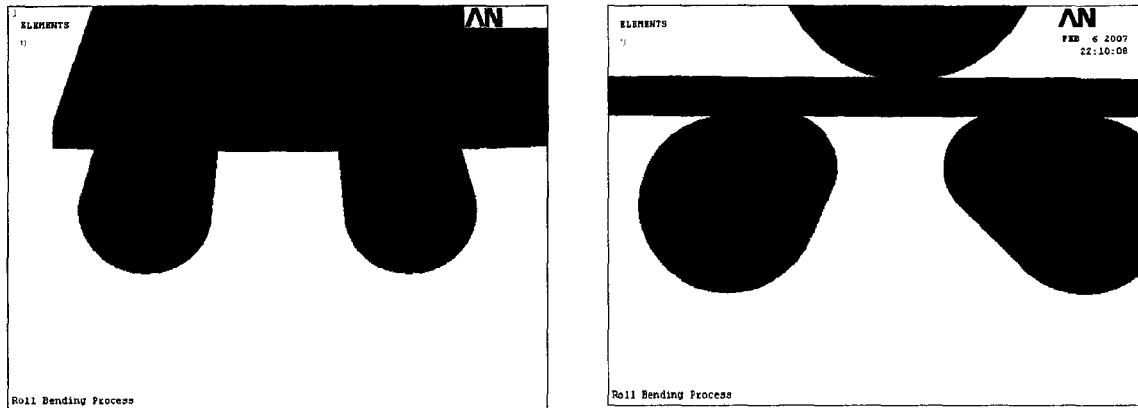


Figure 22 Constraints of the bottom and top central node of the outer rolls

The constraint of the explicit dynamic analysis is defined differently from that of the implicit analysis. Instead of using the *D* command, the command *EDMP* is used to define a material and its attribution. The following command defines a rigid body whose material number is 2, and which has neither translation nor rotation:

EDMP, rigid, 2, 7, 7

All rolls and all cylinders are defined as having neither translation nor rotation. However, applying some loads on this body will produce a response. For example, the two outer rolls only have a rotation, and only a rotation load is applied on the two rolls during the process to cause them to rotate. After the load is discharged, the action is stopped. This method facilitates the control of the load on the rolls.

2.2.6 Material specification

ANSYS LS-DYNA includes over 40 material models that can be used to represent a wide range of material behaviours.

An irreversible plastic deformation is produced during the roll bending process. Therefore, the bilinear material is specified in the simulation to represent the behaviour of this material. The material (ASTM A743 grade CA-6NM) used for the Francis Turbine can be simplified by a bilinear material with two slopes for elastic deformation and plastic deformation. ANSYS with LS-DYNA supports two kinds of bilinear materials: Bilinear Isotropic Model or Bilinear Kinematics Model. [1]

The classical bilinear isotropic hardening model (strain rate-independent) uses two slopes (elastic and plastic; shown in Figure 23) to represent the stress-strain behaviour of a material. The stress-strain behaviour is only specified at one temperature. If we enter the elastic modulus (EX), the Poisson's ratio (NUXY), and the density (DENS) with the *MP* command, the program calculates the bulk modulus (K) using the EX and NUXY values entered. We then input the yield strength and tangent slope with *TB,BISO* and locations 1 and 2 of the *TBDATA* command: [22]

TB,BISO

TBDATA,1, σ_y (yield stress)

TBDATA,2, E_{tan} (tangent modulus)

Yield stress: The applied stress at which irreversible plastic deformation is first observed across the sample is called the yield stress. It is usually denoted by σ_y .

Tangent Modulus: The Tangent modulus is defined as the slope of a line tangent to the stress-strain curve at a point of interest. The tangent modulus can have different values,

depending on the point at which it is determined. For example, the tangent modulus is equal to the Young's Modulus when the point of tangency falls within the linear range of the stress-strain curve. Outside the linear elastic region, at point A shown for example, the tangent modulus is always less than the Young's modulus. The tangent modulus is mostly used to describe the stiffness of a material in the plastic range, and it is denoted by E_{tan} . The yield stress σ_Y and the tangent modulus E_{tan} are illustrated in Figure 23.

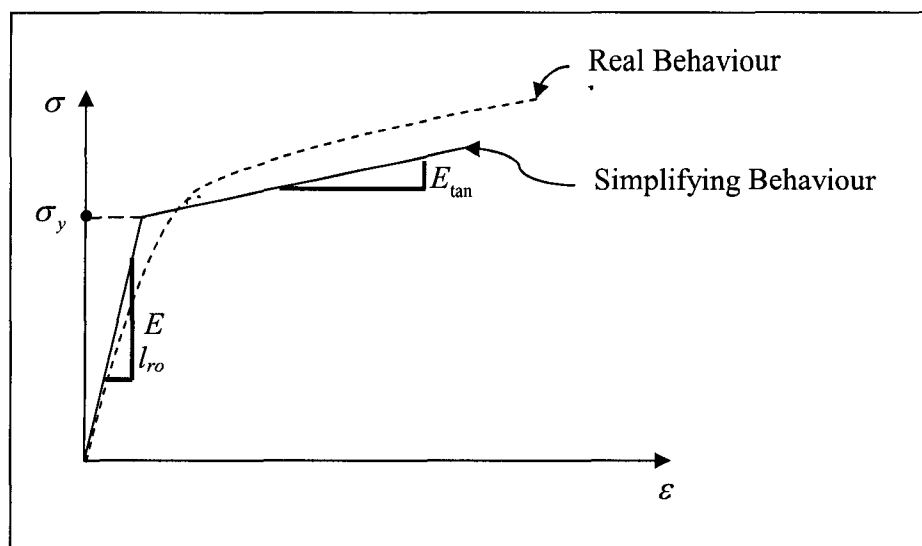


Figure 23 Real behaviour and simplifying behaviour of bilinear material

2.2.7 Loads specification

The problem of the roll bending process is actually an 'inverse dynamic problem'. That means the deformation is known, while the reaction force needs to be determined. The loads in this system are therefore the load causing the deformation and the load driving the plate. There are basically two loads in the roll-bending process. The first load is used to control the curvature of deformation through the inner roll, and the second is used to drive the plate forward or backward by the outer rolls. This section gives an example of the loads used in the three-pass roll bending process.

2.2.7.1 Tilt angle of the inner roll

The deformation of the plate is produced by pressing the inner roll. To press the plate uniformly, the upper roll must be tilted down to press on the plate as illustrated in Figure 24, rather than translated upward or downward. The angle θ_1 , θ_2 , θ_3 represents the tilt angle of each pass in the 3-pass process. Figure 25 illustrates the tilt angle of the inner roll at a given time.

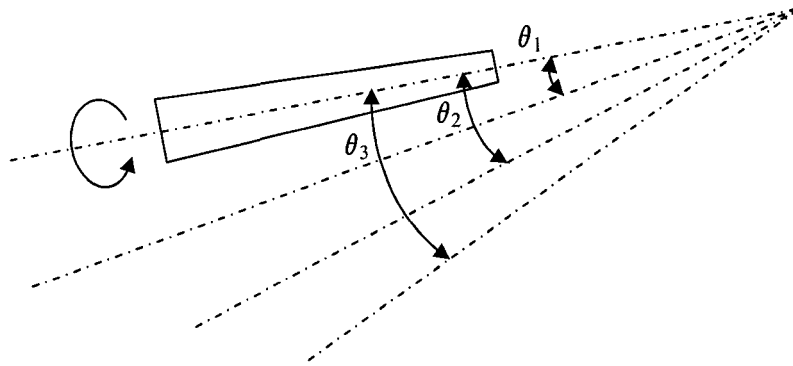


Figure 24 Illustration of the tilt angle for pressing down the upper roll in the three-pass process

ANSYS defines the load by a time array and a load array. Each element in the load array corresponds to an element in the time array. Along with the illustration in Figure 25, this load is easy to define. The command for specifying the load is:

EDLOAD, Option, Lab, KEY, Cname, Par1, Par2, PHASE, LCID, SCALE, BTIME, DTIME

The parameters Par1 and Par2 represent the time array and the load array, respectively.

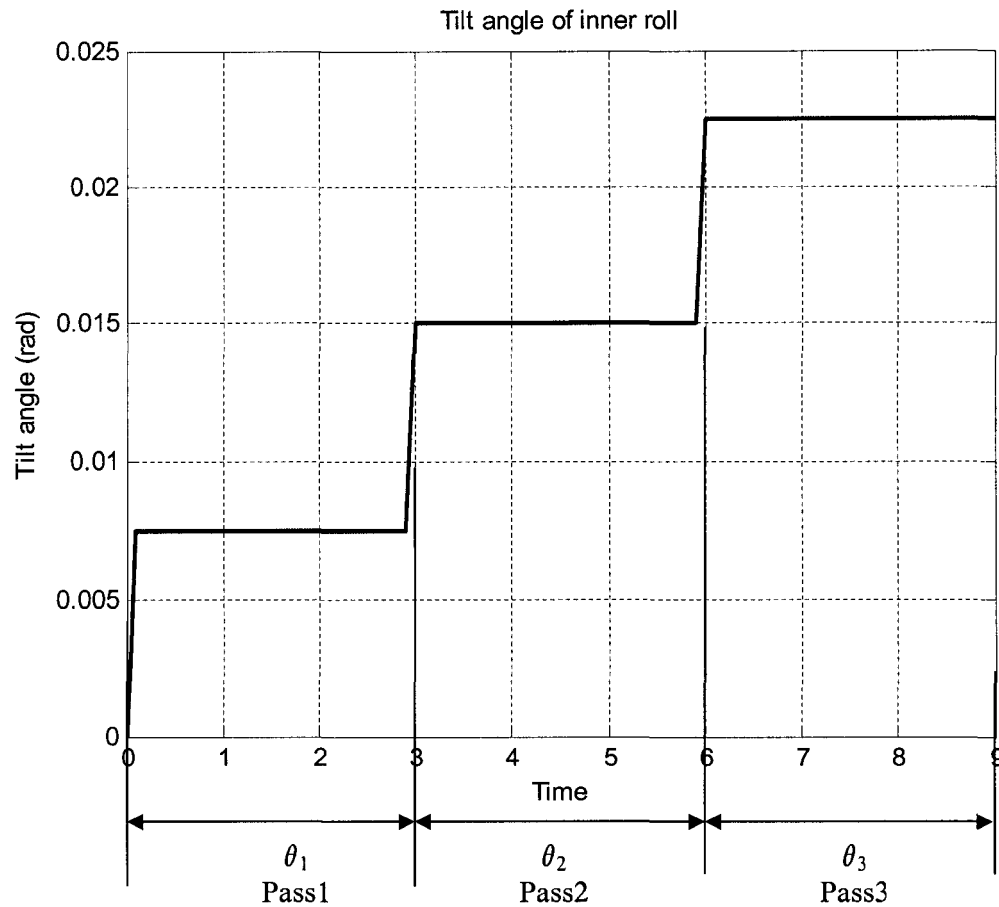


Figure 25 Tilt angle of the upper roll used for pressing the plate during the process

2.2.7.2 Rotation angular speed of the outer roll

In the roll bending process, the plate is driven forward and backward by the friction between the plate and the rolls. When applying the pyramid model, the two outer rolls are rotated to drive the plate forward or backward. As a result, the angular speed needs to be determined. Figure 26 illustrates the rotation angular speed of the outer roll in the 3-pass roll-bending process. When the value is positive, the plate is driven forward, and when it is negative, the plate is driven backward.

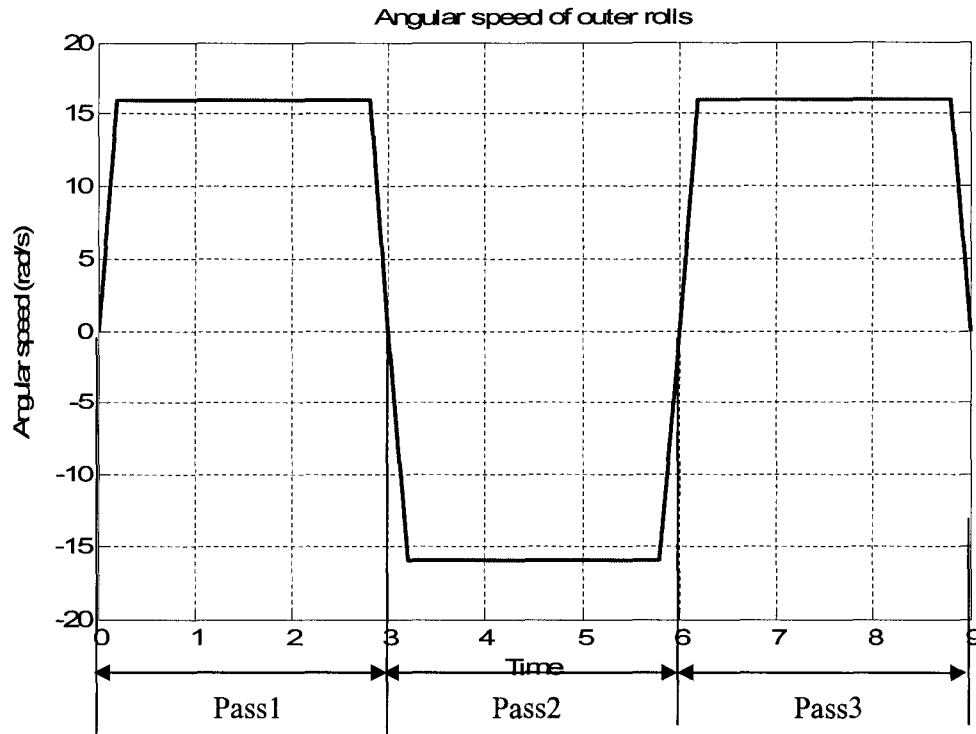


Figure 26 The angular speed of the outer roll for driving the plate forward and backward in the 3-pass roll-bending process

2.3 A typical simulation example and its numerical results

The preceding discussions describe the preparation process for the implementation of a dynamic simulation of the roll bending process using ANSYS and LS-DYNA. After the simulation, ANSYS outputs the corresponding results. This section will examine the simulation results through an example. The convergence and the comparison of the single-pass and multi-pass processes will be discussed.

The following parameters are used in the example:

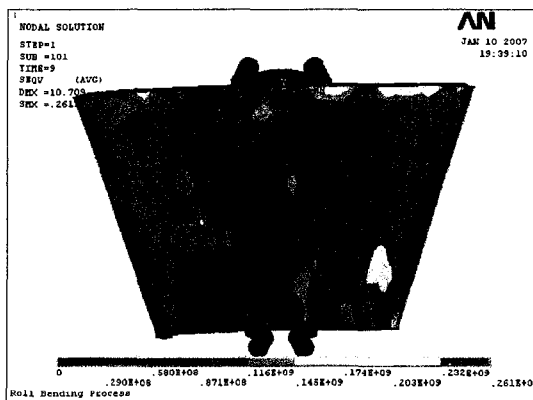
- Geometric parameters: bottom radius, 2.5 m; top radius, 1.5 m; height, 3.0 m and thickness of the plate, 10 cm

- Material: Stainless Steel at 20°C
- Material properties: Elastic Modulus=200 GPa, Yield Stress=250MPa, Density=7850 kg/m³, Poisson's Ratio=0.28, Tangent Modulus=0
- Rolls configuration: bottom radius=2.5 m, span of the outer rolls=1 m
- Mesh size: length division=100, width division=20
- Number of passes: 3

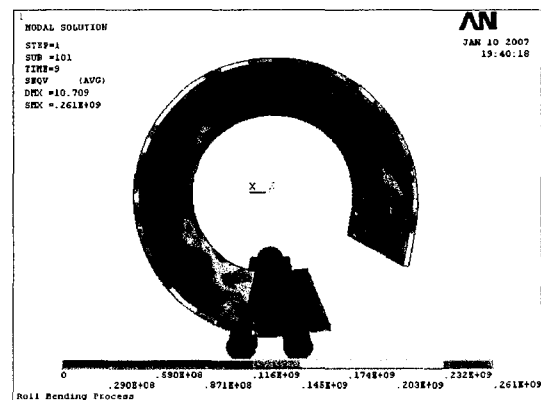
Generally, ANSYS outputs the results through an animation, contour display and numerical result list. While the animation cannot be illustrated in this document, the contour display of the final shape will be presented here to illustrate the final workpiece.

2.3.1 The contour display of the final shape

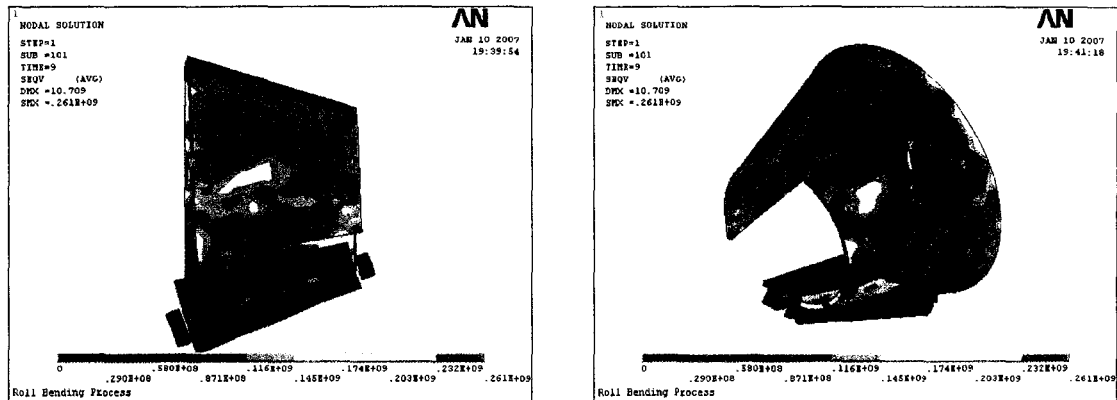
The contour display illustrates the whole workpiece at a specific time. What we are interested in is the final shape. The following pictures (Figure 27) represent the different views of the final shape of this workpiece.



a: Top view



b: Front view



c: Left view

d: 3D view

Figure 27 The contour display of the final shape formed in a typical simulation

Figure 27 presents only a direct visual qualitative representation of the final shape. However, the contour display cannot provide a more precise measurement of the difference between this workpiece and the desired shape. The next chapter will implement a numerical method to evaluate this final shape and verify its geometric parameters.

2.3.2 The reaction force on the roll

The reaction force on the roll is actually the force on the contact surface between the roll and the plate. This force varies with time. ANSYS records this force value at specified time intervals, and presents it in postprocessor POST26.

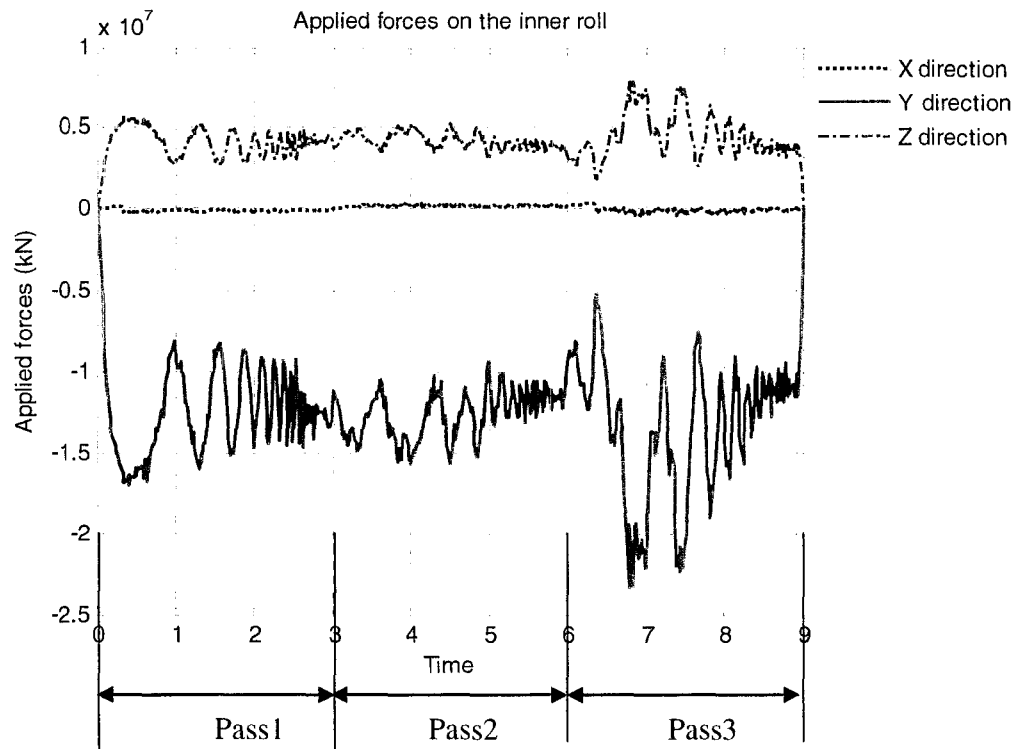


Figure 28 Reaction forces on the upper roll

Figure 28 illustrates the time-history of the reaction forces on the upper roll. All curves demonstrate the complicated vibrating behaviour of these forces. The following discussion adopts the average value of the reaction force. Moreover, all values of the force will be converted to their absolute values.

2.4 Discussion of convergence and number of passes in the process

FEM is applied to analyse this dynamic roll bending process. Therefore, this method should be convergent with an increase in the number of elements. However, the performance will become poorer as the number of elements is increased. As a result, the convergence is examined, and the balance of performance and the accuracy is discussed. The bending type denotes the number of passes in the process. As indicated in the

introduction, the roll bending process can be single-pass or multi-pass. This section compares the two types of processes and discusses the reason for choosing the multi-pass type.

2.4.1 Convergence studies and comparison of performance

FEM is a numerical method which is normally used to find approximate solutions to certain complicated problems. FEM provides the method for obtaining such approximate solutions. However, the degree of approximation varies with specific sector examined. For implicit static analyses, the approximation is generally sensible to the element size, while for explicit dynamic analyses, besides the element size, the time step size also influences the approximation. Generally, the smaller the element size applied, the more precise the result that can be obtained, even though more computation time is needed. This section discusses convergence by comparing the reaction force and time consumption with respect to different element sizes.

The roll bending process is a dynamic problem, and the explicit dynamic analysis method is applied. Two sectors influence convergence: element size and time step, and this section will discuss the influence of these two sectors.

To obtain precise results, the element size should be as small as possible. However, when the element size decreases, the computation time increases rapidly. In addition, when the element size reaches a certain value, continuing to decrease it will have little impact on the precision.

This project studies 11 cases with different element sizes. Figure 29 illustrates the average reaction forces on the inner roll in the Y direction when applying different element sizes. The element size in the figure is represented by a division of the plate (see Figure 20). For example, 25x8 means 25 elements length-wise 8 elements width-wise.

As illustrated in Figure 29, the reaction force value converges to a certain value as the division of elements increases. That means this simulation is convergent.

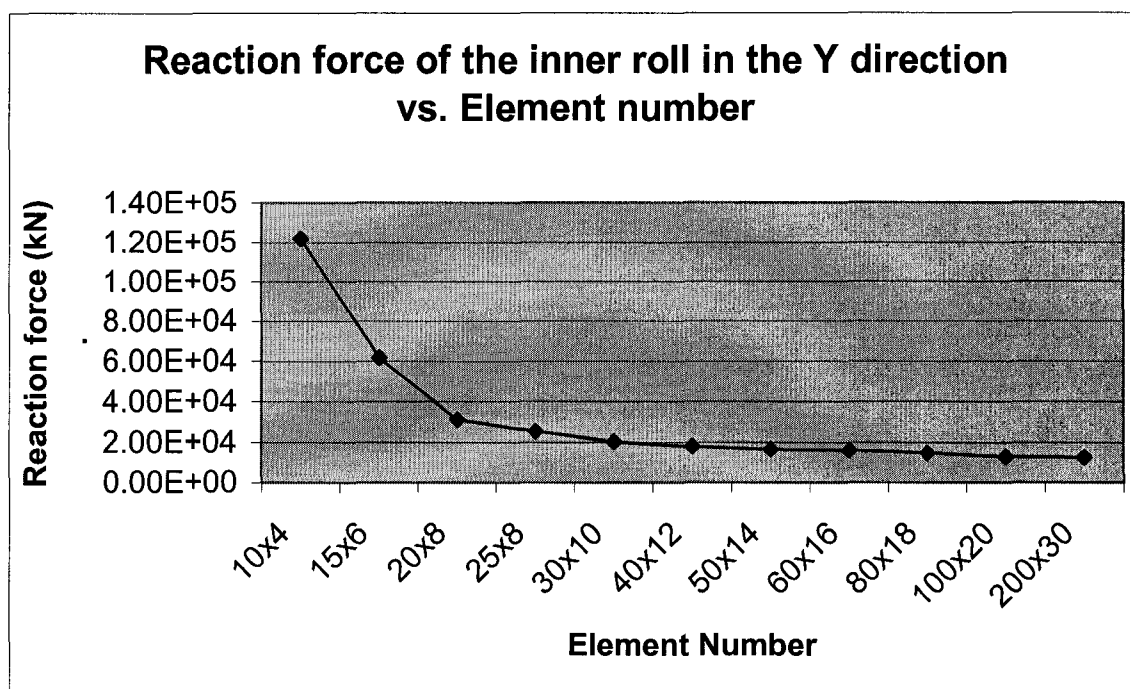


Figure 29 Convergence study conducted by comparing the reaction force of the inner roll in the Y direction when applying different mesh sizes

When a smaller element size is applied, more accurate results can be obtained. However, the greater the number of elements, the poorer the performance. With an increase in the number of elements, the run-time increases rapidly, as shown in Figure 30. Therefore, in simulation, a suitable element size should be chosen to balance the precision and the performance. If we compare Figure 29 and Figure 30, when the division is increased from 100x20 to 200x30, the run-time is increased fourfold while the precision hardly changes. Based on this consideration, the meshing division is set to 100x20 for the following simulations.

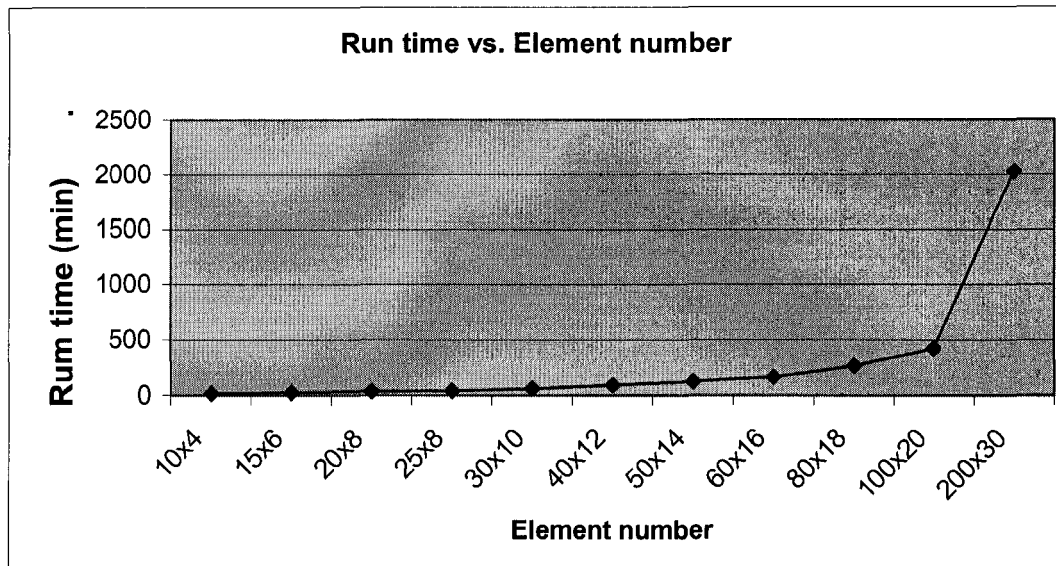


Figure 30 Rapid increase in run-time along with the increase of element

An explicit dynamic analysis is generally applied to resolve the dynamic problem, such as in the roll-bending process. For an explicit dynamic analysis, the time step is very important for convergence purposes. However, the time step size is set automatically by LS-DYNA, and its value is generally $10E-5$ seconds.

2.4.2 Number of passes

The single-pass and multi-pass bending processes were partly described in the introduction. In this section, these two types of bending will be compared based on the simulation result.

Figure 31 illustrates the final shape obtained by applying single-pass bending. All parameters for a single-pass simulation are the same as those for the three-pass simulation. Compared with Figure 27 which illustrates the final shape obtained by applying three-pass roll bending, the single-pass roll bending does not bend the plate

completely. In addition, the radius (see Figure 31-b) is smaller than that for the three-pass bending. As a result, three-pass bending provides a more precise final shape.

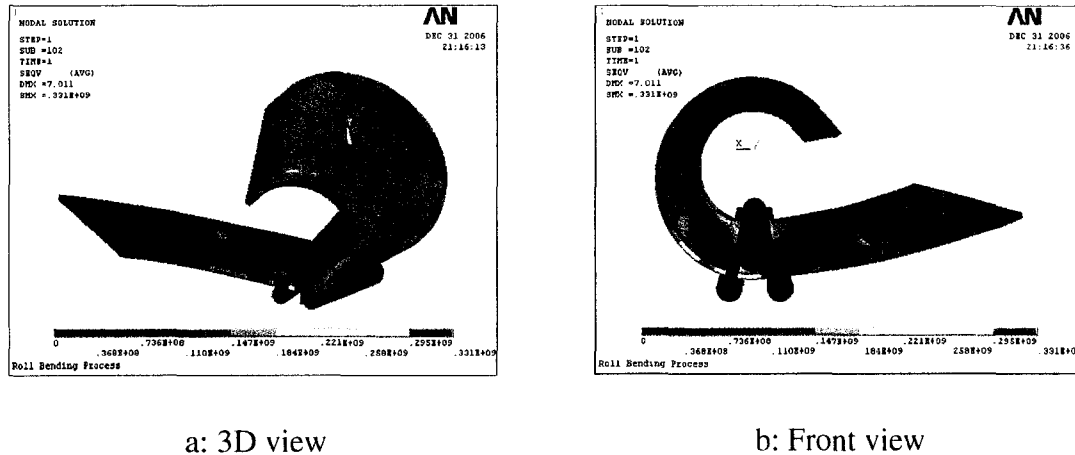


Figure 31 Two views of the contour display of the final shape obtained by applying the single-pass roll bending process

The reaction force on the inner roll in the Y direction is $1.68E+4$ kN when the single-pass roll bending is applied, and $1.27E+4$ kN, when the three-pass roll bending is applied. This indicates that applying the three-pass roll bending requires less force.

In conclusion, a three-pass roll bending achieves a better bending quality and requires less bending force than a single-pass roll bending. Therefore, all the simulations that follow in this document are based on the three-pass roll bending process.

2.5 Comparison between FEM results and the theoretical calculation for the roll-bending of a cylindrical shape

The simulation in ANSYS provides the reaction forces on the rolls and the residual stress in the plate. For the model to form a cylindrical tube, these forces and the residual stress can be estimated in ref. [5]. Nevertheless, the typical simulation presented in this chapter is for the formation of a conical tube using the three-pass process. In order to

validate the result, a simulation of the formation of a cylindrical tube using the single-pass process should be executed. This simulation is based on following parameters:

- Geometry of target shape:
 - Outside radius $R=2.5$ m
 - Height of the cylinder $H=3$ m
 - Plate thickness $t=0.1$ m
- Material properties:
 - Elastic modulus $E=200$ GPa
 - Yield stress $\sigma_Y=250$ MPa
 - Poisson's ratio $\mu=0.3$,
 - Density $\rho=7850$ kg/m³
- Process configuration:
 - Span of the outer rolls $d = 1$ m,
 - Diameter of the outer roll $d_r = 0.5$ m
- Number of passes: single pass

2.5.1 Validation of reaction force

Depending on the simulation result, the maximum reaction force on the inner roll in the Y direction is: $F_{\max}=1.978E+4$ kN, while the average reaction force is: $F_{\text{avg}}=1.425E+4$ kN.

The reaction force can be estimated using the formula provided in [5]; when the radius of target tube satisfies the condition: $R<100*t$, the reaction force can be calculated by the formula:

$$F = \frac{0.7 \cdot \sigma_Y \cdot l \cdot t^2}{\lambda} \quad (2.2)$$

where:

σ_Y : Yield stress

l : Width of the plate

t : Thickness of the plate

λ : Distance between contact points of two outer rolls and the plate

$$\lambda = \frac{d}{1 + \frac{d_r}{2R}}$$

d : Span of two outer rolls

d_r : Diameter of the outer rolls

R : Outer radius of the target cone

The parameters above are illustrated in Figure 32.

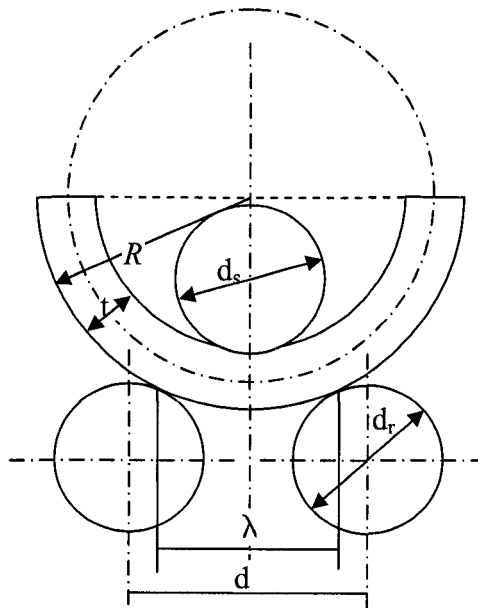


Figure 32 Parameters for the theoretical estimation of the reaction forces on the inner roll

In the simulation, all parameter values are specified as above, except for the length l which is 70% of the perimeter of the target cylinder. Rather, the value is:

$$l = 0.7 \cdot 2\pi R = 10.9956m$$

According to equation 2.1, the reaction force of the inner roll is:

$$F = \frac{0.7 \cdot \sigma_Y \cdot l \cdot t^2}{\lambda} = \frac{0.7 \cdot \sigma_Y \cdot l \cdot t^2}{d} \cdot \left(1 + \frac{d_r}{2R}\right) = 2.02 \times 10^4 \text{ kN}$$

Using this formula, the reaction forces for more examples are calculated for the sake of comparison.

Table XIV lists the comparisons with the result of simulation.

Table XIV

Validation of reaction force on the inner roll with the theoretical result

Yield stress (MPa)	Theoretical result (kN)	Maximum value of simulation (kN)	Relative Difference (%)
562	4.542E+4	3.42E+4	24.7
250	2.02E+4	1.978E+4	2.1
218	1.762E+4	1.831E+4	3.9
134	1.083E+4	1.372E+4	26.7

According to Table XIV, there is an acceptable difference between theoretical results and the simulation results. Despite equation (2.2) is a simplified equation which neglects the influence of the friction, the tangent modulus and the elastic modulus on the reaction forces, it gives an acceptable approximation as can be seen in the last column of the table.

2.5.2 Validation of residual stress

Residual stress can also be estimated theoretically using the method in [5]. Figure 33 illustrates this method for determining the residual stress. After obtaining the value of

$2 \frac{R_f}{t} \cdot \frac{\sigma_Y}{E}$, the residual stress can be determine based on that value and the position through the thickness. Residual stress is validated using the same example as the one used to validate the reaction force. Then,

$$2 \frac{R_f}{t} \cdot \frac{\sigma_Y}{E} = 2 \cdot \frac{2.45}{0.1} \cdot \frac{250E6}{200E9} = 0.0612 \approx 0.1$$

To estimate the residual stress, the value of 0.1 is used in Figure 33. Therefore, on the inner layer, the residual stress is about half of σ_Y , that is $\sigma_r = 125\text{MPa}$. Table XV lists other comparisons for different materials.

Table XV

Comparison of residual stress in simulation with the theoretical result

Yield stress (MPa)	Interpreted result from graph (MPa)	Average value of simulation (MPa)	Relative Difference (%)
250	125	138	9.4
562	281	178	57.8
218	109	90	21.1
134	67	68	1.5

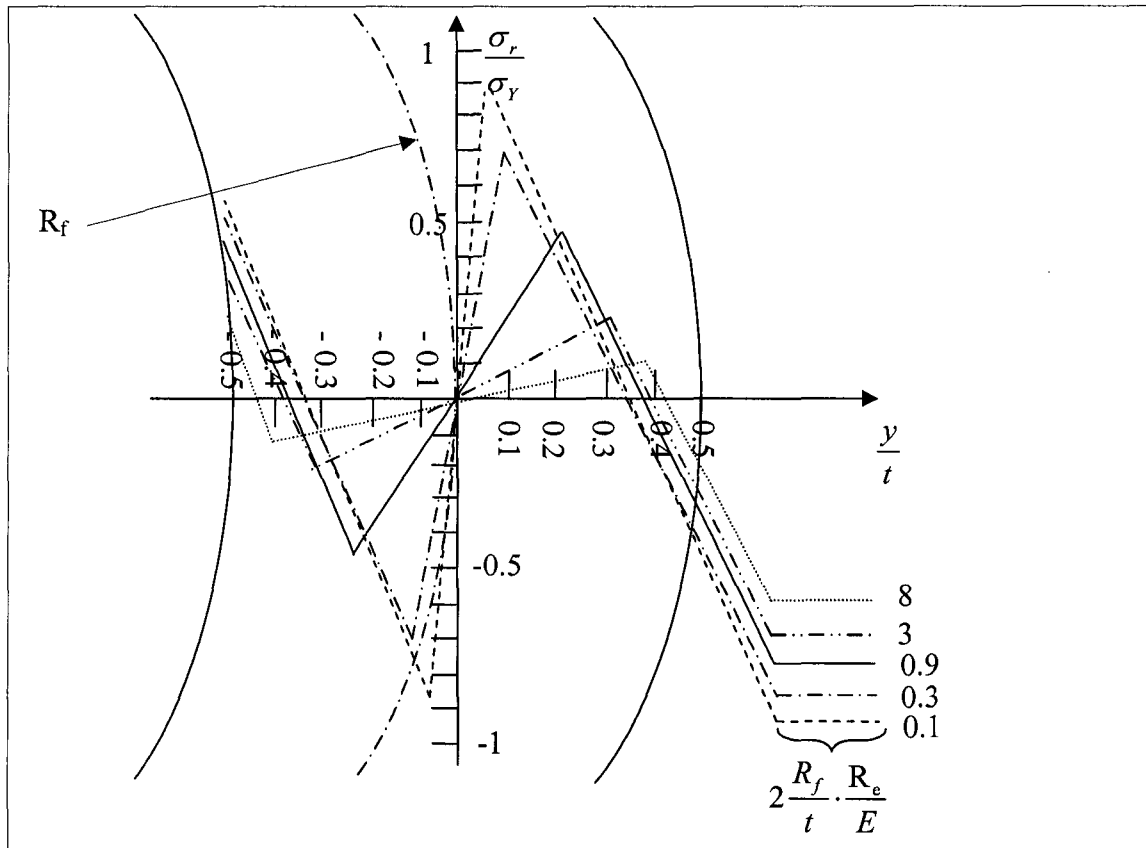


Figure 33 Determination of residual stress using graphic interpretation [5]

According to Table XV, there is also a difference between the interpreted results and the simulation results. There are two reasons for this: the first one is that the value of $2 \frac{R_f}{t} \cdot \frac{R_e}{E}$ is not exactly that illustrated in the graph, and the second one is that the results listed in the first column are an estimate. That being said, the difference in residual stress is nonetheless acceptable.

2.6 Summary

This chapter has discussed some issues relating to the finite element model simulation using ANSYS. The convergence and comparison of single-pass and three-pass bending

have also been discussed. The contour display illustrates the final shape of the simulation of the roll bending process. However, further analysis is required in order to perform a numerical measurement of the final shape, otherwise the bending quality cannot be determined. The next chapter presents a numerical method to verify the geometric parameters of the final shape. The procedure is called geometric verification.

CHAPTER 3

VERIFICATION OF THE GEOMETRIC ACCORDANCE OF THE FINAL PIECE

For a designer, the final shape must be measured numerically because no matter what the parametric analysis or evaluation are used, the bending quality requires a numerical measurement. If different parameters are used, different bending qualities are also realized. A designer can get a pretty good idea of the final shape by looking at the final shape presented in ANSYS. However, for the parametric analysis, a numerical measurement must be implemented for the simulation result. This chapter discusses the procedure for validating the geometric shape using a numerical algorithm, a process called geometric verification.

When discussing simulation in ANSYS in the last chapter, the interface between ANSYS and other software such as MATLAB was described. The coordinates of the nodes produced is imported into MATLAB, and then a least-squares fitted cone is obtained from this coordinate information using the Levenberg-Marquardt algorithm. The deviation of the bended workpiece is calculated by comparing the fitted cone and the target cone.

3.1 Purpose of geometric verification

Ideally, the roll bending process should result in the bended workpiece being exactly the same as the expected shape. However, it is generally impossible to achieve such a shape due to the influence of the roll configuration, the sliding movement and the material, etc. When rolls are well configured, the final shape is close to the target shape. From the simulation result in ANSYS illustrated in the last chapter, the bending quality can be recognized directly, but cannot be measured numerically. Nevertheless, the numerical measurement is necessary for parametric analysis. The procedure for implementing the

numerical measurement for the final shape is called geometric verification, which is thus aimed at calculating the deviation of the final shape from the target shape. Another goal of this verification is to assess the distortion of the final shape produced in the roll bending process.

3.1.1 Assessment of the circularity and the distortion

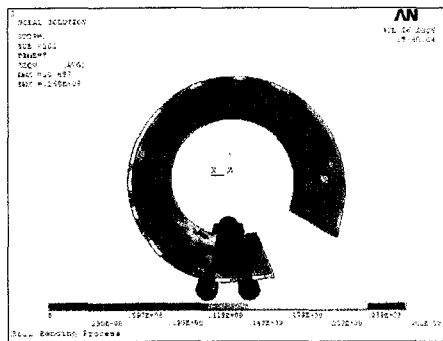
The final workpiece is generally not an exact conical shape because it is distorted during the roll bending process. Moreover, the top and bottom views of the final shape do not look exactly a circle, as do those of an ideal conical shape. This criterion, known as circularity joins distortion as a bending quality criterion. The better the bending quality, the less distorted is the piece and the better its circularity. Geometric verification must therefore primarily assess these two criteria.

3.1.1.1 Comparison of circularity

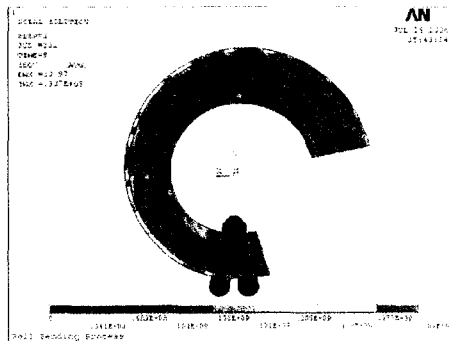
Circularity measures the quality of deformation in the radial direction, as illustrated in Figure 34. From the bottom view of the contour display in ANSYS, the direct qualitative visual representation is given. As shown in Figure 34-*a* illustrates a workpiece with better circularity while that in Figure 32-*b* has worse circularity.

3.1.1.2 Comparison of distortion

Distortion is produced in the roll bending process because of sliding or unbalanced movements. Figure 35 illustrates two examples with different distortions. Distortion displaces the bottom of the workpiece, moving it to another plane. The same effect is present for the top of the workpiece or any other plane parallel with the bottom. Obviously, less distortion implies a better bending quality.

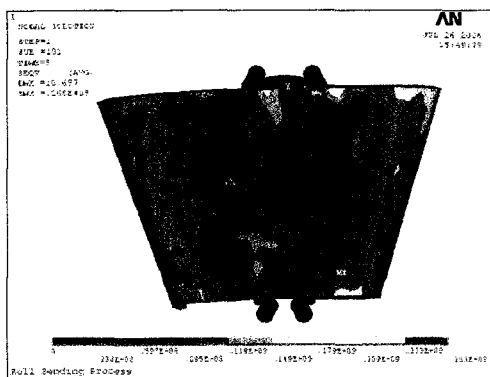


a: good shape, span of the outer rolls is 1 m

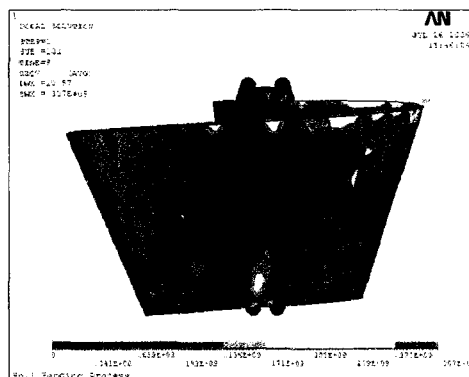


b: bad shape, span of the outer rolls is 0.8 m

Figure 34 Comparison of circularity on different configurations



a: good shape, span of the outer rolls is 1 m



b: bad shape, span of the outer rolls is 0.8 m

Figure 35 Comparison of distortion on different configurations

Generally, distortion cannot be avoided in the roll bending process unless there is no sliding movement present between the rolls and the plate. Since the conical rolls are applied in this project, the dimension of the rolls is chosen to satisfy the kinematics

relationship of the plate. If there is no sliding, the final shape should have no distortion. Thus an increase in the rate of friction may eliminate some sliding, but the friction must really be in realistic range. In this simulation, four cylinders are used to restrict the sliding of the plate (see Figure 16).

As discussed above, geometric verification aims mainly to assess the circularity and the distortion of the final workpiece.

3.1.2 Assesment of the deviation between the fitted cone and the target cone

In order to determine the bending quality, the deviation between the workpiece and the target cone must also be evaluated in addition of the circularity and the distortion. This is because the circularity and the distortion can measure only the similarity of the final shape to an exact conical shape.

3.1.3 Analysis of sensitivity of the bending quality

The bending quality depends on the configuration of the rolls. One of the goals of the simulation is to determine the relationship between the bending quality and the configuration. Suppose the roll bending process is a black box, as shown in Figure 36; changing the configuration results in a change in the bending quality. By comparing the bending quality on different configurations, we are able to reach a conclusion as to the sensitivity of the configurations to bending quality. However, it is impossible to compare the bending quality unless we perform a numeric inspection of the final geometric shape. Consequently, the first step of the geometric sensitivity analysis is the geometric verification.

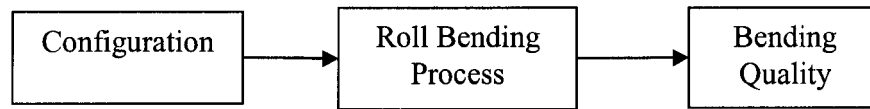


Figure 36 Relationship between configuration and bending quality

3.2 Realization of geometric verification

There are two methods used to verify the geometric shape of the final workpiece. The first involves obtaining the fitted plane and fitted circle, and then evaluating their distortion and the circularity, respectively. This method is suitable for 2D geometric verification. The next method involves obtaining the fitted cone and comparing the similarity of the workpiece to an exact cone. This method is suitable for 3D geometric verification, and is the one applied in this project. We discuss the implementation of this method below.

First, the least-squares fitted cone is obtained from the final workpiece. Then, the similarity of the final shape to an exact conical shape is presented by the sum of squares distance between the final workpiece and the fitted cone. The smaller this value is, the more similar the final shape is to an exact cone. However, similarity to a cone does not indicate good bending quality. The deviation between the fitted cone and the target cone must be calculated in order to evaluate the bending quality. Finding the fitted cone is a nonlinear optimization problem, which is resolved using the Levenberg-Marquardt algorithm, which will be discussed in section 3.4. For more details on this method, refer to lecture [23, 24].

3.2.1 Procedure of geometric verification

Figure 37 illustrates the geometric verification procedure. The coordinates of the nodes produced in ANSYS are imported into MATLAB, which is more suitable for implementing certain numerical optimization algorithms to obtain the least-squares fitted cone.

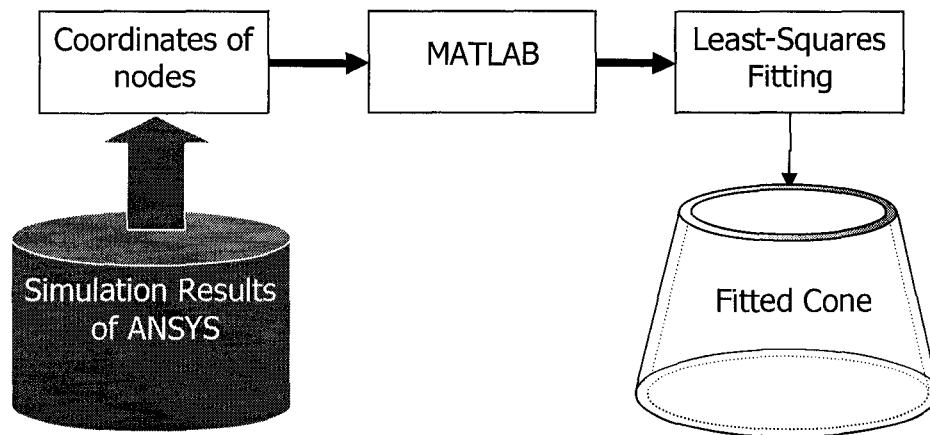


Figure 37 Geometric verification procedure

3.3 Geometric verification criteria

As discussed in section 3.1, the evaluation of the final shape is based on two criteria: similarity to an exact cone and deviation from the target cone.

3.3.1 Similarity to an exact cone

The final workpiece is generally similar to, but is not exactly like a cone. The similarity to an exact cone can be used to evaluate the geometric shape of the final workpiece. As discussed in section 3.2, the sum of squares distance can be applied to present this

criterion, that is, $\sum_{i=1}^n d_i^2$. The smaller this value, the more similar the workpiece is to an exact cone. Furthermore, this value can estimate the circularity and the distortion present. Therefore, in the evaluation of the geometry of the final shape, only this criterion is used.

3.3.2 Deviation from the target cone

The geometric shape criterion can only carry out an assessment of whether the final shape is similar to an exact cone, and of how different it is from an exact cone. However, the bending quality cannot be evaluated because the deviation from the target cone is unknown. This deviation must therefore be assessed. Actually, it can easily be determined after the fitted cone is obtained, just by comparing the fitted cone with the target cone. Because the original parameters of the target cone are the bottom radii, the top radii and the height, the deviation of these three parameters are also assessed in evaluating the bending quality. Equations (3.1) and (3.2) present the calculation of the deviation of the radii and the height.

$$d_r = \frac{|R_f - R_t|}{R_t} \quad (3.1)$$

where,

R_f : Radius of fitted cone

R_t : Radius of target cone

$$d_h = \frac{|H_f - H_t|}{H_t} \quad (3.2)$$

where,

H_f : Height of fitted cone

H_t : Height of target cone

3.4 Levenberg-Marquardt Algorithm [25]

The Levenberg-Marquardt algorithm provides a numerical solution to the mathematical problem of minimizing a sum of squares of several generally nonlinear functions that depend on a common set of parameters.

This minimization problem arises especially in a least-squares curve fitting.

The Levenberg-Marquardt algorithm (LMA) interpolates between the Gauss-Newton algorithm (GNA) and the method of gradient descent. The LMA is more *robust* than the GNA, which means that in many cases it finds a solution even if it starts very far off from the final minimum. On the other hand, for well-behaved functions and reasonable starting parameters, the LMA tends to be a bit slower than the GNA. The LMA is the most popular curve-fitting algorithm; it is used in almost any software that provides a generic curve-fitting tool; few users will ever need another curve-fitting algorithm.

3.4.1 The problem

Given m functions f_1, \dots, f_m of n parameters p_1, \dots, p_n with $m \geq n$, it is convenient to use vector notation for both the functions and the parameters:

$$f^T = (f_1, \dots, f_m) \text{ and } p^T = (p_1, \dots, p_n)$$

The least-squares problem consists in finding the parameter vector \mathbf{p} for which the cost function $J(p) = d^T d = \sum_{i=1}^n [d_i(p)]^2$ becomes is at a minimum.

The main application is in the least-squares curve fitting problem: given a set of empirical data pairs (t_i, y_i) , optimize the parameters \mathbf{p} of the model curve $c(t|\mathbf{p})$ so that the sum of the squares of the deviations $d_i(p) = y_i - c(t_i | p)$ is at a minimum.

3.4.2 The solution

Like other numeric minimization algorithms, the Levenberg-Marquardt algorithm is an iterative procedure. To start a minimization, the user must provide an initial guess for the parameter vector \mathbf{p} . In many cases, an uninformed standard guess such as $\mathbf{p}^T=(1,1,\dots,1)$ will work just fine; in other cases, the algorithm will only converge if the initial guess is already somewhat close to the final solution.

In each iteration step, the parameter vector \mathbf{p} is replaced by a new estimate $\mathbf{p} + \mathbf{q}$. To determine \mathbf{q} , the functions $f_i(\mathbf{p} + \mathbf{q})$ are approximated by their linearization

$$f(p + q) \approx f(p) + J_q$$

where: \mathbf{J} is the Jacobian of \mathbf{f} at \mathbf{p} .

At a minimum of the sum of squares S , we have $\nabla S = 0$. With the above linearization, this leads to the following equation:

$$(J^T J)q = -J^T f$$

from which \mathbf{q} can be obtained by inverting $\mathbf{J}^T \mathbf{J}$. The key to the LMA is to replace this equation with a 'damped version':

$$(J^T J + \lambda)q = -J^T f$$

The (non-negative) damping factor λ is adjusted at each iteration. If the reduction of S is rapid, a smaller value can be used, bringing the algorithm closer to the GNA, whereas if an iteration produces an insufficient reduction in the residual, λ can be increased, taking it a step closer in the direction of gradient descent. A similar damping factor appears in the Tikhonov regularization, which is used to solve linear ill-posed problems.

If a retrieved step length or the reduction in the sum of squares to the latest parameter vector \mathbf{p} falls short of predefined limits, the iteration is aborted, and the last parameter vector \mathbf{p} is considered to be the solution.

3.4.3 Choice of damping parameter

Various more or less heuristic arguments have been put forward for the best choice for the damping parameter λ . There are theoretical arguments showing why some of these choices guarantee a local convergence of the algorithm; however these choices can cause the overall convergence of the algorithm to suffer from the undesirable properties of steepest-descent, in particular, very slow convergence closer to the optimum.

Obviously, the absolute value of any choice depends on how well-scaled the initial problem is. Marquadt recommended starting with a value λ_0 and a factor $\nu > 1$. Initially it involves setting $\lambda = \lambda_0$ and computing the residual sum of squares $S(\mathbf{p})$ after one step from the starting point with the damping factor of $\lambda = \lambda_0$ and secondly with λ/ν . If both of these are worse than the initial point, then the damping is increased by successive multiplication by ν until a better point is found, with a new damping factor of $\lambda\nu^k$ for some k .

If the use of the damping factor λ/ν results in a reduction in the squared residual, then this is taken as the new value of λ (and the new optimum location is taken to be that obtained with this damping factor), and the process continues; if using λ/ν results in a worse residual, but using λ results in a better residual, then λ is left unchanged, and the new optimum is taken to be the value obtained with λ as the damping factor.

3.4.4 Algorithm

Figure 38 illustrates the procedure for the Levenberg-Marquardt algorithm [23]. While the F is the Jacobian matrix of the objective function, λ is the damping parameter.

Input is an initial guess vector p_0 , containing the defining parameters. Returns p_0 that minimizes J .

Set $\lambda \leftarrow 0.001$

Repeat

Decrement λ ; Normalize p_0

Set $U \leftarrow F_0^T F$; $v \leftarrow F_0^T d(p_0)$; $J_0 \leftarrow \sum d_i^2(p_0)$

Repeat

Increment λ

Set $H \leftarrow U + \lambda(I + \text{diag}(u_{11}, u_{22}, \dots, u_{nn}))$

Solve the system $Hx = -v$

Set $p_{new} \leftarrow p_0 + x$; $J_{new} \leftarrow \sum d_i^2(p_{new})$

If converged, Set $p_0 \leftarrow$ Normalized p_{new} ; return p_0

Until $J_{new} < J_0$ or an iteration limit is reached

If $J_{new} < J_0$, $p_0 \leftarrow p_{new}$

Until an iteration limit is reached

Figure 38 Procedure for Levenberg-Marquardt algorithm

3.5 Determination of fitted cone

The points produced in ANSYS are called Points Clouds, and are shown in Figure 39. The procedure for determining the fitted cone is aimed at finding the fitted cone from these points. As discussed in the last section, the least-squares fitting method is aimed at obtaining a fitted shape with the minimum least-squares distance to the points clouds.

As demonstrated in Figure 39, the real line denotes the fitted cone, while the dotted line denotes the points clouds, and the arrows denote the distance from the point to the fitted cone. The least-squares fitting method is used to calculate the sum of the distance and to obtain the minimum value.

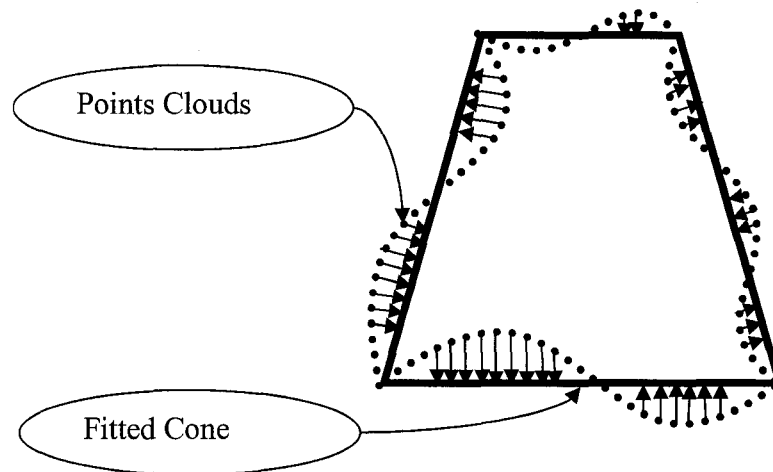


Figure 39 Demonstration of fitting cone

In order to calculate the distance between a point and the fitted cone, the distance from this point to the axis of the fitted cone and the distance from this point to the bottom plane must be calculated. Therefore, the distance between the point and the line and between the points and the plane must first be calculated. This procedure will be discussed in the next section (section 3.5.1)

3.5.1 Distance from a point to a plane (g_i) and to a line (f_i)

Figure 40 shows the distance from one point p_i to a plane defined by p and a normal direction A (Figure 40-a), and the distance from one point p_i to a line defined by p and direction A (Figure 40-b). [23]

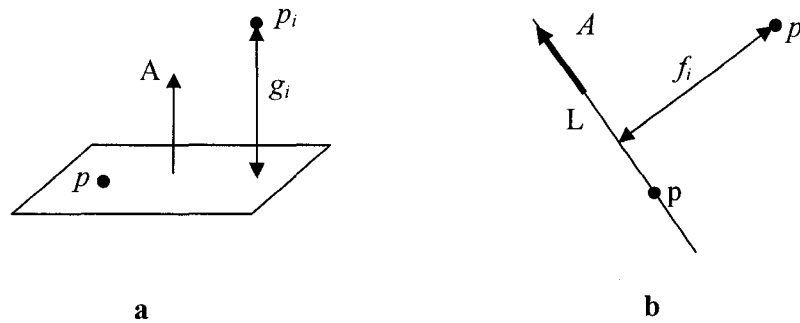


Figure 40 Distance from point to line and distance from point to plane

3.5.1.1 Distance from a point to a plane

Let $g(p_i, p, A)$ denote the distance from the point, $p_i = [x_i, y_i, z_i]$, to the plane defined by the point, $p = [x, y, z]$, and the normal direction, $\vec{a} = \frac{A}{|A|} = [a, b, c]$, where

$\sqrt{a^2 + b^2 + c^2} = 1$. The value of g is given by equation 4.3. [23]

$$g_i = g(p_i, p, A) = a \cdot (x_i - x) + b \cdot (y_i - y) + c \cdot (z_i - z) \quad (3.3)$$

3.5.1.2 Distance from a point to a line

Let $f(p_i, p, A)$ denote the distance from point, $p_i = [x_i, y_i, z_i]$, to line L defined by the point, $p = [x, y, z]$, and the direction, $\vec{a} = \frac{A}{|A|} = [a, b, c]$, where $\sqrt{a^2 + b^2 + c^2} = 1$

The value of f is given by: $f_i = f(p_i, p, A) = |\vec{a} \times (p - p_i)|$. That is equation 4.4. [23]

$$f_i = \sqrt{u^2 + v^2 + w^2} \quad (3.4)$$

where:

$$\begin{aligned}
u &= c(y_i - y) - b(z_i - z) \\
v &= a(z_i - z) - c(x_i - x) \\
w &= b(x_i - x) - a(y_i - y)
\end{aligned}$$

3.5.2 The derivation for f_i and g_i

The algorithm applied to obtain the least-squares fitted cone, the Levenberg-Marquardt Algorithm, was discussed in section 3.4. This algorithm requires both the gradient of the direction of the plane and of the axis. Therefore, the derivations for g_i and f_i must be conducted. Equations 4.5-4.8 show the derivations for g_i and f_i . [23]

$$\nabla g = \begin{bmatrix} \frac{\partial g_i}{\partial x} \\ \frac{\partial g_i}{\partial y} \\ \frac{\partial g_i}{\partial z} \end{bmatrix} = \begin{bmatrix} -a \\ -b \\ -c \end{bmatrix} \quad (3.5)$$

$$\begin{bmatrix} \frac{\partial g_i}{\partial A} \\ \frac{\partial g_i}{\partial B} \\ \frac{\partial g_i}{\partial C} \end{bmatrix} = \begin{bmatrix} (x_i - x) - a \cdot g_i \\ (y_i - y) - b \cdot g_i \\ (z_i - z) - c \cdot g_i \end{bmatrix} \quad (3.6)$$

$$\nabla f = \begin{bmatrix} \frac{\partial f_i}{\partial x} \\ \frac{\partial f_i}{\partial y} \\ \frac{\partial f_i}{\partial z} \end{bmatrix} = \begin{bmatrix} [a \cdot g_i - (x_i - x)] / f_i \\ [b \cdot g_i - (y_i - y)] / f_i \\ [c \cdot g_i - (z_i - z)] / f_i \end{bmatrix} \quad (3.7)$$

$$\begin{bmatrix} \frac{\partial f_i}{\partial A} \\ \frac{\partial f_i}{\partial B} \\ \frac{\partial f_i}{\partial C} \end{bmatrix} = \begin{bmatrix} g_i \cdot [a \cdot g_i - (x_i - x)] / f_i \\ g_i \cdot [b \cdot g_i - (y_i - y)] / f_i \\ g_i \cdot [c \cdot g_i - (z_i - z)] / f_i \end{bmatrix} \quad (3.8)$$

3.5.3 Distance between the point and the plane

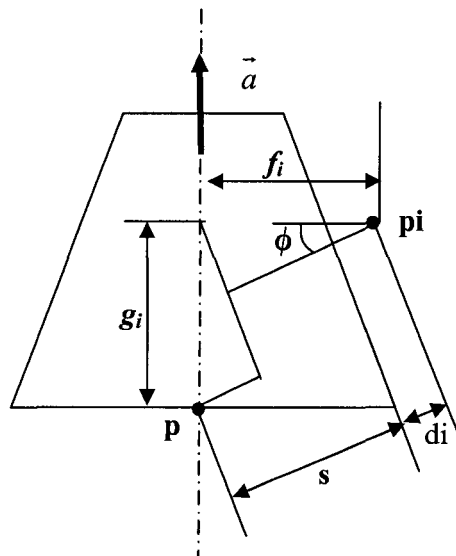


Figure 41 Distance from i^{th} point to fitted cone

Figure 41 illustrates the distance from the i^{th} point to the fitted cone. The point p_i is a point within the points clouds, and p is one point on the axis of the fitted cone. The vector \vec{a} represents the direction of the axis. f_i and g_i are the distance from p_i to axis and from p_i to the bottom of fitted cone, respectively. s is the distance from point p to the fitted cone and d_i is the distance from point p_i to the fitted cone. To construct the objective function, the distance d_i must be calculated primarily as demonstrated in equation 4.9. [23]

$$d_i = f_i \cos(\varphi) + g_i \sin(\varphi) - s \quad (3.9)$$

where:

f_i : Distance from i^{th} point to axis of the cone

g_i : Distance from i^{th} point to bottom plane of the cone

φ : Semi-angle of the fitted cone

s : Distance from center of bottom to the cone

3.5.4 Objective function

The objective is to find a cone, with the distance between this fitted cone and the points clouds being at a minimum. This objective is demonstrated in equation 4.10. [23]

$$\text{Minimize : } J(x, \vec{a}, \varphi, s) = \sum_{i=1}^n d_i^2 \quad (3.10)$$

where:

p : Vector (p_x, p_y, p_z) . a point on the cone axis (not the apex)

\vec{a} : Vector (a_x, a_y, a_z) . the direction numbers of the cone axis (pointing toward the apex)

φ : Semi-angle of the fitted cone

s : the orthogonal distance from point p to the cone

This objective function is a nonlinear problem, which is generally solved using the Levenbeg-Marguardt Algorithm.

3.5.5 Normalization

Normalization is a necessary step when applying the Levenberg-Marquardt Algorithm to solve the problem of equation 4.10 (refer to section 3.4). The procedure is shown below.

$$A \leftarrow A/|A|$$

$$x \leftarrow (\text{center of bottom plane})$$

$$\varphi \leftarrow \varphi(\text{mod } 2\pi)$$

if $\varphi > \pi$ then $[\varphi \leftarrow \varphi(\text{mod } 2\pi); A \leftarrow -A]$

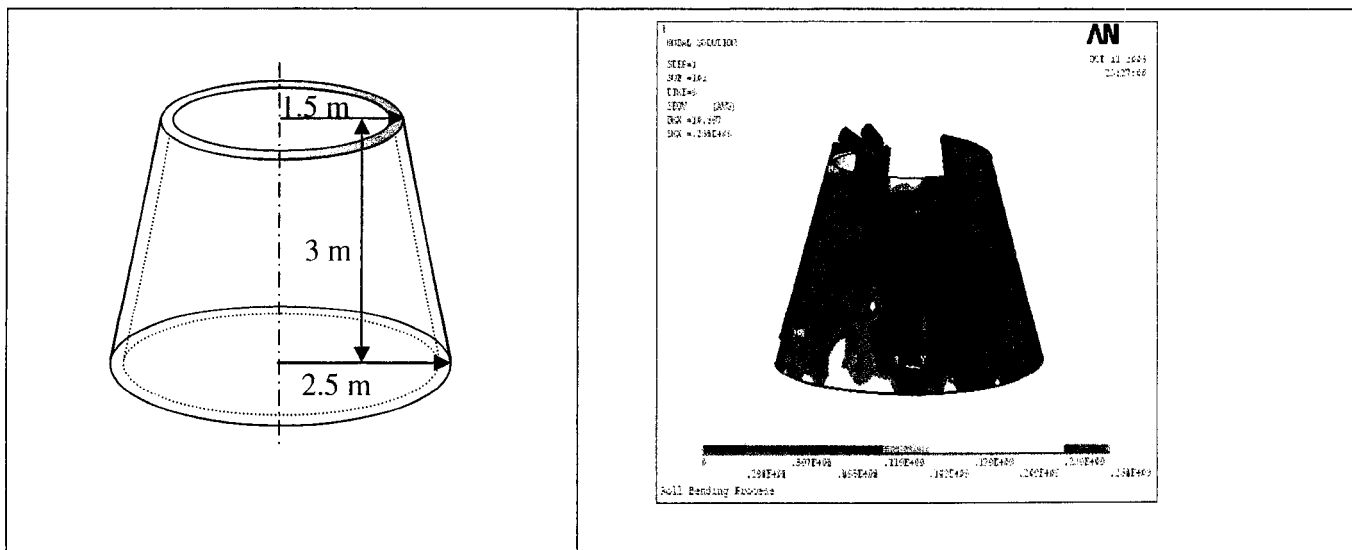
if $\varphi > \frac{\pi}{2}$ then $\varphi \leftarrow \pi - \varphi$

if $s < 0$ then $[s \leftarrow -s; A \leftarrow -A]$

3.6 Typical example of geometric verification

This section provides a typical example to demonstrate the geometric verification procedure. The example is based on the simulation presented in CHAPTER 2.

Figure 42 illustrates the procedure, going from the requirement specifications to the completion of the geometric verification. Figure 42(a) specifies the dimension of the target cone. Figure 42(b) shows the contour display of the final shape of the simulation in ANSYS. Figure 42(c) shows the point clouds imported from the simulation results of a formed cone in ANSYS. This set of three-dimensional points is then passed to the cone fitting algorithm to fit a truncated cone. The graphical results are shown in Figure 42(d), with two shapes superimposed: the fitted cone and the final workpiece produced in the simulation.



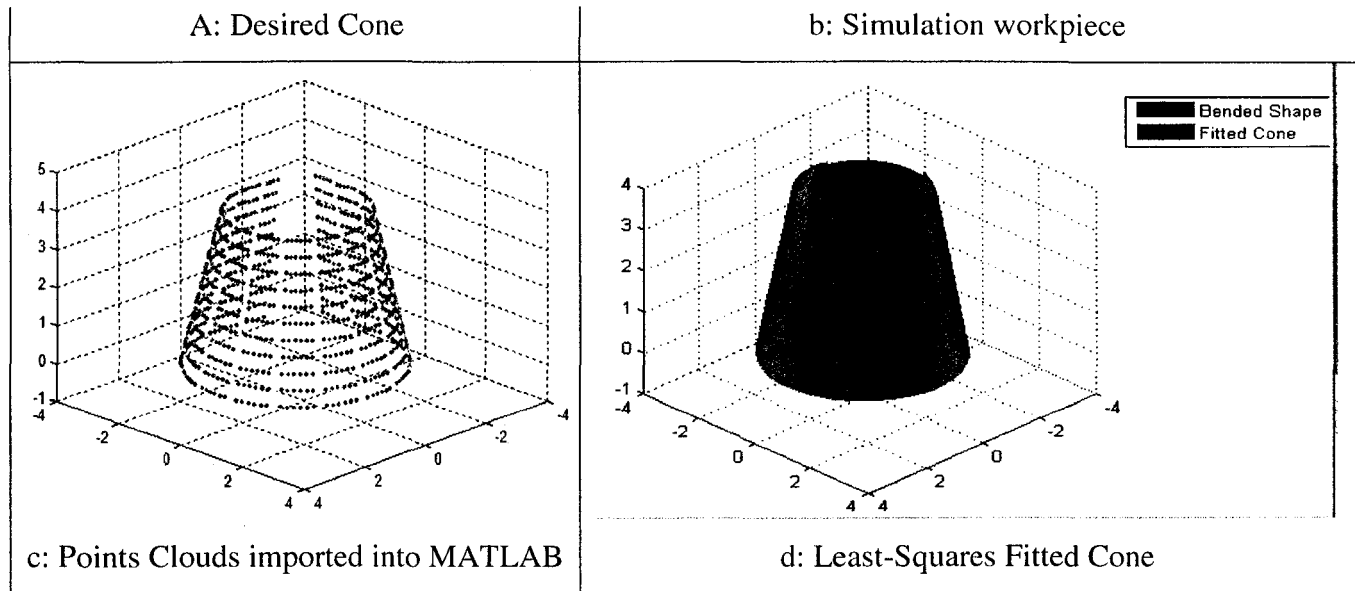


Figure 42 Simulation and geometric verification sequence

After the geometric verification, a least-squares fitted cone is obtained. One of the criteria applied at this stage is a similarity to an exact cone. It is represented by the sum of square distance (s) from the workpiece to the fitted cone. In this example, $s=0.2541 \text{ m}^2$. The smaller the value, the more similar the workpiece is to an exact cone.

The other criteria applied for the bending quality are deviations between the fitted cone and the target cone. Figure 43 and Table XVI illustrate the graphical and numerical comparisons of the target cone and the fitted cone, respectively.

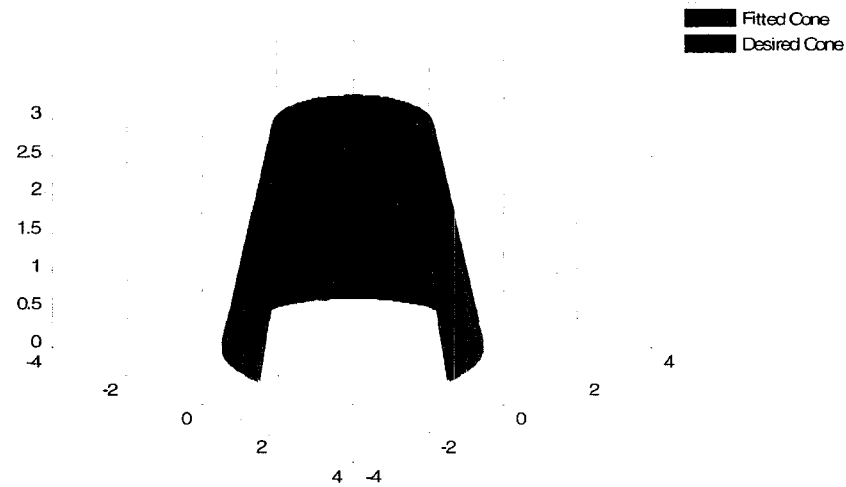


Figure 43 Graphical comparison of the target cone and fitted cone

Table XVI

Numerical comparison of the target cone and the fitted cone

	Top Radius (m)	Bottom Radius (m)	Height (m)
Target Cone (A)	1.5	2.5	3
Fitted Cone of Final Shape (B)	1.5150	2.5069	3.0008
Deviation	0.015	0.0069	0.0008
Deviation (%)	1%	0.28%	0.03%

Based on the result of the geometric verification, the quality of the final shape can be numerically measured, and moreover, the influence of input parameters can be studied in order to improve the bending quality. In the next chapter, the sensitivity of the quality to the input variable parameters will be discussed.

CHAPTER 4

SENSITIVITY ANALYSIS OF THE THREE-ROLL BENDING PROCESS

One of main goals of the simulation is to study the parametric sensitivity to simulation results. As discussed in CHAPTER 2, simulation parameters are chosen as static values. Therefore, the actual parameters influencing the simulation results are geometric parameters, material parameters and configuration parameters. If one of these parameters is changed, the simulation result changes accordingly. This chapter will discuss how these input parameters influence the bending quality, the reaction forces and the residual stress.

4.1 Study parameters and approach

A specific output can be influenced by many parameters. For example, both changes in materials or in the configuration of the rolls can influence the bending quality. Therefore, different parameters must be studied separately. On the other hand, changing the input parameters leads to variations in results. For instance, changing the configuration of the rolls will influence the bending quality, will have but no impact on the residual stress.

4.1.1 Input parameters and output results

The input parameters have a direct influence on the output results. Their relation is illustrated in Figure 44. Input parameters are configured before the simulation, and can be modified by the designer. There are three groups of input parameters listed, as below. Simulation parameters for their part, are set to static values (see section 2.4.1)

- Geometric parameters: including thickness of the plate and the radius of the target cone
- Material properties: elastic modulus and yield stress
- Configuration parameters: the friction, the temperature and the span of outer rolls

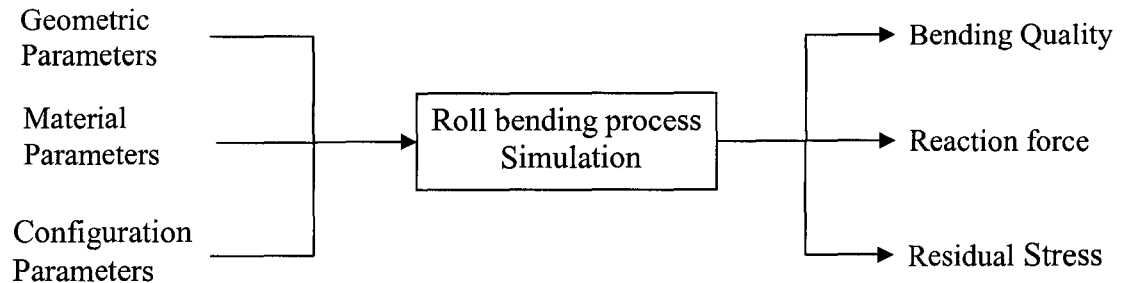


Figure 44 Relation between input parameters and output results

Each simulation in ANSYS produces many types of results. However, the following are the important results for an engineer:

- Bending quality
- Reaction forces
- Residual stress

Generally, when input parameters are changed, different simulation results are obtained. The analysis method involves changing input parameters and observing their influence on all these three output results.

4.1.2 The study approach

Based on Figure 44, when a given parameter is being studied, the others should be kept constant in order to ensure that no interference is introduced. The following section discusses how output results are influenced by geometric parameters, material parameters and configuration parameters, respectively.

4.2 Sensitivity of geometric parameters

Geometric parameters include the plate thickness, the bottom radii, the top radii and the height of the target cone. The plate thickness influences directly the final shape, the reaction forces and the residual stress. This section will discuss this parameter. In addition, the semi-angle of the target cone might influence the precision of the final shape. Generally, the variation of the geometry of the target cone causes the change of rolls configuration. In this situation, it is hard to determine the exact influence of reaction forces or residual stress because there is more than one sensitivity factor at play. Consequently, only the precision of the final shape will be discussed when changing the semi-angle of the target shape.

When studying the sensitivity of the plate thickness, the other parameters must be constant. They are listed in Table XIII.

Seventeen plate thicknesses are studied, from 2 cm to 10 cm, with an interval of 0.5 cm. The material used in this simulation is the ASTM A743 grade CA-6NM, at a temperature of 20°C.

Table XVII

Constant parameters for studying plate thickness sensitivity

Geometric Parameters				
Bottom Radius (m)		Top Radius (m)		Height (m)
2.5		1.5		3.0
Material Parameters (ASTM A743 grade CA-6NM)				
Elastic Modulus (GPa)	Yield stress (MPa)	Tangent Modulus (GPa)	Poisson's Ratio	Density (kg/m ³)
200	754	2	0.3	7850
Configuration Parameters				
Span of outer rolls (m)		Static friction		Dynamic friction
2.0		0.3		0.3

4.2.1 Influence of plate thickness on bending quality

Bending quality represents the deviation of the final workpiece from the target cone. This value is always positive because an absolute value is used. Thus, the value closest to zero indicates the optimal bending quality.

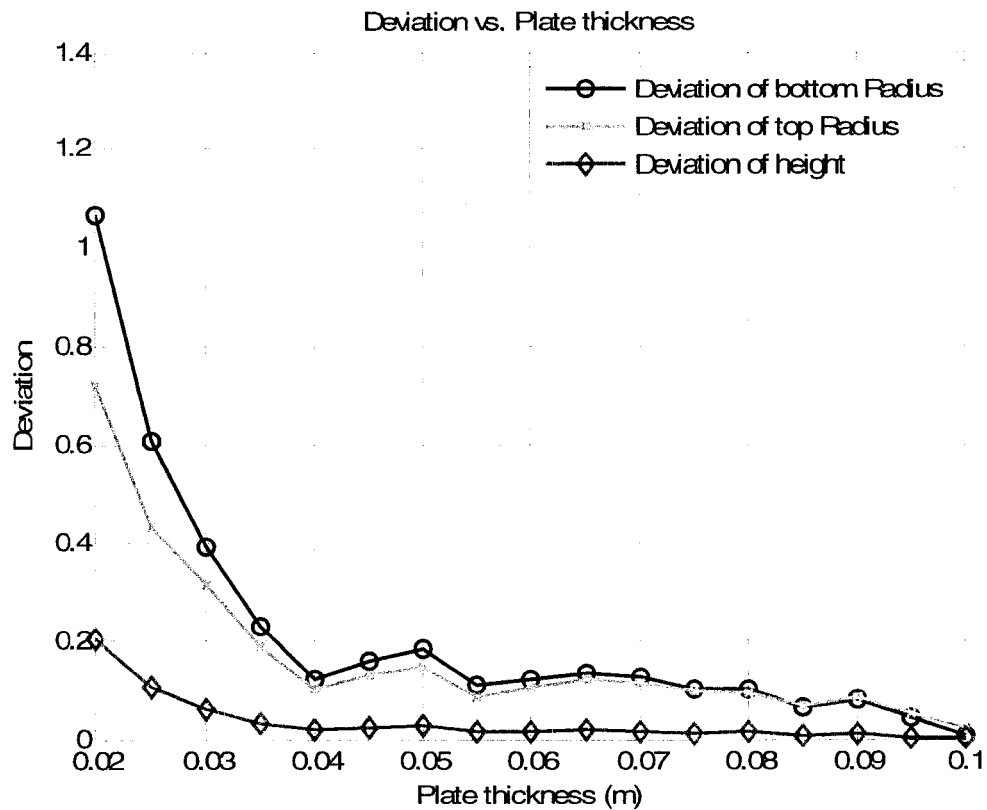


Figure 45 Variation of bending quality with different plate thicknesses

Figure 45 illustrates the variation in the bending quality as the plate thickness is changed. As can be seen in this figure, the deviation of the radius and height become smaller as the plate thickness increases. This implies that better bending quality is obtained with thicker plates. However, a thicker plate also requires more bending force.

4.2.2 Influence of plate thickness on reaction forces on the rolls

The plate thickness directly influences the reaction forces on the rolls. Obviously, for a given target cone, more reaction forces are needed if the plate is thicker. The goal of this study is to determine the relationship of the reaction force with the plate thickness; it

then examines studies whether the reaction forces are increased linearly as the plate thickness is increased.

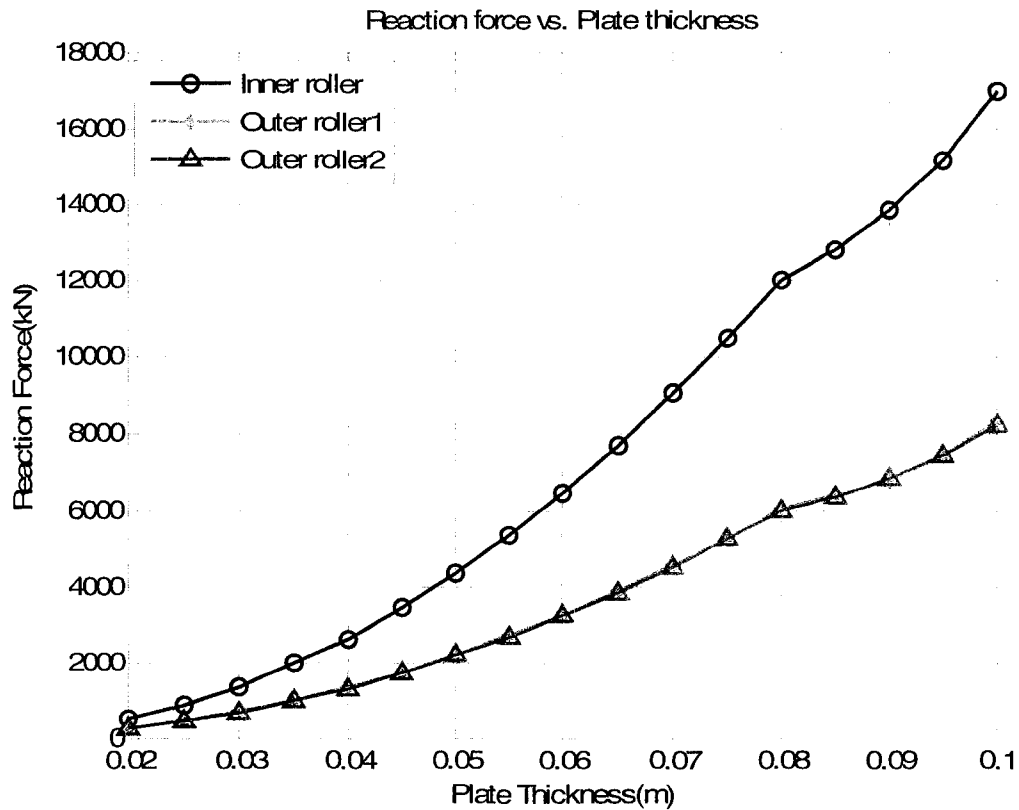


Figure 46 Tendency of reaction forces as plate thickness is increased

Figure 46 illustrates the reaction force in the Y direction on the three rolls. In accordance with the illustration of Figure 46, the reaction forces are increased almost quasi linearly with the plate thickness increase. This conclusion also conforms to equation (2.2).

4.2.3 Influence of plate thickness on residual stresses

The maximum residual stress value is chosen for this study because it is unevenly distributed across the surface.

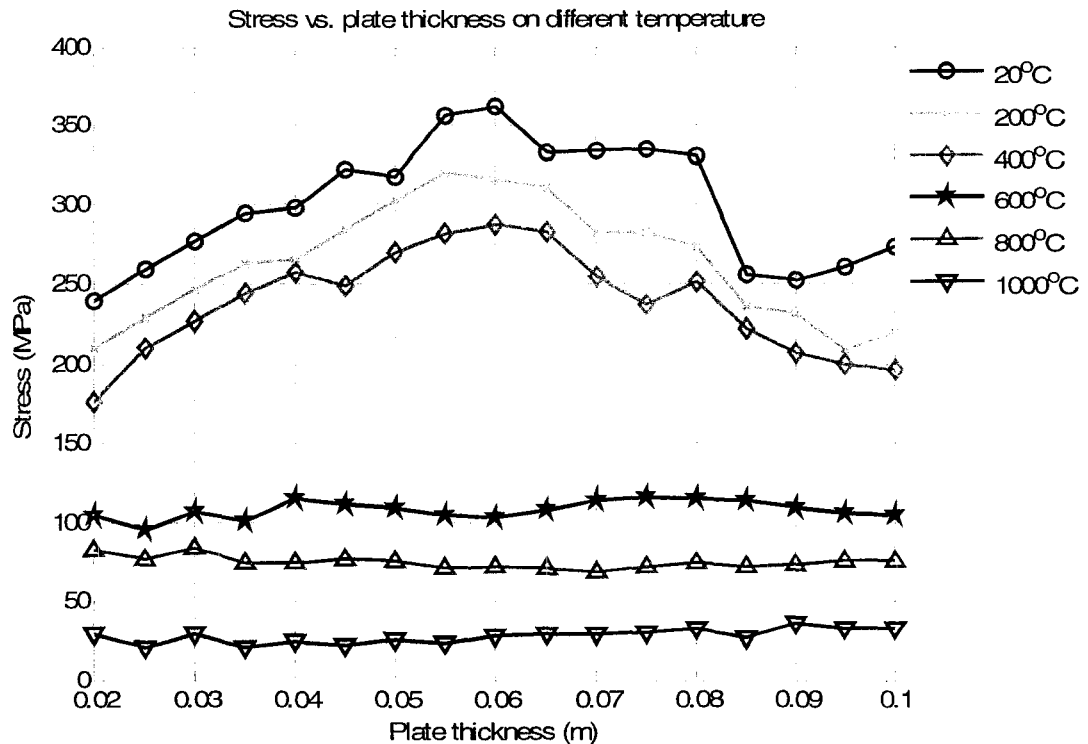


Figure 47 Variation of residual stress with changes in plate thickness

Figure 47 illustrates the variation of the residual stress as a function of plate thickness for different temperatures. The residual stress in this study is the average value of all points on the inner surface. According to the illustration, the temperature is above 600°C, and the residual stress does not vary as the plate thickness is changed. However, if the temperature is below to 400°C, the residual stress becomes greater when the plate thickness is around 6 cm.

4.2.4 Influence of the semi-angle of the target cone on bending quality

In accordance with the roll bending process simulation, the cylindrical shape is easier to bend. For a conical tube, its semi-angle denotes the similarity with a cylindrical shape. Therefore, the semi-angle might influence the bending quality. This section discusses this influence by comparing some simulations on different semi-angles.

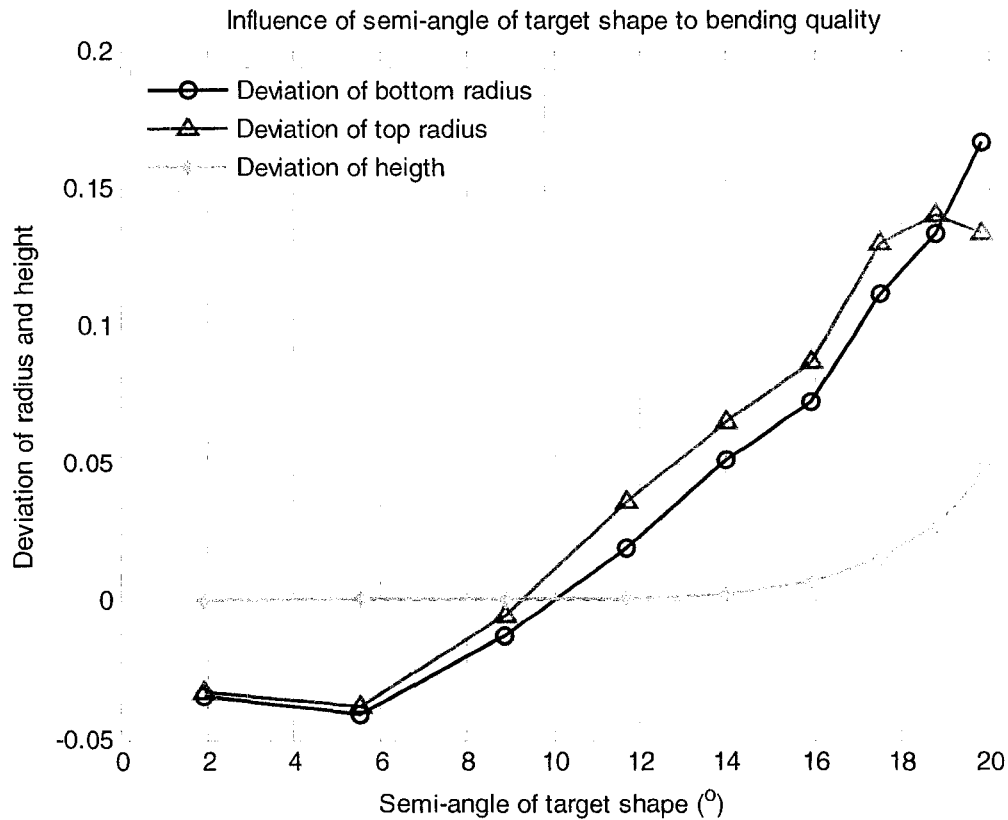


Figure 48 Influence of the semi-angle of the target shape on the bending quality

As illustrated in Figure 48, the deviation of the final shape varies with the semi-angle of the target shape. Generally, the higher the value of the semi-angle, the worse the final shape will be. However, the best final shape does not occur when we have the minimum semi-angle. Rather, the minimum deviation is obtained when the semi-angle is about 8.5° . If the semi-angle falls below 8.5° , the radius of the workpiece becomes smaller than that of the ideal shape.

4.3 Sensitivity of material properties

In this simulation, the different material properties are obtained by changing the plate temperature rather than the material. As the temperature increases, the material becomes

softer, and its elastic modulus and yield stress are smaller. This difference will cause a variation in simulation results. Table XVIII lists the constant parameters for studying the material properties and Table XIX lists the material properties of the ASTM A743 grade CA-6NM at specific temperatures.

Table XVIII

Constant parameters for studying the sensitivity of the temperature

Geometric Parameters			
Bottom radius (m)	Top radius (m)	Height (m)	Plate thickness (cm)
2.5	1.5	3.0	10
Configuration Parameters			
Span of outer rolls (m)	Static friction	Dynamic friction	
1.0	0.3	0.3	

Table XIX

Material ASTM A743 grade CA-6NM at different temperatures

Temperature (°C)	Elastic Modulus (GPa)	Yield stress (MPa)	Tangent Modulus (GPa)	Poisson's Ratio	Density (kg/m³)
20	200	754	2	0.3	7850
200	180	635	1.8	0.3	7850
400	166	562	1.6	0.3	7850
600	107	218	1	0.3	7850
800	92	134	0.9	0.3	7850
1000	62	24	0.6	0.3	7850

4.3.1 Influence of temperature on the bending quality

The bending quality also varies with changes in temperature, as illustrated in Figure 49. In this simulation group, the roll configuration is unvaried. However, different bending qualities are obtained at different temperatures, which, indicates that changing the temperature can improve the bending quality.

Figure 49 shows the radius of the final workpiece becoming smaller and smaller. When the temperature is increased, the workpiece gets closer and closer to the target cone, and at 800°C, it is closest to the target cone. Then, the deviation starts widening again. This illustration indicates that the ideal temperature can be set in order to obtain the optimal bending quality.

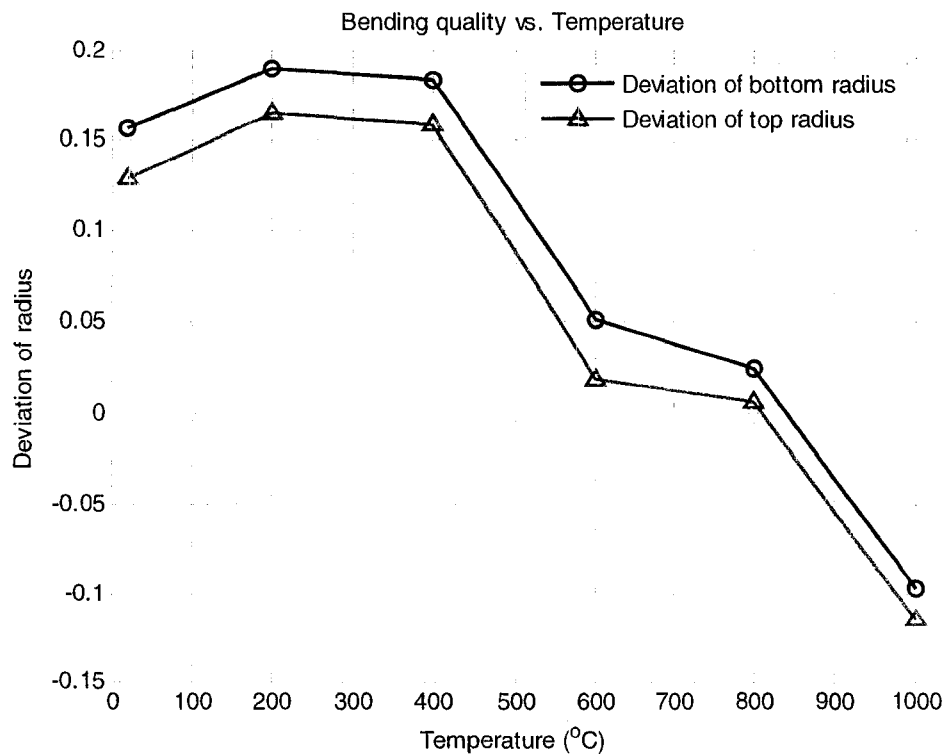


Figure 49 Bending quality obtained at different temperatures

4.3.2 Influence of temperature on the reaction forces on the rolls

Increasing the temperature causes the material to become softer. Apparently, the bending forces required are lower. The illustration in

Figure 50 proves this assertion. The figure merely illustrates the reaction force in the Y direction. For the X and Z directions, they have a similar performance.

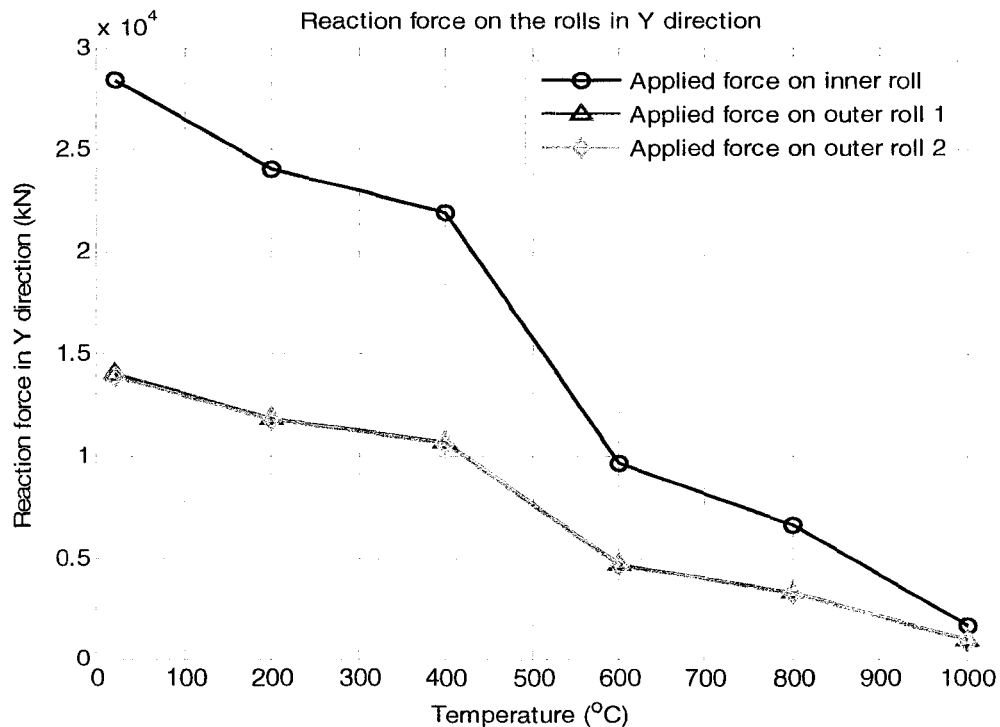


Figure 50 Reaction force of three rolls at different temperatures in the Y direction

4.3.3 Influence of temperature on residual stress

Obviously, the residual stress decreases as the temperature increases, as illustrated in Figure 51. In this project, the residual stress caused by thermal deformation is not considered. The residual stresses illustrated in Figure 51 are at specific temperatures.

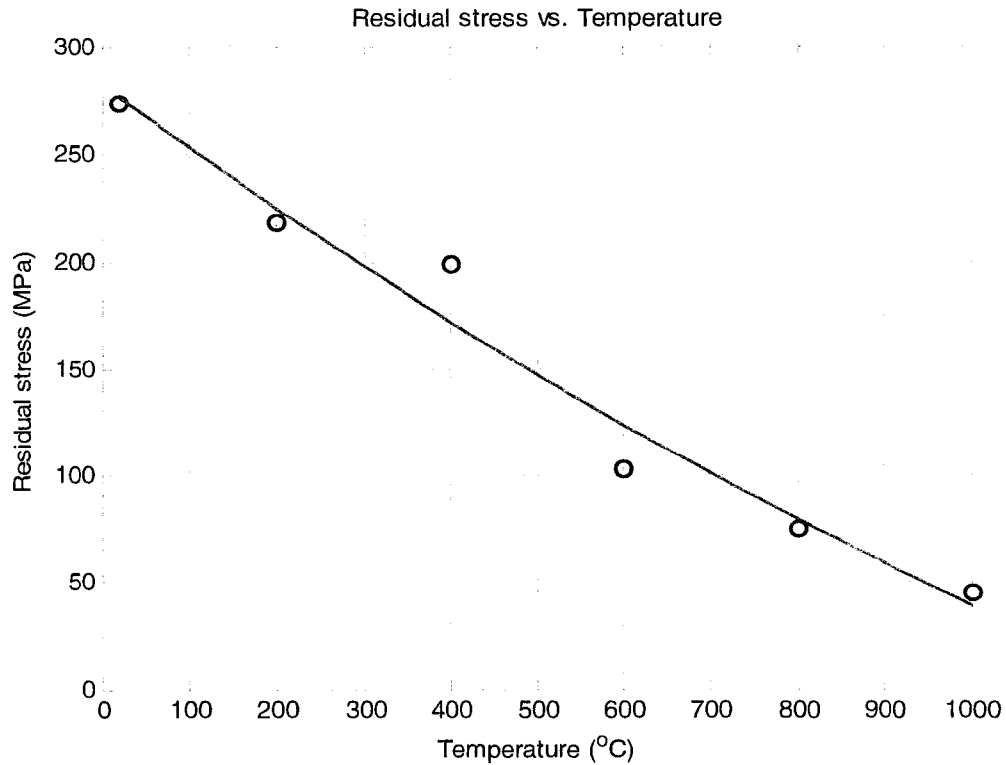


Figure 51 Trend of residual stress with increase in temperature

4.4 Configuration parameters

Configuration parameters include the span of the outer rolls, the friction, the dimension of the rolls, etc. The latter depends on the geometry of the target cone, as discussed in section 1.2. In this study, the span of the outer rolls will be examined in order to verify its influence on the final shape and other output results, etc. Roll configuration denotes the span of the outer rolls. Moreover, the influence of friction is also discussed, based on three values of friction coefficients: 0.1, 0.3 and 0.7.

As observed in simulation results, the span of the outer rolls significantly influences the bending quality and reaction forces. This parameter will be emphasized for discussion.

Table XX lists the constant parameters for studying the span of the outer rolls. In this study, the span of the outer rolls varies from 1.5 m to 3.0 m, while the temperature is kept at 20°C.

Table XX

Constant parameters for studying the sensitivity of the span of outer rolls

Geometric Parameters				
Bottom radius (m)	Top radius (m)	Height (m)	Plate thickness (cm)	
2.5	1.5	3.0	10	
Configuration Parameters				
Static friction		Dynamic friction		
0.3		0.3		
Material Parameters (ASTM A743 grade CA-6NM)				
Elastic Modulus (GPa)	Yield stress (MPa)	Tangent Modulus (GPa)	Poisson's Ratio	Density (kg/m ³)
200	754	2	0.3	7850

4.4.1 Influence of span of the outer rolls on bending quality

A dramatic phenomenon is discovered when analyzing the span of the outer rolls. The bending quality does vary with the application of different spans of the outer rolls. Generally, there is a configuration in which the optimal bending quality can be obtained, even though all configurations satisfy the geometry of the target cone. Actually, for different materials, even if the geometry of the target cone is the same, the optimal configuration is different. For a given material, at different temperatures, this optimal configuration is also different. That means that the optimal configuration is related to the material. This section states the variations seen in the bending quality with the span of

the outer rolls when applying material of ASTM A743 grade CA-6NM at 20°C. To verify whether the optimal configuration indeed exists, the other two materials, stainless steel and aluminum, are also studied. Figure 52 illustrates that the bending quality varies with the span of the outer rolls.

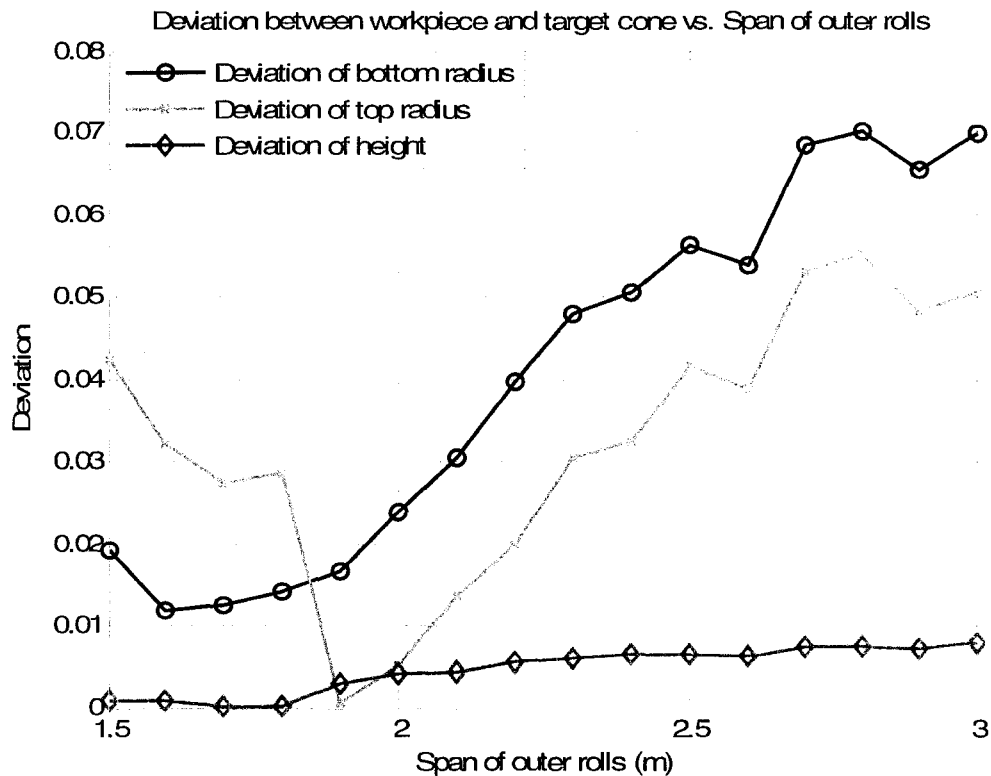


Figure 52 Deviation of the final shape from the target cone on different spans of the outer rolls when applying the ASTM A743 grade CA-6NM material

The other two materials, stainless steel and aluminum alloy, have different mechanical properties. Table XXI lists the material properties of ASTM A36 Steel and Figure 53 illustrates the bending quality changes as the span of the outer rolls is varied as this type of material is applied.

Table XXI

Material properties of ASTM A36 Steel

Material Parameters (ASTM A743 grade CA-6NM)				
Elastic Modulus (GPa)	Yield stress (MPa)	Tangent Modulus (GPa)	Poisson's Ratio	Density (kg/m ³)
200	250	2	0.3	7850

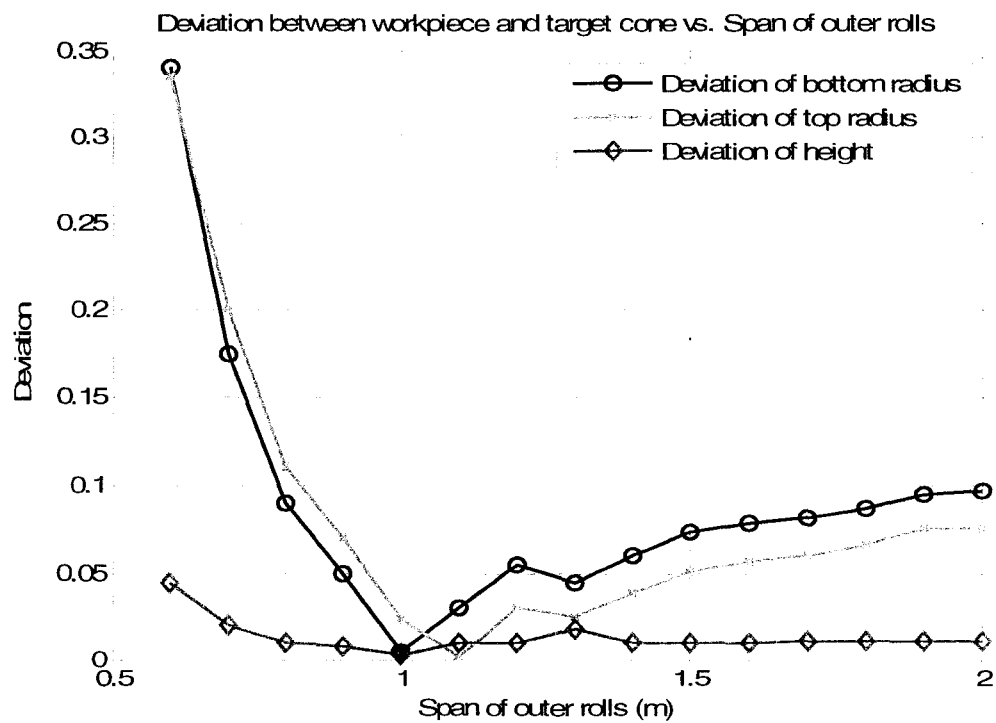


Figure 53 Deviation of the final shape from the target cone on different spans of the outer rolls when applying the ASTM A36 Steel material

Moreover, Table XXII lists the material properties of AA 6063 Aluminum Alloy and Figure 54 illustrates the variation in the bending quality as changes are made to the span of the outer rolls as this type of material is applied.

Table XXII

Material properties of AA 6063 Aluminum Alloy

Material Parameters (ASTM A743 grade CA-6NM)				
Elastic Modulus (GPa)	Yield stress (MPa)	Tangent Modulus (GPa)	Poisson's Ratio	Density (kg/m ³)
75	48	0.75	0.33	2700

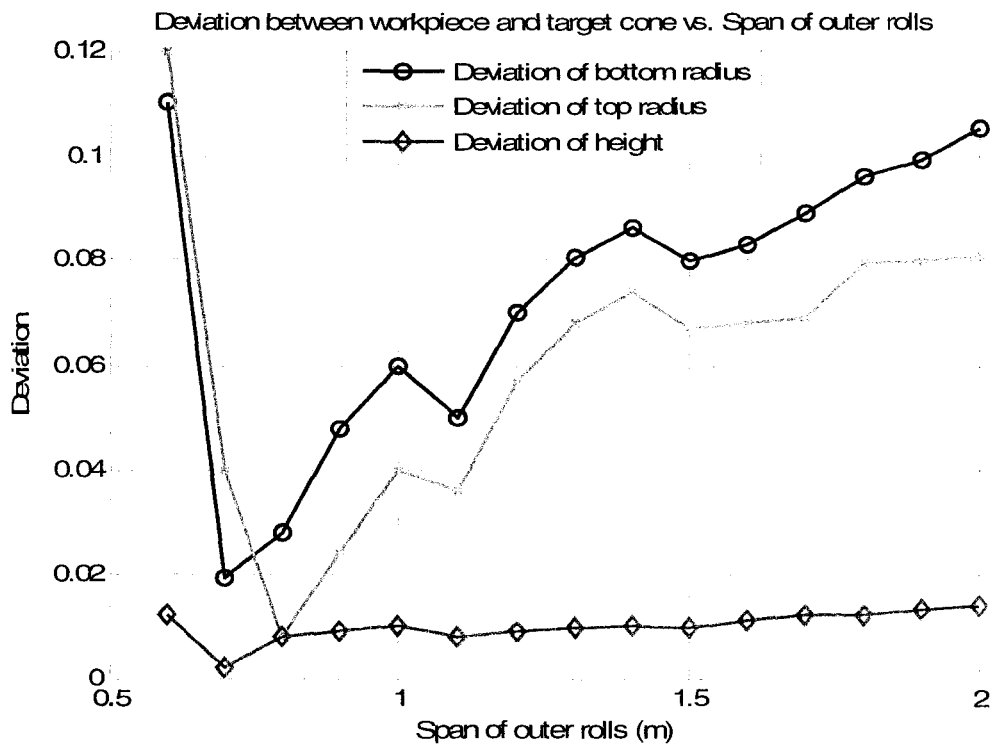


Figure 54 Deviation of the final shape from the target cone on different spans of the outer rolls when applying the AA 6063 Aluminum Alloy material

Figure 52 to Figure 54 indicate that the bending quality depends on the configuration of the rolls (span of the outer rolls). Furthermore, the optimal roll configuration is not static

for different materials. The softer the material applied, the smaller the optimal value of span.

4.4.2 Influence of span of outer rolls on the reaction forces on the rolls

The reaction force on the rolls also varies as the roll configuration is varied. As illustrated in Figure 55, the reaction forces have inverse ratio with the span of the outer rolls. This conclusion also conforms to equation (2.2).

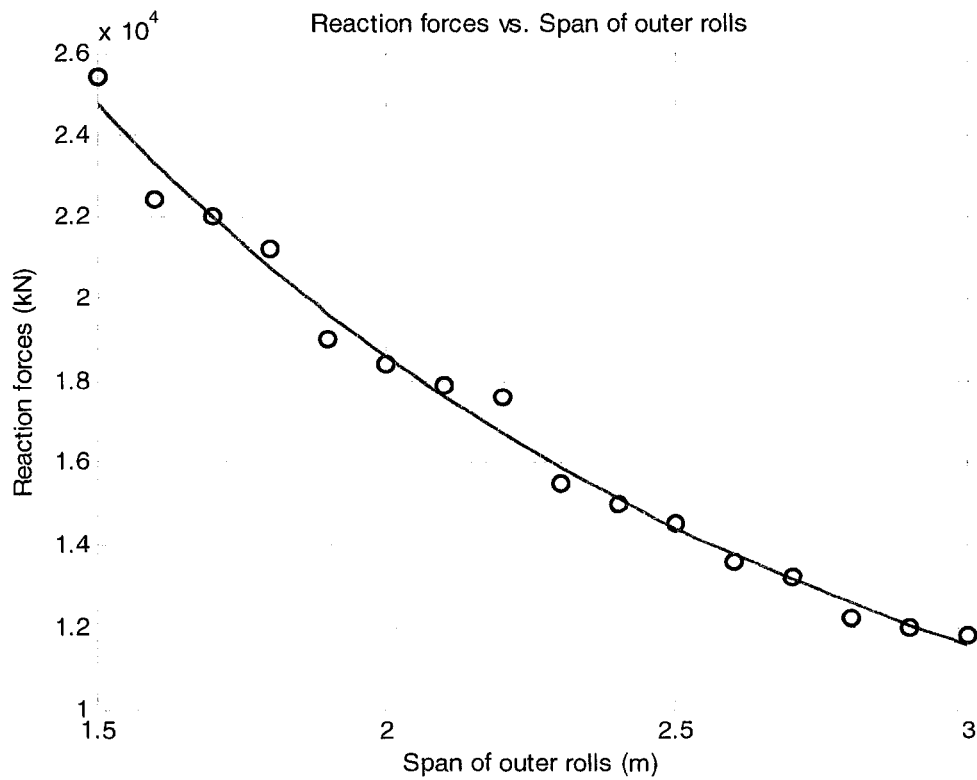


Figure 55 Variation of reaction force when applying different spans of the outer rolls

4.4.3 Influence of span of the outer rolls on residual stress

Figure 56 illustrates the variation of residual stress with an increase in the span of rolls. The residual stress in this figure is the average value of all points on the inner surface.

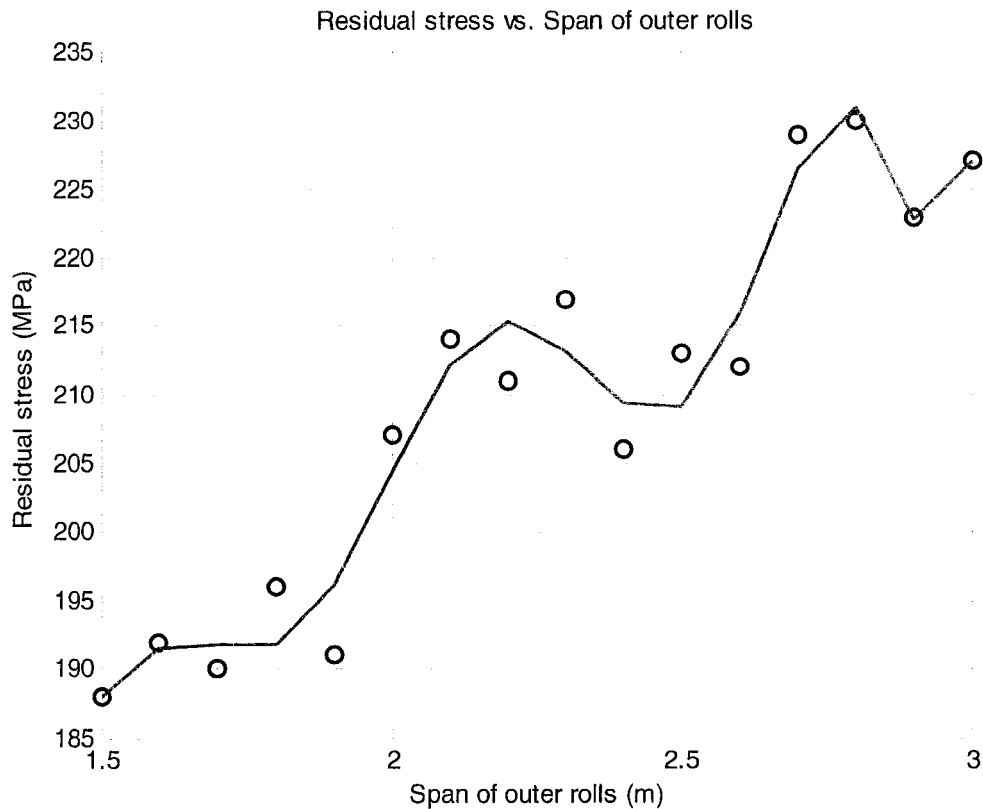


Figure 56 Residual stress on the application of different span of the outer rolls

As illustrated in Figure 56, the residual stress undergoes a slight irregular increase when the span of the outer rolls is enlarged. According to the analytical method for estimating the residual stress discussed in section 2.5.2, the span of the outer rolls cannot influence the residual stress. However, as observed in multiple simulations, the radius of the final piece reduces irregularly with the increase of the span of the outer rolls. Therefore, the residual stress is increased correspondingly, though irregularly.

4.4.4 Sensitivity of friction to the bending process

The friction specification has been discussed in section 2.2.4. Generally, friction can influence the bending process, and so this section therefore performs the simulations with three different friction values, and verifies the influence. For the inner roll and guiding cylinders, their friction is always set to 0. The friction of the outer rolls is set to 0.1, 0.3, and 0.7, respectively, and the static friction and dynamic friction are always set equal.

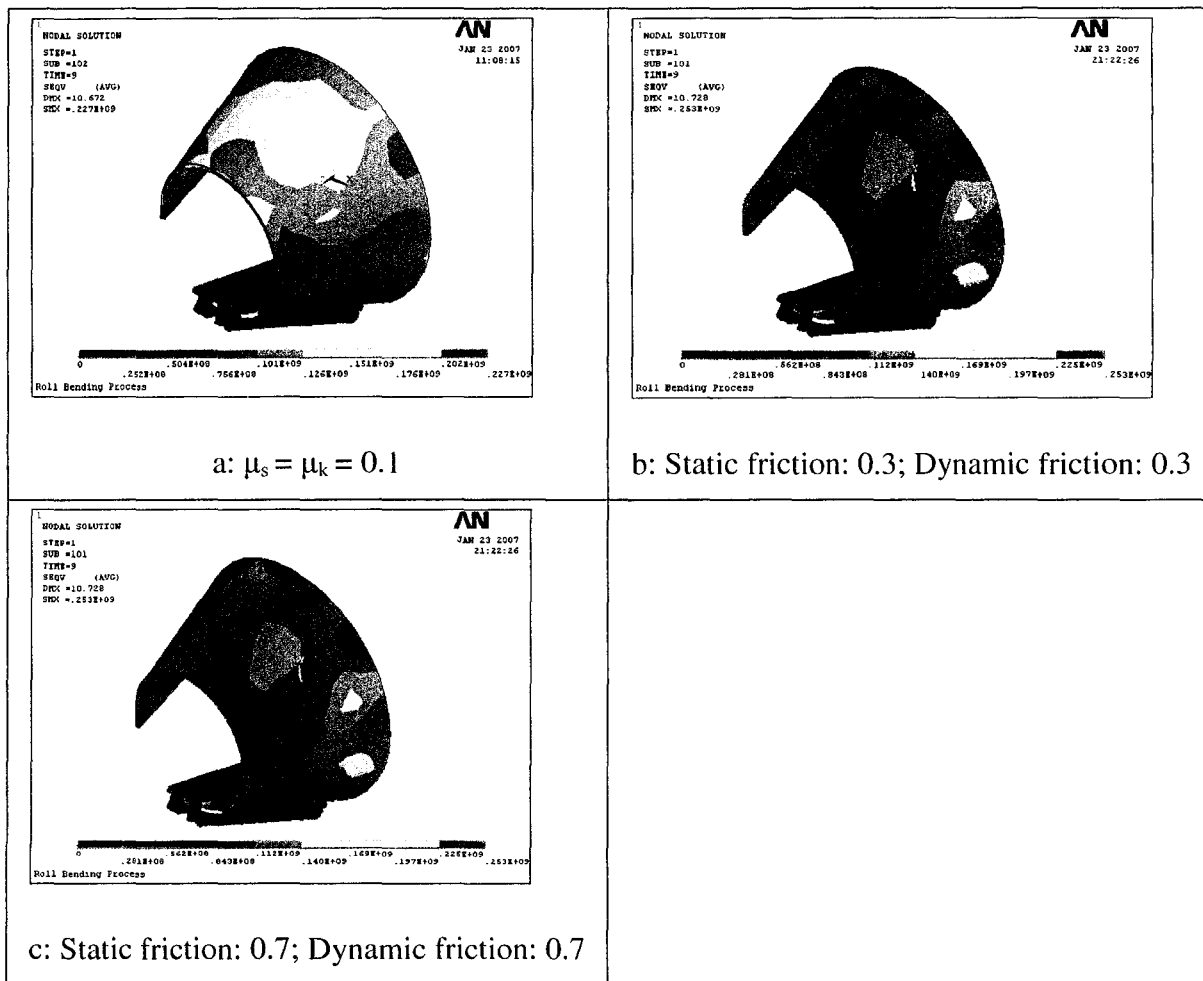


Figure 57 Comparison of the final shape at frictions of 0.1, 0.3 and 0.7

With the illustration in Figure 57, the final shape in Figure *b* and in Figure *c* are nearly the same. Even the stress distribution is almost the same. However, Figure *a* is slightly different, indicating that 0.3 of friction is sufficient for bending a good shape. In reality, the dynamic friction between steel and steel is around 0.3, while the static friction is even higher. In this document, all simulations are based on a friction of 0.3 unless otherwise specified.

4.5 Summary

The analysis performed in this chapter indicates that changing input parameters results in different simulation results. Some input parameters are sensible to specific output results. For instance, the temperature is sensible to reaction forces on the rolls. Nevertheless, some input parameters have nearly no influence whatsoever on certain specific output results. An example of this is the rolls configuration, which hardly has any influence at all on the residual stress.

The study demonstrates that any changes in input parameters can influence the bending quality. For specific materials at certain temperatures to form a specified target cone, the bending quality depends on the roll configuration. This roll configuration can be optimized to obtain the best bending quality. If the roll configuration is solid but the temperature is changed, an optimal temperature can also be obtained for bending the best final shape. For different materials, their optimal roll configurations are not identical either.

The roll configuration also influences the reaction forces. As the span of the outer rolls widens, a minor force is applied. Obviously, the temperature also influences the reaction forces and the constraint, with higher temperature causing a decline in reaction forces and in the constraint.

The plate thickness obviously influences the final shape. A thinner plate implies less force, but does not imply a better bending quality. Actually, when the dimension of the target cone is large, the plate thickness should also be high enough; otherwise, the final shape will be seriously deformed. However, the negative of increasing the plate thickness is that reaction forces are rapidly increased. Therefore, for a thicker plate, the best technique is to first heat up the plate before bending it. In this condition, less force is applied, and a good bending quality can be guaranteed.

CONCLUSION

The goal of the numerical simulation of the roll bending process is to find the optimal roll configuration and to balance the reaction force and bending quality. With the dynamic FE simulation, much valuable information has been obtained, such as the stress, the strain, the reaction force, etc. Moreover, the final shape and the animation of the process have also been produced. To summarize, the dynamic FE simulation decreases the development time and provides a lot of valuable information.

This project implements the simulation of the roll bending process using ANSYS LS-DYNA. This simulation is able to simulate the roll bending process to form various tubular cones with different diameters, different heights and different plate thicknesses. Furthermore, we may choose different materials or the same material, at different temperatures for a simulation study, just by changing material properties. Another important configuration involves the dimension and position of the rolls. Given a specific target cone tubular, different rolls configurations result in different bending qualities. The roll configuration is easy to set up in this simulation, and simply involves the modification of corresponding parameters. For the simulation and FEM, the element type and mesh strategy must be specified. The mesh strategy in this simulation is simple because there is no part with complex geometric shapes. The SHELL element is used in order to decrease the processing time. The configuration parameters are set in corresponding files. By changing the parameters of these files, the simulation runs using the specified parameters.

Based on the simulation result, the roll bending process can be used to form a conical tubular shape. Both simulations with conical or cylindrical rolls work well. However, with the conical rolls applied, it becomes easier to control the curvature of the plate and satisfy the tangent speed relationship. By configuring the roll's dimension and position, we are able to obtain different bending qualities.

Depending on the number of passes involved, the roll bending process can be divided into single-pass or multiple-pass processes. The single-pass process is more efficient, but 3-pass requires less force and allows a better control of the bending curvature. In this project, both the single-pass and 3-pass processes were simulated, and the 3-pass process simulation was finally selected.

For each simulation, the general analysis or Time-History analysis are implemented in ANSYS. Additionally, further analysis is implemented in MATLAB. The curve of the reaction force, the curve of stress, and the geometric verification are all implemented using MATLAB.

In order to measure the bending quality, the geometric shape must be verified after the simulation in ANSYS, in order to obtain the deviation between the bended workpiece and the target cone; furthermore, the sensitivity to the bending quality can also be studied. In this thesis, by comparing the least-squares fitted cone, which is calculated from the bended workpiece using the Levenberg-Marquardt algorithm, with the target cone, the geometric verification is implemented, and the bending quality can therefore be measured.

Another goal of the simulation is to predict the reaction force and the residual stress. From the results obtained in ANSYS, these data (reaction force, residual stress and required energy, etc.) can be obtained directly. Furthermore, the entire roll bending process is illustrated dynamically in ANSYS using an animation display. The workpiece can be displayed at a specified interval, thus providing more details on the workpiece, and providing direct information on bending quality.

The parametric sensitivities were studied through the results of the simulation and the geometric verification. In this project, the geometric parameters, the material properties

and the rolls configuration have been studied in order to analyze their sensitivity to the bending quality, the reaction force and residual stress. For the geometric parameters, the radius of the target cone ranges from 1 to 3 m, and the thickness of the plate ranges from 2 to 10 cm. For the material, several materials, such as stainless steel, aluminum have been studied. Furthermore, the material used for the Francis Turbine at different temperatures was also studied. For the roll configuration, the span of outer rolls was studied. The following conclusions can be drawn from the parametric studies:

- For a specific material and a given target cone, the bending quality depends on the roll configuration. An optimal bending quality is within a certain configuration.
- For a given target cone, a better bending quality can be achieved when a harder material or thicker plate is chosen.
- For a given roll configuration, the reaction force increases quasi linearly with the increase in the plate thickness. Note also that the reaction force decreases as the span of outer rolls increases.
- The span of outer rolls is a major configuration parameter of the roll bending process, and it influences the bending quality directly. The simulation is important for determining the optimal value of this parameter.

In this thesis, the roll bending simulation has been implemented, and been shown to work very well. However, some improvements can be achieved. In the next chapter, some recommendations are listed in that regard.

RECOMMENDATIONS

Until now, the simulation model has been constructed to simulate the roll bending process. However, this simulation model is an open loop system with respect to bending quality. That means that when input parameters are changed, the bending quality varies. The close loop system is better for controlling the bending quality, and to obtain such a system, one module should be added to measure the bending quality and then provide feedback to the input so that the roll's configuration can be adapted accordingly.

Furthermore, the correlation between the bending quality, the target cone, the material properties and the roll's configuration are yet to be derived. Even though this work requires many simulations, it will be a practical tool for optimizing the process.

A parallel computation is also necessary because the current simulation requires too much time (about 4 hours when the mesh division is 200). Decreasing the meshing size can decrease the computation time, but it also decreases the precision of the results as well. A parallel computation can minimize the computation time while maintaining its precision. In the ANSYS environment, a parallel computation might be difficult to realize. These are however avenues that will require further investigation.

Moreover, the feasibility of applying cylindrical rolls deserves additional study because the cylindrical roll is not too expensive. The conical roll for its part is dedicated to one specific cone, but provides the possibility of usage on a large variety of workpieces or conical shapes. Furthermore, the rolls in the current simulation are rigid bodies. Simulations with deformable rolls will be studied in the next research project.

REFERENCES

1. Couture, P., *Simulation du roulage de tôles fortes*, in *Mechanic Engineering*. 2004, École de technologie supérieure, Université du Québec: Montreal. p. 68.
2. *Francis Turbine*, turbine_09-s.jpg, Editor, Topomadica. Available from http://www.topomatika.hr/Applications/Images/turbine_09-s.jpg
3. *Francis Turbine*, P3194956_Twizel_Powerstation_mediu.jpg. Available from http://www.jr-worldwi.de/nzpics/mediu/P3194956_Twizel_Powerstation_mediu.jpg
4. Kohser, E.P.D.J.T.B.R.A., *Materials and Processes in Manufacturing*. 2002: John Wiley & Sons.
5. Bouhelier, C., *Le formage des toles fortes*. Senlis, France : Centre technique des industries mécaniques 1982.
6. Yang, M. and S. Shima, *Simulation of pyramid type three-roll bending process*. International Journal of Mechanical Sciences, 1988. **30**(12): p. 877-886.
7. Hua, M., K. Baines, and I.M. Cole, *Bending mechanisms, experimental techniques and preliminary tests for the continuous four-roll plate bending process*. Journal of Materials Processing Technology 2nd Asia Pacific Conference on Materials Processing, 1995. **48**(1-4): p. 159-172.
8. Hua, M., K. Baines, and I.M. Cole, *Continuous four-roll plate bending: a production process for the manufacture of single seamed tubes of large and medium diameters*. International Journal of Machine Tools and Manufacture, 1999. **39**(6): p. 905-935.
9. Hua, M., et al., *A formulation for determining the single-pass mechanics of the continuous four-roll thin plate bending process*. Journal of Materials Processing Technology Proceedings of the International Conference on Mechanics of Solids and Materials Engineering, 1997. **67**(1-3): p. 189-194.
10. Hua, M. and Y.H. Lin, *Effect of strain hardening on the continuous four-roll plate edge bending process*. Journal of Materials Processing Technology, 1999. **89-90**: p. 12-18.
11. Hua, M., D.H. Sansome, and K. Baines, *Mathematical modeling of the internal bending moment at the top roll contact in multi-pass four-roll thin-plate bending*. Journal of Materials Processing Technology, 1995. **52**(2-4): p. 425-459.
12. Hua, M., et al., *Continuous four-roll plate bending process: Its bending mechanism and influential parameters*. Journal of Materials Processing Technology, 1994. **45**(1-4): p. 181-186.

13. Hu, W. and Z.R. Wang, *Theoretical analysis and experimental study to support the development of a more valuable roll-bending process*. International Journal of Machine Tools and Manufacture, 2001. **41**(5): p. 731-747.
14. Tekiner, Z., *An experimental study on the examination of springback of sheet metals with several thicknesses and properties in bending dies*. Journal of Materials Processing Technology, 2004. **145**(1): p. 109-117.
15. Kalpakjian, *Manufacturing Engineering and Technology*, ed. D.D.L. McGuire. 1995: Addison Wesley Publishing Company. 461-468.
16. ISEL co., Ltd. 2003; Available from: <http://www.isel.co.jp/english/index.htm>.
17. *Basic Analysis Guide*, Release 10.0 Documentation for Ansys, 2007.
18. *ANSYS LS-DYNA User's Guide*. Release 10.0 Documentation for Ansys, 2007.
19. *ANSYS LS-DYNA*; Available from: <http://www.ansys.com/products/lsdyna.asp>.
20. A.C.UGURAL, *Mechanics of Materials*. 1991: McGRAW-HILL,INC. 252-280.
21. R.CRAIG, R., *Mechanics of Materials*. 1996: John Wiley & Sons.
22. ANSYS, I. *Structural Analysis*. [cited.
23. Shakarji, C.M., et al., *Least-Squares Fitting Algorithms of the NIST Algorithm Testing System*. Journal of Research of the National Institute of Standards and Technology, 1998. **Volume 103**(Number 6).
24. Miller, A. *Curve Fitting, Data Modelling, Interpolation, Extrapolation.*; Available from: <http://www.mathcom.com/corpdir/techinfo.mdir/scifaq/q230.html>.
25. Wikipedia. *Levenberg-Marquardt algorithm*. 2006; Available from: http://en.wikipedia.org/wiki/Levenberg-Marquardt_algorithm.